

PDF hosted at the Radboud Repository of the Radboud University Nijmegen

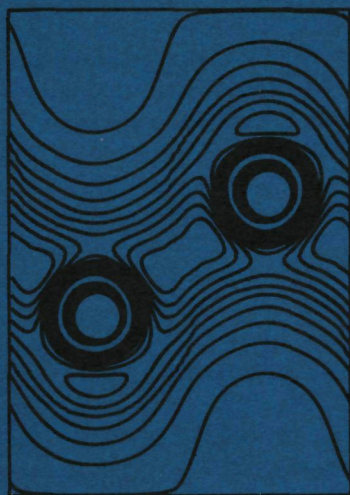
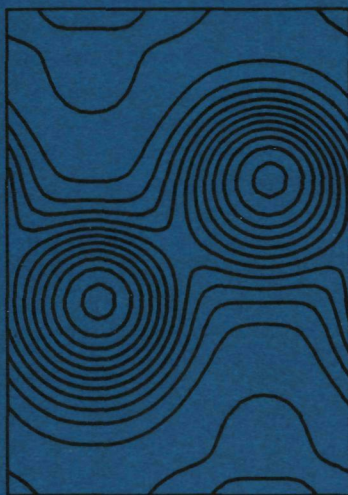
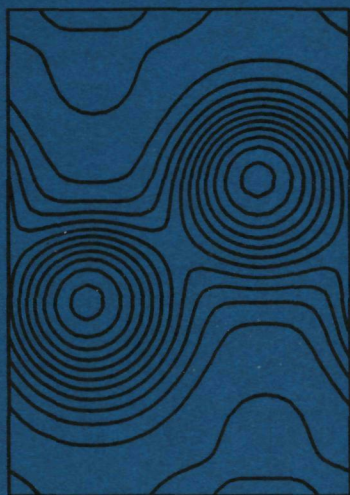
The following full text is a publisher's version.

For additional information about this publication click this link.

<http://hdl.handle.net/2066/113307>

Please be advised that this information was generated on 2018-07-08 and may be subject to change.

3283



Multipole Green Functions for Electronic Structure Calculations

M.S. Methfessel

Multipole Green Functions for Electronic Structure Calculations

Multipole Green Functions for Electronic Structure Calculations

PROEFSCHRIFT

ter verkrijging van de graad van
doctor in de wiskunde en natuurwetenschappen
aan de Katholieke Universiteit te Nijmegen,
op gezag van de Rector Magnificus,
Prof.Dr. J.H.G.I. Giesbers,
volgens besluit van het College van Dekanen
in het openbaar te verdedigen
op donderdag 29 mei 1986
des namiddags te 2 uur precies

door

Michael Siegfried Methfessel

geboren te Clausthal-Zellerfeld

druk: Springelkamp, Groningen

1986

promotores: **Prof. Dr. J. Kübler** (Technische Hochschule Darmstadt)
Prof. Dr. A.G.M. Janner

co-referent: **Dr. M.H. Boon**

MIJN DANK GAAT UIT NAAR ALLE MENSEN
DIE MIJN VERBLIJF IN NEDERLAND ZO AANGENAAM
GEMAAKT HEBBEN.

CONTENTS

CHAPTER 1: Introduction 1

CHAPTER 2: Background 3

2.1 Goal 3

2.2 Methods for muffin-tin potentials 4

(A) Muffin-tin geometry and potential 5

(B) Augmented plane wave method (APW) 6

(C) Methods based on spherical waves 8

(D) Comparison of plane wave and spherical wave approaches 10

(E) Linearized versions of APW and KKR 12

CHAPTER 3: Generalization of Multiple Scattering Methods to Non-Uniform Interstitial Potentials 14

3.1 Formal properties of solid Hankel and Bessel functions 14

(A) Defining equations 14

(B) Generation of the H_L and Fourier transforms 17

(C) Bloch-Hankel functions and structure constants 20

(D) Smoothed Hankel functions 22

3.2 Generalization to varying interstitial potential 23

(A) Multipole Green function 23

(B) Transfer of boundary conditions 26

3.3 Calculating multipole Green functions in practice 29

(A) Separation into singular and smooth part 29

(B) Calculation of the singular part 31

CHAPTER 4: Implementation for Periodic Systems 36

4.1 Calculation of eigenstates 36

(A) Smooth part of the multipole Green function 36

(B) Augmentation and matrix elements 38

(C) L-truncation of augmentation sums 41

(D) Choice of energy parameters 43

4.2 Charge density and self-consistency 44

(A) Local-density approximation 46

(B) Representation of the charge density 48

(C) Hartree and exchange-correlation potentials 51

(D) Self-consistency cycle 55

(E) Total energy 56

CHAPTER 5: Applications 59

5.1 Covalent crystals 59

(A) Methods and results to date 60

(B) Application to silicon: eigenvalues and bulk properties 62

(C) Charge density 65

(D) Distortion energies 69

5.2 Metals 75

5.3 Conclusions 76

CHAPTER 6: The Analytic-Quadratic Integration Method 79

6.1 Analytic-Quadratic Method of Calculating the Density of States 80

6.2 Singular Integrals over the Brillouin Zone:

The Analytic-Quadratic Method for the Density of States 86

6.3 Singular Integrals over the Brillouin Zone:

Inclusion of \mathbf{k} -dependent Matrix Elements 106

APPENDIX A: Mathematical Formulae 118

APPENDIX B: Singular Part of the Multipole Green function 128

APPENDIX C: Almost Degenerate Rayleigh-Ritz Basis 132

SUMMARY 135

SAMENVATTING 138

REFERENCES 142

CHAPTER 1

Introduction

One of the consequences of quantum mechanics was the disappearance of the clear-cut separation of theoretical materials science into physics and chemistry. With the Schrodinger equation, the proper description for the behaviour of electrons in a potential was given. In principle this made it possible to derive all the properties of atoms, molecules, and condensed matter from first principles. However, this program has not yet been executed because of what might be called technical difficulties. The distinction between the chemical and the physical approach has therefore remained, not so much in the subject matter or objective but in the means used to deal with the computational problems. An example is given by the electron-electron interaction, which makes it necessary to treat a large number of highly correlated electrons instead of a single particle moving in an external potential. Theoretical chemists often work with methods based on Slater determinants, which are suited for the accurate treatment of small systems such as molecules. Theoretical physicists emphasize the concept of the effective single-particle potential, an idea designed for the practically infinite number of electrons in a solid or liquid. As a consequence of the differences in the two approaches, there has been a specialization on different types of systems which can be treated by the various methods, with a large gray zone of unsolved problems in the middle.

In the last few years the distinction between the two approaches has blurred again because the computational techniques in both sciences have become more advanced and are now applied to more complicated systems. As interest is extended to include surfaces and impurities in addition to crystals in solid state physics, problems are encountered which are very similar to those which have to be solved for a molecular calculation. Central among these is to solve a single-particle Schrodinger equation in a potential of general shape. Existing methods either use a large basis set of some type to get enough degrees of freedom, or simplify the task in some way as by making use of a pseudopotential approximation. In addition there are a number of elegant and efficient methods which describe the stationary electron states as standing waves resulting from multiple scattering between the constituent atoms, the best-known of these is Korringa, Kohn, and Rostoker (KKR) method. Unfortunately, this approach requires in practice a shape approximation for the potential. It must be taken uniform in the 'interstitial region' between the atoms. The first part of this thesis considers the

question of how the multiple-scattering approach can be generalized in order to avoid this approximation for the potential. A new way of doing this is presented together with test calculations which demonstrate the value of the method.

In the course of the work another problem of computational solid state physics was encountered: the precise numerical evaluation of singular Brillouin integrals such as those occurring when the density of states is calculated. A new technique has been found which is presented in the last chapter. The new method is based on a local quadratic expansion of the energy band as a function of the k -vector whereas all existing methods do not go higher than the linear term. A quadratic expansion is necessary to give a proper description of the Van Hove singularities. These play a large role in determining the character of the density of states or similar quantities. The results show that the new approach is considerably more efficient and precise than those which are in use at the present time.

The general plan of the subsequent chapters is as follows. In chapter 2, the multiple scattering approach in the present form is discussed and compared to other techniques which use the same shape approximation for the potential. In chapter 3 the generalization to potentials of arbitrary shape is done. Chapter 4 describes the implementation of the new approach for periodic systems, and chapter 5 presents the results of the calculations and the conclusions. Finally, the integration of singular Brillouin zone integrals is the subject of chapter 6. Additional mathematical information is collected in the appendices.

CHAPTER 2

Background

2.1 Goal

The major part of this thesis is concerned with one question: how to solve the single-particle time-independent Schrödinger equation. It might be supposed that this has been adequately discussed in the time since the equation was introduced. However, one can say that there have been two separate periods of interest in the problem. At the present time, we are in the middle of the second period.

In the *first* period, the Schrödinger equation was the central tool for the new quantum-mechanical description of nature. For example, the Bohr-Sommerfeld model of the atom was put on a sound theoretical footing, the existence of energy bands could be explained, and phenomena such as tunneling were discovered. Also, interesting philosophical questions were raised. For these discussions of a more qualitative nature it was sufficient (and indeed advantageous to physical understanding) to consider simple systems in conjunction with some perturbation theory. For example, a lot was learned about energy bands from the nearly-free electron and tight-binding models. But one problem which could not be solved satisfactorily was the task of deriving the ground state properties of condensed matter from first principles. There were two difficulties: first, the problem of the strong interaction between electrons and second, the inherent complexity of many-atom systems even if non-interacting electrons are considered.

The *second* period of interest started considerably later than the first after means to deal with the two difficulties were found. The first step was of course the development of large computers, making possible new numerical approaches; for example, matrix diagonalizations are done routinely today which were simply impossible fifty years ago. The second ingredient was the somewhat unexpected discovery that a simple treatment of the electron-electron interaction can lead to an adequate description of the ground state for many systems. These approaches consider each electron as moving in an effective potential which models the influence of the other electrons. The final effect is to reduce the many-electron problem to the iteration of single-electron problems. This was first done in practice by the Slater $X\alpha$ method [85] and later in a more sophisticated way by local-density theory [43,55,41]. It became possible to

calculate small effects properly such as cohesive energies and phonon frequencies. However, for studies of this type a method for solving the Schrödinger equation is required which is at the same time precise and efficient. A typical case is the calculation of phonon frequencies from first principles: the energy changes are very small but it is also necessary to use a large unit 'supercell' containing one complete period of the atomic displacements.

Consider some configuration of atoms in space, for example, a crystal or a molecule. Assume that the electron-electron interaction is described adequately by some effective single-particle potential but that one does not want to sidestep the problem of the core states by using a pseudopotential method [6]. Then difficulties can be expected for the following reasons when solving the single-particle Schrödinger equation:

- (i) Partial differential equations are generally difficult to solve unless there is sufficient symmetry to reduce the number of variables. Eigenvalue problems are more difficult than inversion problems.
- (ii) The interaction part of the potential is given numerically so that elegant analytical approaches are impossible.
- (iii) The $1/r$ Coulomb potential of the nuclei is especially unpleasant, since it is at the same time singular and long-range.
- (iv) The set of wave functions contains at the same time highly localized core states as well as valence states which extend over the whole system.
- (v) Because they are orthogonal to the core states, the valence wave functions have strong oscillations near the nuclei.

A number of techniques have been developed to deal with these problems. On one hand there is the pseudopotential approximation (see section 5.1). Focus will be here on methods using a muffin-tin potential in particular methods based on the concept of multiple scattering. In chapter 3 these will be adapted to potentials of arbitrary shape.

2.2 Methods for muffin-tin potentials

Points (iii), (iv) and (v) above strongly suggest that it is best to treat those parts of space which are close to a nucleus differently from the rest.

(A) MUFFIN-TIN GEOMETRY AND POTENTIAL

Muffin-tins were introduced into electronic structure calculations by Slater [84]. The term 'muffin-tin geometry' will be used to denote the following way of dividing space: A set of non-overlapping spheres centered on the nuclei is chosen*. Inside such an atomic sphere, the potential is nearly spherical and it is natural to use a description in polar coordinates. The interstitial region is then defined as that part of space lying between the spheres. Here, both the potential and the wave function are slowly varying and are best represented using basis functions adapted to this behaviour. By choosing different representations in the spheres and the interstitial, a high degree of precision is made possible in both. Proper behaviour at the Coulomb singularity, good core states, and a sound orthogonality of valence states on the core are obtained easily by numerical integration along the radial variable. In principle the choice of sphere radii is arbitrary as long as the spheres do not overlap.

It is a standard practice to simplify the problem further by means of the muffin-tin potential approximation. Inside the atomic spheres, the potential is replaced by its spherical average. The approximation is good because the dominating Coulomb term close to the nucleus forces the charge density (and consequently the interaction potential) into a spherically symmetric shape. For this potential the angular momentum components decouple which simplifies the solution of the Schrödinger equation. Perturbation methods are usually adequate if non-spherical terms become important inside the spheres [51,77]. The second approximation is to take the potential constant throughout the interstitial region. This makes it possible to write down analytical solutions of the Schrödinger equation there. The choice between plane waves and spherical waves then leads to the augmented plane wave and multiple scattering methods, respectively. For a close-packed structure such as a simple metal, the error introduced by the muffin-tin potential approximation is very small [26,77]. Partly this is because the interstitial volume is small and partly because of the high symmetry around each site. However, for many other systems of interest the approximation is too crude. In a loosely packed structure such as a diamond lattice, the interstitial volume is much larger and the potential has a pronounced maximum at the interstices. A similar situation is found for molecules where the potential rises to the vacuum level in a complicated way. Other examples are systems in which the disturbance of the symmetry is important for the effects under study, such as

* When a molecule is considered, one often adds another sphere surrounding the whole system [34,49].

phonon frequencies or elastic distortion energies. The large errors which the muffin-tin approximation produces for these systems can be traced to the inadequate treatment of the potential in the interstitial region [51,54]

In the following, the two competing approaches which are used to solve the Schrodinger equation in a muffin-tin potential are described

(B) AUGMENTED PLANE-WAVE METHOD (APW)

Characteristic of the APW method (Slater [84]) is that it uses plane waves to expand the wave function in the interstitial. This is only possible in a periodic system. In that case Bloch boundary conditions to a Bloch vector \mathbf{k} are used to define the functions. A truncated Fourier series defines a function over all of the cell which, however, is equal to the wave function only in the interstitial region

$$\psi_I(\mathbf{r}) = \sum_{\mathbf{G}} A_{\mathbf{G}} e^{i(\mathbf{k}+\mathbf{G}) \cdot \mathbf{r}} \quad (2.1)$$

\mathbf{G} runs over some finite subset of the reciprocal lattice, usually the vectors lying within a sphere around the origin. The Fourier representation is only suited for moderately smooth functions and cannot describe the oscillations of the wave function near the nuclei. To introduce atomic detail into the smooth function, Slater invented a simple but effective device called augmentation. Inside a muffin-tin sphere, the potential has spherical symmetry so that a solution can be written as

$$\psi_{\tau}(\mathbf{r}) = \sum_{L} C_L \frac{u_L(r)}{r} Y_L(\mathbf{r}) \quad (2.2)$$

Here the Y_L are real spherical harmonics indexed by the composite index $L=(\ell, m)$ and \mathbf{r} is taken relative to the sphere center τ . The radial functions $u_L(r)$ are obtained by integrating the radial equation numerically

$$\frac{d^2}{dr^2} u_L(r) = \left\{ \frac{\ell(\ell+1)}{r^2} + V(r) - \epsilon \right\} u_L(r) \quad (2.3)$$

Augmentation consists of replacing the function given by the Fourier series (2.1) by a linear combination (2.2) inside each sphere, whereby the amplitudes C_L are chosen so that ψ_I and ψ_{τ} match continuously on the sphere surface. For a given energy ϵ this construction gives a unique result for any function ψ_I . It is especially easy to augment plane waves due to the well-known theorem which expresses a plane wave as a linear combination of regular spherical waves [67]

$$e^{i\mathbf{k}\cdot\mathbf{r}} = 4\pi \sum_{\mathbf{L}} i^{\ell} j_{\ell}(kr) Y_{\mathbf{L}}(\mathbf{k}) Y_{\mathbf{L}}(\mathbf{r}). \quad (2.4)$$

A comparison of the values at the sphere radius gives immediately the coefficients $C_{\mathbf{L}}$.

The functions constructed in this way are used as basis for the Rayleigh-Ritz variational principle. The energy functional $E[\phi]$ is defined as

$$E[\phi] =: \frac{\int (|\nabla\phi|^2 + V|\phi|^2) d\mathbf{r}}{\int |\phi|^2 d\mathbf{r}} \quad (2.5)$$

for any once-differentiable function $\phi(\mathbf{r})$. The functional is stationary at those vectors which are the best approximations to the eigenfunctions in the space spanned by the basis. The wave function is written as a linear combination of the augmented plane waves $\phi_{\mathbf{G}}$ with undefined coefficients $A_{\mathbf{G}}$. The condition that $E[\psi]$ be stationary leads to a matrix eigenvalue equation

$$\mathbf{H}\mathbf{A} = \epsilon\mathbf{S}\mathbf{A} \quad (2.6)$$

where \mathbf{A} is the vector of all the $A_{\mathbf{G}}$. \mathbf{H} and \mathbf{S} are the Hamiltonian and overlap matrices:

$$\begin{aligned} \mathbf{H}_{\mathbf{G}\mathbf{G}'} &= \int (\nabla\phi_{\mathbf{G}}^* \cdot \nabla\phi_{\mathbf{G}'} + V\phi_{\mathbf{G}}^*\phi_{\mathbf{G}'}) d\mathbf{r} \\ \mathbf{S}_{\mathbf{G}\mathbf{G}'} &= \int \phi_{\mathbf{G}}^*\phi_{\mathbf{G}'} d\mathbf{r}. \end{aligned} \quad (2.7)$$

A complication is that the augmentation procedure and therefore both matrices depend on the energy chosen in the radial equation (2.3). An acceptable solution must have the eigenvalue of the matrix equation equal to this energy. In practice this means that the eigenvalue must be approached by repeatedly setting up and diagonalizing the matrices ('root tracing'). The details of the APW method in this form can be found in the book by Loucks [63] and in ref. [22].

At first sight it might be surprising that the APW's should make an efficient basis set. While it is true that each APW is locally a solution of the Schrödinger equation, the eigenvalues in the different parts of space are not the same. The eigenvalue associated with the interstitial is $|\mathbf{k}+\mathbf{G}|^2$ which is far above the range of interest for most functions in the basis. Also, each APW has a discontinuous derivative or kink at the sphere surfaces. However, the functions do satisfy a number of the requirements for a good Rayleigh-Ritz basis:

- (i) They are complete in both the atomic and the interstitial regions.
- (ii) They are perfectly orthogonal to all core states; this is a major advantage when compared to methods such as OPW [42].
- (iii) The matrix elements are easy to calculate.
- (iv) The functions have the qualitative behaviour which one expects of the valence wave functions: they are extended functions which have the correct strong oscillations near the nuclei.

If enough basis functions are included, the exact solutions for the muffin-tin potential are found. The method has been used very successfully for close packed systems; see ref. [22] for a review.

(C) METHODS BASED ON SPHERICAL WAVES

There are number of methods for muffin-tin potentials which can be grouped under this heading. For periodic systems, there are the LMTO (linear muffin-tin orbital [3,4]), ASW (augmented spherical wave [98]) and the KKR or Green function methods [56,57] and for molecules one has the scattered-wave description of Johnson [49,50]. The difference to the APW method described above is that spherical waves take the place of plane waves to represent the wave function in the interstitial. It will be seen later on that atom-centered spherical waves are more suitable for a number of reasons. Specifically, they make it possible to use a smaller basis. Here, emphasis is on the 'classical' KKR method whereas the more efficient methods (LMTO, ASW) are described under (E).

The outgoing spherical waves $H_L(\mathbf{r})$ are defined in eq. (3.2). These functions satisfy $\Delta H_L = -\epsilon H_L$ at all points of space except at $\mathbf{r}=0$, where they have a singularity proportional to $r^{-\ell-1}Y_L(\mathbf{r})$. Since this representation of the wave function is only required to be valid in the interstitial region, the singularities are not a problem as long as they are located inside the spheres. It is known that a complete basis for the functions satisfying the zero-potential Schrodinger equation to energy ϵ throughout the interstitial region are the functions $H_{L\nu}(\mathbf{r})=H_L(\mathbf{r}-\mathbf{R}_\nu)$, where \mathbf{R}_ν runs over the centers of all spheres and all L 's up to infinity are included. Functions centered on other points within the spheres are acceptable in principle but lead to an overcomplete set.

Proceeding along the lines described for the APW case, one first selects a finite basis set by choosing a truncation value $L_{\max,\nu}$ for each site and a trial energy ϵ . These functions are augmented with numerical radial solutions to the same energy. Again, augmentation is made easy by an expansion in regular

spherical waves (eq. 3.12). The augmented functions, denoted by $\tilde{H}_{L,v}$ are similar to the APW's in that they are continuous but have discontinuous derivatives on the sphere surfaces. The wave function is expanded in the form

$$\psi(\mathbf{r}) = \sum_{vL} A_{vL} \tilde{H}_{vL}(\mathbf{r}). \quad (2.8)$$

The condition that ψ must be smooth on the interface between the interstitial region and the atomic spheres leads to a homogeneous matrix equation

$$0 = \sum_{vL} M_{\mu K, vL} A_{vL} \quad (2.9)$$

which is solvable only if $\det M=0$. The matrix M depends on the trial energy which must be varied until the determinant vanishes. The trial energy then is equal to the eigenvalue and the coefficients determined by (2.9) give the wave function when substituted in (2.8). The general discussion above is modified only slightly for periodic systems: the outgoing spherical waves $H_L(\mathbf{r})$ are replaced by Bloch sums over the lattice

$$\mathcal{H}_L(\mathbf{k}, \mathbf{r}) = \sum_{\mathbf{R}} e^{i\mathbf{k}\cdot\mathbf{R}} H_L(\mathbf{r}-\mathbf{R})$$

and the basis for the Bloch solution $\psi(\mathbf{k}, \mathbf{r})$ consists of these functions, centered on all sites in the unit cell and augmented inside all atomic spheres. Augmentation, the set-up of the matrix, and the search for the eigenvalue are done exactly as above.

In fact, the approach described in this part was first developed for periodic systems (Korringa, Kohn and Rostoker [56,57]). For close-packed crystalline metals, the method (called KKR) has been very successful. Later, the scheme was re-formulated for molecules [49,50] but for these it produced quite wrong results [18]. For example, minimalization of the total energy predicted a straight water molecule [16]. These errors arise because the muffin-tin approximation is inadequate for molecules and not because of errors made when solving the Schrödinger equation. The presentation in this part departs from the historical order to emphasize this point: the KKR approach is in principle applicable to any kind of system, but because it needs a spatially constant interstitial potential, a straightforward application is only possible for close-packed metals in practice.

(D) COMPARISON OF PLANE WAVE AND SPHERICAL WAVE APPROACHES

From the preceding, it can be seen that the augmented plane wave and spherical-wave method are in many ways very similar. The distinguishing feature is the seemingly superficial difference in the choice of the interstitial basis functions. However, experience has shown that the plane wave basis must be chosen larger than the spherical-wave basis to attain the same precision. The following discussion tries to isolate the factors determining the basis size in each case.

For a *plane wave basis*, the important factor is the shortest wavelength which is needed to describe the variation of the interstitial function. This defines the cutoff radius for the reciprocal vectors to be included. A moderate amount of variation quickly leads to large numbers of plane waves. A sign that something inefficient is being done is that the kinetic energy $|\mathbf{k}+\mathbf{G}|^2$ for most of the plane waves is much higher than the energy of the eigenfunction. The high kinetic energies are the consequence of using functions which are analytic over the whole cell whereas this behaviour is only required for the interstitial.

For a *spherical-wave basis*, the logic goes the other way. First the kinetic energy of the interstitial wave function is prescribed to lie in the range of interest. Unless this happens to be a free electron energy there is no solution of the free particle Schrödinger equation which is regular over all of space. Therefore there must be a singularity somewhere and to get a valid solution for the interstitial this must be put inside one of the spheres. Thus the suitable spherical waves are classified by specifying the sphere which contains the singularity and the type of singularity. The latter can be specified using angular momentum. The next question is, which of all the possible degrees of freedom must be included for a good basis. The answer is given by elementary scattering theory [66]. There, one tries to match an incoming wave (i.e. a solid Bessel function) to a solution for the potential inside the sphere and finds that this is only possible if certain amounts of outgoing Hankel functions are added. For the higher angular momenta, the scattering phase shifts go to zero which means that the unadulterated incoming Bessel functions alone are sufficient. Thus, it can be concluded that a certain outgoing spherical wave can be left out of the basis if the atomic potential at the wave's center does not scatter at that angular momentum. In this way exactly the necessary degrees of freedom are included in the basis. Even for the case that more than one interstitial energy is used (see part E), the resulting set is smaller than a plane wave basis. To express this differently, assume that the wave function is known to have an eigenvalue ϵ which is not a free-electron eigenvalue. Then there must be an expansion of the function in

the atom-centered singular spherical waves for the same energy ϵ . Their singularities are noticeable as atom-oriented behaviour outside the spheres. So in effect the plane wave basis must build up a representation of the spherical waves by tedious summation.

By considering the scattering at all atomic sites simultaneously, one quickly comes to the useful and elegant multiple-scattering description of the spherical-wave methods [49,62]. For some selected atom, the spherical waves centered at all other sites add up to a total incoming wave. To match the interstitial function to the solution inside the sphere, some Hankel terms at the site must be added for all those angular momenta with non-zero phase shift. These outgoing waves contribute in turn to the incoming waves at the other atoms. An eigenstate of the system as a non-trivial stationary state must be 'self-consistent' at all sites, the ratios of outgoing to incoming waves must be compatible with the phase shifts. This is of course just another way of stating that the interstitial wave function must match smoothly to all atomic wave functions. However, the multiple scattering viewpoint is more appealing to the intuition as well as a useful starting point for problems such as impurities [104] or disorder [23,30].

All together, the following advantages of the spherical-wave approach can be seen when compared to the plane wave basis

- (i) Because of the smaller basis, it is more *efficient*
- (ii) It is in principle applicable not only to periodic systems but to any kind of structure, that is, it is *versatile*
- (iii) The multiple scattering formulation is *intuitive* and leads to useful attacks on complicated problems

On the other hand, there is one disadvantage in the plane wave basis it is straightforward to go beyond a flat interstitial potential [51,7,100]. For the spherical waves there is no satisfactory equivalent, even simple perturbation theory leads to difficult integrals. Thus an application of the latter method is mainly restricted to system for which the muffin-tin potential is an adequate approximation. These are the close-packed periodic systems for which only the first advantage is of any importance. Still, the concept of scattering between atomic sites should make sense even if there is a non-uniform 'medium' between the atoms. This will be discussed further in chapter 3.

(E) LINEARIZED VERSIONS OF APW AND KKR

Both the methods presented work by approaching each eigenstate iteratively. This makes it necessary to set up and diagonalize the matrices many times before the energy bands for a single \mathbf{k} -point are mapped out. Later, versions of the methods were developed which avoid this time-consuming root-tracing without reducing precision. In the process of iterating towards the eigenvalue, one is in fact adjusting the energies in the different parts of space with the aim of eliminating the kinks at the interfaces. Therefore it makes sense to start from a set of smooth basis functions. This is done by augmenting with two linearly independent radial functions for each angular momentum in place of one. The extra degree of freedom makes it possible to match the slope as well as the value. A frequently used scheme is to use the energy derivatives of the radial solutions (2.3) as the second function set. This was introduced and discussed in detail by Andersen [4], see also ref. [53]. For the plane wave case, the resulting method is called linearized APW or LAPW. In this basis set, the matrix eigenvalue problem (2.6) must be diagonalized only once per \mathbf{k} -point to give the proper eigenstates in the relevant part of the bands. The exact choice of the energy defining the functions inside the spheres is uncritical as long as the radial function has the proper number of nodes for the valence state and the boundary conditions are somewhere between bonding and antibonding.

The KKR method can be linearized in a similar way. However, there is a difference in that the interstitial function also depends on the trial energy. The energy dependence for both parts must be linearized. One possible way is to include spherical waves for two different interstitial energies ϵ_1, ϵ_2 in the basis. These functions are augmented to make smooth functions as for LAPW, the (twice as large) matrices are set up and diagonalized. The resulting eigenvalues are essentially the same as those of the full KKR method.

Some further approximations lead to the very efficient linear muffin-tin orbital (LMTO) method [4]. When the atomic spheres are expanded until the interstitial volume reduces to zero (whatever that means exactly), it turns out that only *one* basis function per site and angular momentum already gives good results. The eigenvalues are more or less independent of the single interstitial energy. A double basis would lead to an almost singular overlap matrix. The LMTO method of Anderson simply sets the kinetic energy of the interstitial wave function equal to zero. The augmented spherical wave (ASW) method [98] was devised as an extension of the renormalized-atom description of solids [28] and is similar to LMTO in practice. It considers the interstitial energy as a parameter controlling the localization of the trial orbitals. Both methods are

very fast and have made it possible to calculate systems with large unit cells [31,58,59,86] These accelerated methods also have the advantage of simplifying the way of thinking about the band structure problem The Wigner-Seitz cell has been approximated by a sphere of equal volume and the task of the interstitial functions is to prescribe k -dependent boundary conditions at the surface In this sense one is considering an extension of the Wigner-Seitz method [96], whereby the spherical approximation to the cell makes it easier to formulate the boundary conditions One also gains a clean separation of the inter- and intra-atomic parts of the problem The potential inside a given sphere can be characterized by a few numbers which in effect parametrize the phase shifts Andersen has used this reduction of the input information to define 'canonical bands' which describe the bands of simple metals in a compact way Since the crystal is described as a collection of interacting atomic spheres, effects such as bonding can be analyzed in terms of atoms responding to changes in their environment [68], similar to Miedema's theory [70] Finally, it is satisfying to work with a 'minimal basis' of one function per site and angular momentum These advantages are offset to some extent by the fact that, due to the overlapping spheres, one sometimes does not know exactly what one is calculating

CHAPTER 3

Generalization of Multiple Scattering Methods to Non-Uniform Interstitial Potentials

From the discussion of chapter 2, it was concluded that for muffin-tin potentials, the atom-centered, KKR-like methods are superior to plane wave methods in several important respects. The extension to non-muffin-tin potentials, however, is trivial for the latter but quite involved for the former. A straightforward perturbative approach is possible but the evaluation of the perturbation matrix element is difficult for the atom-centered basis functions [77,34]. In this chapter, a different way to extend multipole scattering to general potentials is presented. Basically, the aim is to solve the Schrodinger equation exactly in the interstitial region.

The first section collects some formal properties and formulae needed here and in chapter 4. In section 3.2 the atom-centered functions for the general potential case are introduced ('multipole Green functions'). Finally, section 3.3 shows how the functions can be calculated in practice.

3.1 Formal properties of solid Hankel and Bessel functions

(A) DEFINING EQUATIONS

The names 'solid Hankel' and 'solid Bessel' functions will be used to denote special solutions of Helmholtz's equation in three dimensions

$$(\Delta + \epsilon)\phi(\mathbf{r}) = 0 \quad (3.1)$$

where ϵ is any real number. This is of course just the Schrodinger equation for zero potential. For reasons which will become clear later on, it is useful to define the functions with multiplicative factors in the following way

$$\left. \begin{aligned} H_L &= i^\ell k^{\ell+1} n_\ell(kr) Y_L(\mathbf{r}) \\ J_L &= i^\ell k^{-\ell} j_\ell(kr) Y_L(\mathbf{r}) \end{aligned} \right\} \text{for } k^2 = \epsilon > 0 \quad (3.2a)$$

$$\left. \begin{aligned} H_L &= r^{\ell(\kappa)^{\ell+1}} h_{\ell}(\kappa r) Y_L(\mathbf{r}) \\ J_L &= r^{\ell(\kappa)^{-\ell}} J_{\ell}(\kappa r) Y_L(\mathbf{r}) \end{aligned} \right\} \text{for } -\kappa^2 = \epsilon < 0 \quad (3.2b)$$

The functions $n_{\ell, j_{\ell}}, h_{\ell} (= h_{\ell}^+)$ are defined as in Messiah [67], Appendix B6. $Y_L(\mathbf{r})$ is a real spherical harmonic with the composite index $L = (\ell, m_{\ell})$. Each H_L and J_L is a function of both \mathbf{r} and the energy ϵ . The energy is considered as a parameter and will usually be suppressed in the notation. Both sets of functions are important in KKR or multiple-scattering methods.

The 'solid Hankel functions' $H_L(\mathbf{r})$ are singular at $\mathbf{r} = 0$. For any scattering potential located at the origin, the outgoing scattered wave is a linear combination of the H_L .

The 'solid Bessel functions' $J_L(\mathbf{r})$ have no singularities and are analytic for all \mathbf{r} . They can be used to expand a given solution of the Helmholtz equation in a sphere around the origin, provided that there are no singularities inside the sphere. Specifically, expansion theorems in J_L 's exist for plane waves $e^{i\mathbf{k} \cdot \mathbf{r}}$ with $\epsilon = k^2$ (valid throughout all space) and for functions $H_L(\mathbf{r}-\mathbf{R})$ (valid in the sphere of radius R).

The leading terms of the functions for $r \rightarrow 0$ are

$$\begin{aligned} H_L &\approx r^{\ell} \frac{(2\ell+1)!!}{2^{\ell+1}} r^{-\ell-1} Y_L(\mathbf{r}) \\ J_L &\approx r^{\ell} \frac{1}{(2\ell+1)!!} r^{\ell} Y_L(\mathbf{r}) \end{aligned} \quad (3.3)$$

These expressions also give H_L and J_L exactly for the case $\epsilon = 0$. The leading term of J_L is proportional to the spherical harmonic polynomial $y_L(\mathbf{r}) = r^{\ell} Y_L(\mathbf{r})$ which satisfies $\Delta y_L = 0$.

The singular functions H_L are seen as outgoing spherical waves while the functions J_L can be used to expand any incoming wave. This is the starting point for conventional description of scattering (see e.g. Merzbacher [66]). As described in chapter 2, the functions H_L are central to multiple scattering theory. Later on, the H_L 's will be generalized to a non-flat interstitial potential, which means that the Helmholtz equation (3.1) will be replaced by the Schrodinger equation. The potential used in this step will not have spherical symmetry so that the solutions of the Schrodinger equation will be a combination of different angular momentum components. Nevertheless, one expects that scattering can still be classified by angular momentum. In this context it is useful to combine equations (3.3) and (3.1) (which are both necessary to define $H_L(\epsilon, \mathbf{r})$ uniquely) into one differential equation. Any linear combination of the

functions $H_L(\epsilon, r)$ satisfies the Helmholtz equation (3.1) in all points except $r=0$. To eliminate the arbitrariness, the zero on the right-hand side, is replaced by a distribution concentrated at $r=0$ and the equation is required to be valid there also. For the $\ell=0$ case, an expression of this type follows from the well-known Green function for the zero potential. One has

$$H_0(r) = \begin{cases} \frac{\cos kr}{r} Y_0 & \epsilon > 0 \\ \frac{e^{-kr}}{r} Y_0 & \epsilon < 0 \end{cases} \quad (3.4)$$

so that [67]:

$$(\Delta + \epsilon)H_0(r) = -4\pi Y_0 \delta(r).$$

To find a similar expression, valid for general L , one multiplies $(\Delta + \epsilon)H_L$ by an arbitrary testfunction ϕ , integrates over a sphere S_R of radius R and then takes the limit for $R \rightarrow 0$:

$$I = \lim_{R \rightarrow 0} \int_{S_R} \phi(\Delta + \epsilon)H_L dr. \quad (3.5)$$

The testfunction is expanded in a Taylor series which can be rewritten as

$$\phi(r) = \sum_K \sum_{m=0}^{\infty} C_{Km} r^{2m} y_K(r). \quad (3.6)$$

The angular integration makes I independent of all C_{Kn} with $K \neq L$. By taking the leading term of H_L , one sees that $\int r^{2m} y_L H_L dr$ is proportional to R^{2m+2} for small R and consequently $\epsilon \int \phi H_L dr$ gives zero in the limit $R \rightarrow 0$. To get the contribution from the ΔH_L -part, one transforms to a surface integral:

$$\begin{aligned} \int_{S_R} y_L \Delta H_L dr &= \int_{S_R} [\nabla \cdot [y_L \nabla H_L - H_L \nabla y_L] dr \\ &= \oint_{\partial S_R} [y_L \nabla H_L - H_L \nabla y_L] \cdot da. \end{aligned} \quad (3.7)$$

Using (3.3), this evaluates to $-i^\ell (2\ell + 1)!!$ for $R \rightarrow 0$. For a function $r^{2m} y_L$ in place of y_L , a higher power of R comes into the integral, giving zero in the limit. The final result is

$$\lim_{R \rightarrow 0} \int_{S_R} r^{2m} y_K(\mathbf{r})(\Delta + \epsilon)H_L(\mathbf{r})d\mathbf{r} = -i^\ell(2\ell + 1)!! \delta_{m0} \delta_{KL}. \quad (3.8)$$

Thus the distribution we are looking for has the property of picking out the coefficient C_{L0} in the expansion (3.6). This is the special case $n=0$ of equation (A24) of Appendix A from which it follows that

$$(\Delta + \epsilon)H_L(\mathbf{r}) = -4\pi D_L(\mathbf{r}). \quad (3.9)$$

As described in Appendix A, the distribution D_L is derived from the δ -function by means of the very useful differential operator $\mathcal{Y}_L(-i\nabla)$:

$$D_L(\mathbf{r}) = \mathcal{Y}_L(-i\nabla)\delta(\mathbf{r}) \quad (3.10)$$

There are no problems of a subtle nature in the definition of D_L : since $\mathcal{Y}_L(\mathbf{r})$ is a polynomial in x, y, z , the operator $\mathcal{Y}_L(-i\nabla)$ is defined by substituting $-i\partial/\partial x$ for x etc. Thus D_L is a linear combination of ℓ -th order derivatives of the δ -function. Equation (3.10) is convenient shorthand for the usual construction of dipoles or higher multipoles out of δ -functions with infinitesimal displacements.

The inhomogeneous equation (3.9) defines H_L uniquely except for a possible additive solution of the homogeneous equation. This last arbitrariness is eliminated by prescribing boundary conditions for the functions. At the same time, the choice of boundary conditions selects the system to be considered. The functions H_L result if regularity at infinity is demanded. Alternatively, one can consider the unit cell of a periodic system and prescribe Bloch boundary conditions on the cell surface. Then the solutions of (3.9) are Bloch-sums of the solid Hankel functions. In each case the solutions can be interpreted as the response of the system under consideration to a monopole, dipole, quadrupole... disturbance. This is similar to the interpretation of the usual free-particle Green function, which is just the $\ell=0$ case of (3.9). The solutions of an equation such as eq. (3.9) will be denoted as 'multipole Green functions'. Of course, the disturbance can be put anywhere in space by taking $-4\pi D_L(\mathbf{r}-\mathbf{R})$ as the inhomogeneous term. These statements become more important in view of the fact that eq. (3.9) has an obvious generalization to a non-zero, varying potential.

(B) GENERATION OF THE H_L AND FOURIER TRANSFORMS

Next, note that the functions H_L and J_L can be derived from the first function in each family as was the case with the $D_L(\mathbf{r})$:

$$\begin{aligned} H_L &= \mathcal{Y}_L(-i\nabla)h(r) \\ J_L &= \epsilon^{-\epsilon} \mathcal{Y}_L(-i\nabla)j(r) \end{aligned} \quad (3.11a)$$

with

$$\left. \begin{aligned} h(r) &= \frac{\cos(kr)}{r} \\ j(r) &= \frac{\sin(kr)}{r} \end{aligned} \right\} \epsilon > 0 \quad (3.11b)$$

$$\left. \begin{aligned} h(r) &= \frac{e^{-\kappa r}}{r} \\ j(r) &= \frac{\sinh(\kappa r)}{r} \end{aligned} \right\} \epsilon < 0 \quad (3.11c)$$

and k, κ defined as in eq (3.2). This type of ladder operator was first used by Kasterin [52] in 1898⁽¹⁾ and later by Nozawa [75] and Segall [82]. Equation (3.11) is valid at all points including $r=0$, meaning that neither side has a distribution part (see Appendix A). The energy dependence enters only over the functions $h(r)$ and $j(r)$. Also $\mathcal{Y}_L(-i\nabla)$ is homogeneous in space, in the sense that the operator applied to a shifted h or j will generate the corresponding shifted function. These facts make it possible to derive many properties of the function families very easily.

- (i) *Differential equation* To recover the equation (3.9), apply $\mathcal{Y}_L(-i\nabla)$ to both sides of the Green function equation $(\Delta + \epsilon)h(r) = -4\pi\delta$. Since the partial derivatives all commute, one can exchange the order of the operators and recover equation (3.9) immediately.
- (ii) *The recursion relations* for the Hankel and Bessel functions follow immediately from the general relations in Appendix A.
- (iii) *Expansion theorem* The aim is to expand $H_L(\mathbf{r}-\mathbf{R})$ as a linear combination of the $J_L(\mathbf{r})$. A theorem of this type is known for the zero-potential Green function

$$h_0(\mathbf{r}-\mathbf{R}) = 4\pi \sum_L H_L(\mathbf{R}) J_L(\mathbf{r})$$

This is valid for $r < R$ and for any energy ϵ (which is the same for all functions in the equation). Substitute $\epsilon^{-\epsilon} \mathcal{Y}_L(-i\nabla)j$ for J_L and apply $\mathcal{Y}_K(-i\nabla)$ on both sides, giving

$$H_{\mathbf{K}}(\mathbf{r}-\mathbf{R}) = 4\pi \sum_{\mathbf{L}} H_{\mathbf{L}}(\mathbf{R}) \epsilon^{-\ell} y_{\mathbf{K}}(-i\nabla) y_{\mathbf{L}}(-i\nabla) j(\mathbf{r}).$$

As usual, the product of two spherical harmonics is rewritten using Clebsch-Gordon coefficients:

$$\begin{aligned} Y_{\mathbf{K}}(\mathbf{r}) Y_{\mathbf{L}}(\mathbf{r}) &= \sum_{\mathbf{M}} C_{\mathbf{KLM}} Y_{\mathbf{M}}(\mathbf{r}) \\ \Rightarrow y_{\mathbf{K}}(\mathbf{r}) y_{\mathbf{L}}(\mathbf{r}) &= \sum_{\mathbf{M}} C_{\mathbf{KLM}} r^{k+\ell-m} y_{\mathbf{M}}(\mathbf{r}) \\ \Rightarrow y_{\mathbf{K}}(-i\nabla) y_{\mathbf{L}}(-i\nabla) &= \sum_{\mathbf{M}} C_{\mathbf{KLM}} (-\Delta)^{(k+\ell-m)/2} y_{\mathbf{M}}(-i\nabla). \end{aligned}$$

The last step used that $k+\ell-m$ is an even positive integer if $C_{\mathbf{KLM}} \neq 0$. The final expansion theorem then is:

$$\begin{aligned} H_{\mathbf{K}}(\mathbf{r}-\mathbf{R}) &= \sum_{\mathbf{M}} B_{\mathbf{KM}}(\mathbf{R}) J_{\mathbf{M}}(\mathbf{r}) \quad (3.12) \\ B_{\mathbf{KM}}(\mathbf{R}) &= 4\pi \sum_{\mathbf{L}} C_{\mathbf{KLM}} \epsilon^{(k+m-\ell)/2} H_{\mathbf{L}}(\mathbf{R}). \end{aligned}$$

Theorems of this type have been derived in different ways [19,75], for example from group theory by using the fact that the solid Hankel and Bessel functions are related to matrix elements of representations of the Euclidean group in three dimensions [89].

- (iv) *Fourier transforms*: These are especially simple. The Fourier transforms of $-i\nabla$ of a function $f(\mathbf{r})$ is the transform $\hat{f}(\mathbf{q})$ multiplied by \mathbf{q} . Thus one has the following relationship between the Fourier transforms of f and of $F_{\mathbf{L}} = y_{\mathbf{L}}(-i\nabla)f$:

$$\begin{aligned} f(\mathbf{r}) &\mapsto \hat{f}(\mathbf{q}) \\ F_{\mathbf{L}}(\mathbf{r}) &\mapsto y_{\mathbf{L}}(\mathbf{q}) \hat{f}(\mathbf{q}). \end{aligned} \quad (3.13)$$

For the solid Hankel functions, this gives:

$$\hat{h}(\mathbf{q}) = \frac{4\pi}{\epsilon - q^2} \Rightarrow \hat{H}_{\mathbf{L}}(\mathbf{q}) = \frac{-4\pi y_{\mathbf{L}}(\mathbf{q})}{\epsilon - q^2}. \quad (3.14)$$

The expression for $\hat{H}_{\mathbf{L}}(\mathbf{q})$ also can be derived by solving the differential equation (3.9) in Fourier space:

$$(-q^2 + \epsilon) \hat{H}_{\mathbf{L}}(\mathbf{q}) = -4\pi \hat{D}_{\mathbf{L}}(\mathbf{q}).$$

Since the Fourier transform of the δ -function is the constant $\hat{\delta}(\mathbf{q})=1$, it follows from (3.13) that $\hat{D}_{\mathbf{L}}(\mathbf{q})=Y_{\mathbf{L}}(\mathbf{q})$, giving $\hat{H}_{\mathbf{L}}(\mathbf{q})$ as in eq. (3.14).

When solving the differential equation in Fourier space, one has the freedom of adding a homogeneous solution. In this context the choice of the boundary conditions defining the function $H_L(\mathbf{r})$ uniquely is equivalent to deciding on a certain way of integrating around the singularities of (3.14) when evaluating the back transform at positive energies. At negative energies, the exclusion of the terms proportional to $e^{x\tau}$ is implicit in the Fourier transform.

(C) BLOCH-HANKEL FUNCTIONS AND STRUCTURE CONSTANTS

A large part of the following will deal with periodic systems, i.e., crystals. In that case one considers functions defined on the unit cell (or alternatively the Wigner-Seitz cell). Bloch boundary conditions are prescribed on the surface of the cell

$$\begin{aligned}\psi_2 &= +e^{i\mathbf{k}\cdot\boldsymbol{\tau}}\psi_1 \\ \frac{\partial\psi_2}{\partial\mathbf{n}} &= -e^{i\mathbf{k}\cdot\boldsymbol{\tau}}\frac{\partial\psi_1}{\partial\mathbf{n}}\end{aligned}\tag{3.15}$$

where ψ_1 and ψ_2 are the function values at equivalent points on opposite faces, $\boldsymbol{\tau}$ is the connecting vector between the points and \mathbf{n} is the outward normal. The set of functions satisfying eq. (3.15) is a vector space and the aim is to find solutions of the Schrodinger equation in this space. The central functions of KKR theory then are the solutions of

$$(\Delta + \epsilon)\phi_{L\boldsymbol{\tau}}(\mathbf{r}) = -4\pi D_L(\mathbf{r} - \boldsymbol{\tau})\tag{3.16}$$

in the space, with $\boldsymbol{\tau}$ running over the positions of the atoms in the cell. As before, $\phi_{L\boldsymbol{\tau}}$ describes the propagation of an 2^ℓ -pole disturbance located at $\boldsymbol{\tau}$ through the cell. $\phi_{L\boldsymbol{\tau}}$ is a Bloch sum of the Hankel functions H_L over the lattice

$$\begin{aligned}\phi_{L\boldsymbol{\tau}}(\mathbf{r}) &= \mathcal{H}_L(\mathbf{k}, \mathbf{r} - \boldsymbol{\tau}) \\ \mathcal{H}_L(\mathbf{k}, \mathbf{r}) &= \sum_{\mathbf{R}} e^{i\mathbf{k}\cdot\mathbf{R}} H_L(\mathbf{r} - \mathbf{R})\end{aligned}\tag{3.17}$$

This way of constructing $\phi_{L\boldsymbol{\tau}}$ is similar to the use of a lattice of mirror charges in electrostatics. H_L satisfies the differential equation (3.16) for $\boldsymbol{\tau}=0$ and the boundary conditions (3.15).

In many ways, the Bloch-Hankel functions \mathcal{H}_L are very similar to the H_L 's

(i) They can be generated by applying $\mathcal{Y}_L(-i\nabla)$ to

$$\mathcal{H}(\mathbf{k}, \mathbf{r}) = \sum_{\mathbf{R}} h(\mathbf{r}-\mathbf{R}) e^{i\mathbf{k}\cdot\mathbf{R}}.$$

(ii) From the Fourier transform eq. (3.14) it follows that

$$\mathcal{H}_L(\mathbf{k}, \mathbf{r}) = \frac{1}{\Omega} \sum_{\mathbf{G}} \frac{-4\pi\mathcal{Y}_L(\mathbf{k}+\mathbf{G})}{\varepsilon-(\mathbf{k}+\mathbf{G})^2} e^{i(\mathbf{k}+\mathbf{G})\cdot\mathbf{r}} \quad (3.18)$$

where Ω is the volume of the unit cell and the \mathbf{G} runs over the reciprocal lattice.

(iii) By summing the expansion theorem (3.12) over the lattice, one obtains

$$\mathcal{H}_K(\mathbf{r}-\boldsymbol{\tau}) = \sum_{\mathbf{M}} \mathcal{B}_{KM}(\boldsymbol{\tau}) J_{\mathbf{M}}(\mathbf{r}) \quad \text{for } |\mathbf{r}| < |\boldsymbol{\tau}|$$

$$\text{with } \mathcal{B}_{KM}(\boldsymbol{\tau}) = 4\pi \sum_{\mathbf{L}} C_{KLM} \varepsilon^{(\mathbf{k}+\mathbf{m}-\boldsymbol{\ell})/2} \mathcal{H}_L(\boldsymbol{\tau}). \quad (3.19a)$$

The $\mathcal{B}_{KM}(\boldsymbol{\tau})$ are the (site off-diagonal) structure constants of the KKR method for 'complex' lattices (Segall [82]). Due to the tails coming in from the Hankel functions centered at lattice sites different from zero, the \mathcal{H}_L are not of pure L-character. Instead, one has the expansion

$$\mathcal{H}_K(\mathbf{r}) = H_K(\mathbf{r}) + \sum_{\mathbf{M}} \mathcal{B}_{KM}(0) J_{\mathbf{M}}(\mathbf{r}). \quad (3.19b)$$

The expansion coefficients $\mathcal{B}_{KM}(0)$ are similar (but not equal) to the $\mathcal{B}_{KM}(\boldsymbol{\tau})$ for $\boldsymbol{\tau} \rightarrow 0$ and are called the (site diagonal) structure constants (see eq A36). The calculation of $\mathcal{H}_L(\mathbf{r})$ or \mathcal{B}_{KM} in practice is not trivial and is usually done using the Ewald method [27,36] (see Appendix A).

From eq. (3.18), it is apparent that \mathcal{H}_L diverges at the discrete energies given by $\varepsilon = |\mathbf{k}+\mathbf{G}|^2$. At these energies the corresponding plane wave is a solution of the homogeneous version of eq (3.16) and thus an eigenstate of the Schrodinger equation. The singularity in \mathcal{H}_L follows from the divergence of the Green function at eigenenergies or, equivalently, from the fact that $\Delta + \varepsilon$ is then not invertible. The problems connected with these 'free electron singularities' are discussed in section 4.1(D).

For the special case $\mathbf{k}=0$, the $\mathcal{H}_L(\mathbf{r})$ are periodic, atom-centered functions which are useful for representing the interstitial charge density and potential (see section 4.2(B),(C)).

(D) SMOOTHED HANKEL FUNCTIONS

The Gaussian $g(r) = (a^2/\pi)^{3/2} e^{-a^2 r^2}$ is normalized to one in three dimensions and approaches the δ function for $a \rightarrow \infty$. Application of $\mathcal{Y}_L(-i\nabla)$ to g leads to a set of anisotropic Gaussians which converge to the multipole distributions D_L in equation (3 10) and which are given explicitly by

$$G_L(\mathbf{r}) = (a^2/\pi)^{3/2} (2a^2)^\ell e^{-a^2 r^2} \mathcal{Y}_L(\mathbf{r})$$

It is interesting to consider the solutions of (3 9) which result if D_L on the right-hand side is replaced by the Gaussian G_L . In effect, this means that the δ -function is broadened to a width of about $1/a$. For convenience, it is useful to include a factor $e^{\epsilon/4a^2}$ and define the functions F_L by

$$(\Delta + \epsilon)F_L = -4\pi e^{\epsilon/4a^2} G_L \quad (3 20)$$

The F_L can be found by solving the equation $(\Delta + \epsilon)f = -4\pi e^{\epsilon/4a^2} g$ and then applying $\mathcal{Y}_L(-i\nabla)$ to f . Both g and f have spherical symmetry, so that one solves the radial differential equation

$$\frac{1}{r} \frac{\partial^2}{\partial r^2} (rf) + \epsilon f = -4\pi e^{\epsilon/4a^2} g$$

The solution can be written using the complex error function

$$f = \frac{1}{2r} (u_+ - u_-)$$

$$u_{\pm}(r) = \begin{cases} e^{\pm ikr} \operatorname{erf}\left(\frac{ik}{2a} \pm ar\right) & \text{for } \epsilon = k^2 > 0 \\ e^{\mp \kappa r} \left[1 - \operatorname{erf}\left(\frac{\kappa}{2a} \mp ar\right)\right] & \text{for } \epsilon = -\kappa^2 < 0 \end{cases} \quad (3 21)$$

$f(r)$ is analytic at all points including $r=0$ and is equal to $h(r)$ of eq (3 11) for $a^2 r^2 \gg 1$. Thus, the function $F_L = \mathcal{Y}_L(-i\nabla)f$ is the Hankel function H_L with the singularity removed in a very smooth way. The constant a determines how far out one must go for F_L and H_L to be equal. One can alternatively solve (3 20) in the Fourier representation and finds that the Fourier transform of F_L is

$$\hat{F}_L(\mathbf{q}) = -\frac{4\pi e^{(\epsilon - q^2)/4a^2}}{\epsilon - q^2} \mathcal{Y}_L(\mathbf{q}) \quad (3 22)$$

When compared to $\hat{H}_L(\mathbf{q})$, the components for large q are cut off by the

exponential factor By using the explicit expression for (3 21) and the recursion relations in Appendix A, the F_L are easy to calculate The functions are used in the Ewald method for lattice sums and in section 4 2(D)

3.2 Generalization to varying interstitial potential

(A) MULTIPOLE GREEN FUNCTIONS

Multiple scattering theory for a muffin-tin potential is a description in terms of scatterers embedded in a homogeneous medium Waves are emitted by all atoms and the condition for an eigenstate is that the balance of the total incoming and outgoing waves is compatible with the atomic scattering phase shifts at all sites simultaneously To go beyond the muffin-tin potential, the medium will be taken as inhomogeneous It will be described by a smooth but non-uniform potential $V_1(\mathbf{r})$, which is required to be equal to the true potential in the interstitial region only Inside the atomic spheres, it is taken as a smooth interpolation (see Fig 3 1) Analogous to the muffin-tin case, it is now necessary to describe the propagation of waves through the medium from one atomic site to another For the flat interstitial potential this was done via the functions H_L , which were defined by equation (3 9) To include the effect of the medium, one instead uses the similar equation

$$[\Delta - V_1(\mathbf{r}) + \varepsilon]\phi_{L\tau}(\mathbf{r}) = -4\pi D_L(\mathbf{r} - \boldsymbol{\tau}) \quad (3 23)$$

Here $\boldsymbol{\tau}$ is the position of an atom As before, $D_L(\mathbf{r} - \mathbf{R})$ is a multipole of order ℓ located at $\boldsymbol{\tau}$ and the function $\phi_{L\tau}$ gives the response of the system to this disturbance, aptly named 'multipole Green function' $\phi_{L\tau}$ is an outgoing wave which can result from a scattering process by the atomic potential at $\boldsymbol{\tau}$ Thus the $\phi_{L\tau}$ must be determined in the energy range of interest, for all atomic positions, and for all L up to some $L_{\max \tau}$ (the highest L at which scattering from this site is expected) Clearly at least this amount of information is needed about the interstitial potential in order to calculate the relevant eigenstates

The problems when calculating the multipole Green functions are discussed further on Once the functions are known, however, they have the same *advantages* over other choices of basis as the Hankel functions did for flat interstitial potential These are

- (i) The number of basis functions needed is small. By properly choosing the $L_{\max, \tau}$ and the energy range, exactly the right degrees of freedom are included. (Plane waves, for example, do not ‘know’ about the positions of the atoms and involve high kinetic energies. This inefficiency makes a large basis necessary).
- (ii) A calculated eigenstate is a linear combination of solutions of the Schrödinger equation in the interstitial region and therefore is known to be a solution. (This is not true for a basis such as atom-centered Gaussians or Slater-type orbitals).
- (iii) Hamiltonian and overlap matrix elements are trivial to calculate by using equation (3.23) (see section 4.1(B)).

The advantage over the plane wave approach can also be seen in the following way: Plane waves are a useful basis mainly because anything can be expanded in them. However, since a certain amount of spatial variation is expected in the eigenstates, the number of plane waves needed quickly becomes large. Therefore, it makes more sense to first make suitable linear combinations of plane waves which are similar to the function one is looking for. Since this involves a matrix inversion and not a diagonalization, there is an overall gain in efficiency. Thus, the $\phi_{L\tau}$ are infinite sums of plane waves which solve the Schrödinger equation in the interstitial, ‘feel’ the positions of the atoms, and have an energy in proper range.

Once the functions $\phi_{L\tau}$ have been determined, the way in which waves propagate between the sites is known. This information can be put together to calculate eigenvalues and eigenstates in exactly the same way as in KKR or linearized KKR methods:

- (i) KKR: at a trial energy ϵ , one tries to find a linear combination of the $\phi_{L\tau}$ which matches smoothly onto solutions of the Schrödinger equation inside the spheres. If this is not yet possible, the energy is adjusted and the process is repeated.
- (ii) linearized KKR: The $\phi_{L\tau}$ are augmented in all spheres as described in section 2.2(E). The resulting functions are used as a Rayleigh-Ritz basis. Because the functions solve the Schrödinger equation in the interstitial, all matrix elements are easy to calculate; this is where the effort put in when calculating the $\phi_{L\tau}$ is recovered. The implementation described in chapter 4 works in this way.

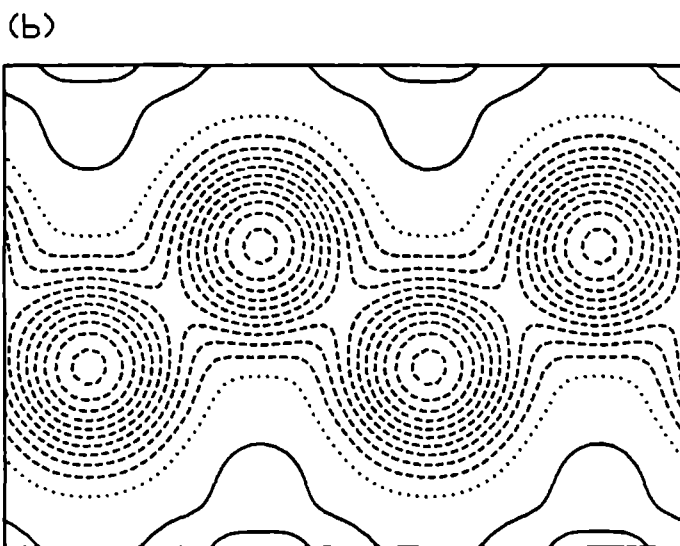
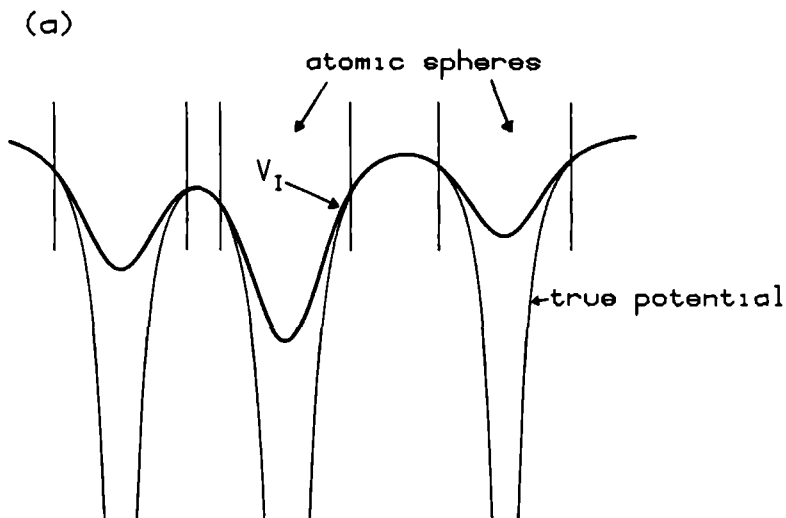


Figure 3.1. Definition of the interstitial potential $V_I(r)$ In (a) it is shown schematically that V_I equals the true potential in the interstitial but interpolates smoothly through the atomic spheres. Since V_I is well-behaved the Green function can be calculated, giving a description for the scattering between atoms embedded in the 'medium' V_I (b) shows V_I for self-consistent silicon in the (110) plane The contour interval is 0.25 Ry

At this point, a comparison with some previous schemes for generalizing multiple scattering to non-flat interstitial potentials will be made. Bross and Anthony [11] have presented a formulation of the KKR method which is suitable for a muffin-tin geometry and which uses different representations for the (arbitrary) potential in the interstitial region and in the atomic spheres. However, while it is true that their method is based on the variational principle of Kohn and Rostoker, they use plane waves to describe the interstitial wave function (see Ziman [105]). It is then not surprising that the interstitial potential enters in the form of Fourier integrals over the interstitial region, just as is the case for general-potential APW methods. Therefore their method should be seen as a step in the development towards the LAPW method rather than as a generalization of multiple scattering. Of more interest is the comparison with the proposal of Williams [99], who formulated multiple scattering for an arbitrary arrangement of *overlapping* scatterers. The consequence of the potential overlap from different sites is that inelastic scattering must be taken into account, whereas only elastic scattering is possible for a flat interstitial potential. The extra effects can be included by perturbation. Thus, the approach of Williams and the one presented in the beginning of this section are two distinct and satisfyingly complementary viewpoints of the same problem, both in the same context of multiple scattering theory. The former considers free-electron propagation in a system of overlapping scatterers, while the latter is concerned with propagation between well-separated scatterers in a non-homogeneous medium. Both approaches are suitable for potentials of general shape, but the role of the potential is quite different in the two cases.

(B) TRANSFER OF BOUNDARY CONDITIONS

Here, the KKR-like general potential approach presented above will briefly be considered from a different viewpoint. The essence is that one wants to treat some parts of space (the atomic spheres) differently than the rest (the interstitial I). The interstitial region was interpreted as a medium through which disturbances propagate from one atom to another. Alternatively, one can say that the interstitial connects together the boundary conditions on different parts of the surface ∂I . This 'transfer' of the boundary conditions depends on both the interstitial potential and the energy. To treat this in a general way, consider a potential V in an arbitrarily shaped volume Ω with surface $\partial\Omega$. For any function f given on $\partial\Omega$, there exists a unique solution ϕ of the Schrodinger equation in Ω with $\phi=f$ on $\partial\Omega$. For if two functions ϕ_1, ϕ_2 exist, then $U = \phi_1 - \phi_2$ is zero on $\partial\Omega$ and $\Delta U = (V - \epsilon)U$ inside. In the usual way this eigenvalue problem only has solutions for certain discrete energies ϵ_n . It follows that $U=0$ if ϵ is different

from all the ϵ_n , which can be assumed in general. For functions given on $\partial\Omega$ define a scalar product and assume a complete orthonormal set f_ν :

$$\langle f_\nu, f_\mu \rangle := \oint_{\partial\Omega} f_\nu^* f_\mu d^2\tau = \delta_{\nu\mu}.$$

Every f_ν defines a unique solution ϕ_ν in Ω which is equal to f_ν on $\partial\Omega$. The normal derivative (slope) of ϕ_ν must be expandable in the f_ν , so

$$\frac{\partial\phi_\nu}{\partial\mathbf{n}} = \sum_\mu f_\mu \langle \phi_\nu, \frac{\partial\phi_\nu}{\partial\mathbf{n}} \rangle =: \sum_\mu f_\mu T_{\mu\nu}.$$

The matrix $T_{\mu\nu}$ describes the operator which transforms prescribed *values* on $\partial\Omega$ into *slopes* in the following way. Any function f on $\partial\Omega$ defines a solution ϕ in Ω , equal to f on $\partial\Omega$, the value and slope of which can be expanded in the f_ν as

$$\phi = \sum_\nu \alpha_\nu f_\nu, \quad \frac{\partial\phi}{\partial\mathbf{n}} = \sum_\nu \beta_\nu f_\nu.$$

Then the connection between value and slope is given by

$$\beta_\nu = \sum_\mu T_{\nu\mu} \alpha_\mu.$$

The Wronski relation shows that $T_{\mu\nu}$ is hermitian: since all ϕ_ν solve the Schrödinger equation to the same energy, one has

$$\nabla \cdot [\phi_\nu^* \nabla \phi_\mu - \phi_\mu \nabla \phi_\nu^*] = \phi_\nu^* (V - \epsilon) \phi_\mu - \phi_\mu (V - \epsilon) \phi_\nu^* = 0$$

$$\oint_{\partial\Omega} [\phi_\nu^* \frac{\partial\phi_\mu}{\partial\mathbf{n}} - \phi_\mu \frac{\partial\phi_\nu^*}{\partial\mathbf{n}}] d^2\tau = T_{\nu\mu} - T_{\mu\nu}^* = 0.$$

In passing, note that $T_{\mu\nu}$ can be diagonalized. The column eigenvector to an eigenvalue D_i then defines a linear combination g_i of the f_ν with the property that, for all points on $\partial\Omega$,

$$\frac{\partial\psi_i}{\partial\mathbf{n}} = D_i \psi_i$$

where ψ_i is the solution which is equal to g_i on $\partial\Omega$. Thus the ratio of slope to value on the whole surface is given by one number, which neatly generalizes the concept of the logarithmic derivative for volumes of general shape.

The matrix $T_{\mu\nu}$ gives the connection between the values and slopes on all pieces of $\partial\Omega$ and this is exactly the information which is needed if solutions in different parts of space are to be matched together. In effect, the matrix gives

the result of integrating from one side of Ω to the other. The information contained in $T_{\mu\nu}$ for $\Omega=I$ is derived in the multipole Green function approach by extending the interstitial potential smoothly into the spheres to make V_I and then solving for the response to various multipoles at the sphere centers. The resulting functions solve the Schrodinger equation in the interstitial and their values on $\partial I=\partial\Omega$ span a large-enough subspace of the space of all possible value boundary conditions. Thus, for each atom there are functions which are large on the corresponding sphere and small on all the others as well as functions with different angular dependences. Note that $T_{\mu\nu}$ is well-defined even at those energies for which the multipole Green functions are singular (the eigenvalues of $-\Delta+V_I$)

In the context of trying to find a suitable treatment for the interstitial potential, it is of interest to consider the way in which $T_{\mu\nu}$ depends on the potential in Ω . A general answer is not possible but the change to linear order $\delta T_{\mu\nu}$ caused by changes δV and $\delta\epsilon$ can be derived. By taking the variation of the Schrodinger equation for ϕ_ν , the equation for $\delta\phi_\nu$ comes out to

$$\Delta\delta\phi_\nu = (V-\epsilon)\delta\phi_\nu + (\delta V-\delta\epsilon)\phi_\nu$$

Then

$$\begin{aligned} \nabla [\phi_\mu^* \nabla \delta\phi_\nu - \delta\phi_\nu \nabla \phi_\mu^*] &= \phi_\mu^* \Delta \delta\phi_\nu - \delta\phi_\nu \Delta \phi_\mu^* \\ &= \phi_\mu^* (\delta V - \delta\epsilon) \phi_\nu \end{aligned}$$

By integrating over Ω , transforming to a surface integral, and using that $\delta\phi_\nu=0$ on $\partial\Omega$, one obtains

$$\begin{aligned} \int_{\Omega} \phi_\mu^* (\delta V - \delta\epsilon) \phi_\nu d\mathbf{r} &= \oint_{\partial\Omega} \phi_\mu^* \nabla \delta\phi_\nu \cdot d\mathbf{a} \\ &= \delta \oint_{\partial\Omega} \phi_\mu^* \nabla \phi_\nu \cdot d\mathbf{a} = \delta T_{\mu\nu} \end{aligned}$$

A special case of this equation is that for $\delta V=0$,

$$\frac{\partial}{\partial\epsilon} T_{\mu\nu} = - \int_{\Omega} \phi_\mu^* \phi_\nu d\mathbf{r} = -S_{\mu\nu}$$

Thus knowledge of $T_{\mu\nu}(\epsilon)$ is sufficient to calculate the interstitial overlap integrals (for the case that the Rayleigh-Ritz method is used to solve the KKR equations)

By setting $\delta\epsilon$ to zero, one sees that the effect of a potential perturbation is given by $\delta T_{\mu\nu} = \int \phi_{\mu}^* \delta V \phi_{\nu} dr$. First of all, this suggests that when non-uniform interstitial potential terms are to be treated as a perturbation, it is better to use the perturbation integrals to correct $T_{\mu\nu}$ than to simply add terms to the Hamiltonian matrix. The work in both cases is the same but the methods are not equivalent. Second, one can estimate the effect of an error in the interstitial potential for the KKR-like approach. The main point is that $\delta T_{\mu\nu}$ will tend to average out to zero if the wavelengths of δV is shorter than that of $\phi_{\mu}^* \phi_{\nu}$. For example, this is the case for the muffin-tin approximation in close-packed systems. Due to the low kinetic energy in the interstitial region, ϕ_{ν} and ϕ_{μ} have long wavelengths there so that details of the potential are not 'seen' by the functions. For structures such as the diamond lattice, however, the interstitial region is so wide that slow variations of the interstitial potential are possible. The wavelengths of potential and wavefunctions are comparable so that the potential has a large effect on $T_{\mu\nu}$, making a muffin-tin treatment impossible.

3.3 Calculating multipole Green functions in practice

(A) SEPARATION INTO SINGULAR AND SMOOTH PART

The solution of eq (3.23) to obtain the multipole Green function is equivalent to a matrix inversion and therefore should not be too difficult. However, what is known about the character of the functions makes for some problems

- (i) The function $\phi_{L\tau}$ has a strong singularity at τ
- (ii) Further away from τ , the functions are smooth but their shape depends on details of the potential $V_I(\mathbf{r})$

A representation must be found which is able to treat both points adequately. For example, assume that one is interested in a periodic system and tries to represent $\phi_{L\tau}$ as a Fourier series (with coefficients A_G). Then eq (3.23) translates to the matrix equation

$$[\epsilon - (\mathbf{k} + \mathbf{G})^2] A_G - \sum_{\mathbf{G}'} V_{\mathbf{G} - \mathbf{G}'} A_{\mathbf{G}'} = -4\pi y_L(\mathbf{k} + \mathbf{G}) e^{-i(\mathbf{k} + \mathbf{G}) \cdot \tau} \quad (3.24)$$

The V_G are the Fourier coefficients of the smooth periodic potential $V_I(\mathbf{r})$. The plane wave Hamiltonian would have to be inverted only once, then applied successively to the different L - and τ -dependent right-hand sides. This seems to

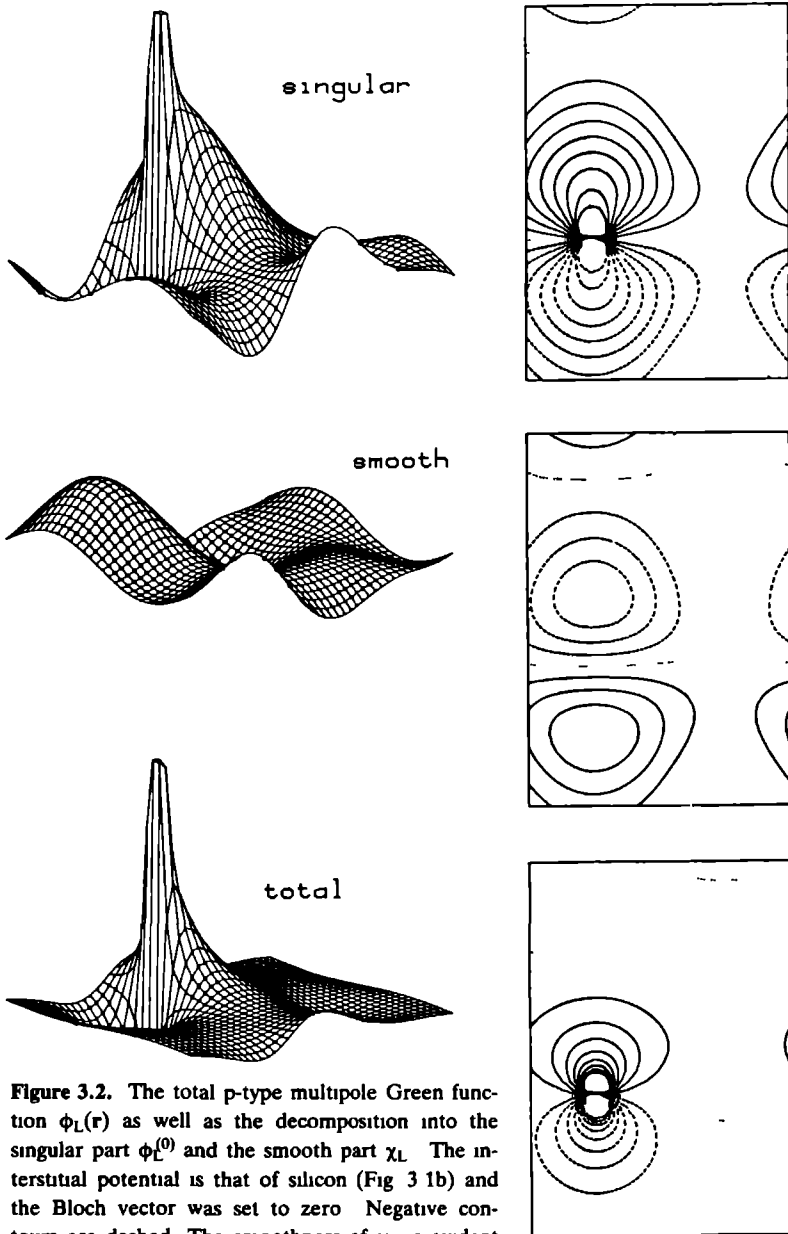


Figure 3.2. The total p-type multipole Green function $\phi_L(\mathbf{r})$ as well as the decomposition into the singular part $\phi_L^{(0)}$ and the smooth part χ_L . The interstitial potential is that of silicon (Fig 3 1b) and the Bloch vector was set to zero. Negative contours are dashed. The smoothness of χ_L is evident from the equidistance of the contours. The separation is necessary when calculating the function in practice for a numerical potential.

be an efficient scheme since V_I , being smooth, can be described by a short Fourier series. The problem lies in the right-hand side. It is a polynomial of order ℓ in $\mathbf{k}+\mathbf{G}$ from which it follows that $|A_G| \sim G^{\ell-2}$ for large $|G|$. Thus the Fourier series for $\phi_{L\tau}$ is at best conditionally convergent and of no use in practice*.

The best solution of the problem is to split off the singular part of $\phi_{L\tau}$ for separate treatment. A function $\phi_{L\tau}^{(0)}$ is constructed which has the same singular behaviour at τ as the sought-for function. Then one has $\phi_{L\tau} = \phi_{L\tau}^{(0)} + \chi$ with a remainder $\chi(\mathbf{r})$ which is smooth everywhere. Different representations are chosen for the two parts. In this approach the following steps are needed to calculate one of the functions $\phi_{L\tau}$.

- (i) Make $\phi_{L\tau}^{(0)}$ (see below).
- (ii) Calculate the residuum for the singular part:

$$R(\mathbf{r}) := (\Delta - V_I + \epsilon)\phi_{L\tau}^{(0)} + 4\pi D_L. \quad (3.25)$$

If $\phi_{L\tau}^{(0)}$ was constructed properly, R is already a smooth function of \mathbf{r} .

- (iii) Calculate χ by solving

$$(\Delta - V_I + \epsilon)\chi = -R. \quad (3.26)$$

Steps (ii) and (iii) can be done in a representation such as plane waves, smooth atom-centered functions, or as values on a mesh of points. The separation into the two parts is shown in Fig. 3.2 for a typical case.

(B) CALCULATION OF THE SINGULAR PART

In principle this is the same as solving a differential equation by power-series expansion around some point. That is, coefficients are calculated recursively and the input information is a Taylor expansion of the potential V_I around τ . Matters are made complicated because the potential couples the angular momentum components together and because the desired solution is singular. Also, the function must finally be given in a form which is usable for the rest of

* One possible solution is to smear out the singularities by using the Gaussians G_L of section 3.1(D) in place of the D_L on the right-hand side. This ultimately leads to factors $e^{-(\mathbf{k}+\mathbf{G})^2/4a^2}$ in the Fourier coefficients A_G which makes the sums absolutely convergent. But since the G_L 's must be localized inside the atomic sphere, the constant a must be chosen so large that the number of plane waves needed is still prohibitive.

the calculation. It will be seen that the best choice is a representation in solid Hankel functions and their energy derivatives.

Assume one wants to calculate $\phi_{L_0, \tau}^{(0)}$. For simplicity the indices will be suppressed and τ will be taken as zero in the following. It might be expected that for r in the neighborhood of zero the approximation $V_I(r) \approx V_I(0)$ is adequate and that a single solid Hankel function (of angular momentum L_0 and energy $\epsilon - V_I(0)$) gives the singularity. To see that this is not sufficient, consider first an expansion of the form

$$\phi = \sum_L R_L(r) Y_L(r) = \sum_{ln} A_{Ln} r^n Y_L(r) \quad (3.27)$$

with n taking positive and negative integer values. The analytic part of ϕ is the sum of the terms with $n = \ell, \ell+2, \ell+4, \dots$; all other terms make up the singular part (see Fig. 3.3). Of course, for positive values of n the singular contributions to ϕ are not infinite at zero but they still hinder a good convergence of, say, a Fourier series. The aim is that $\Delta\phi = (V_I - \epsilon)\phi$ for $r > 0$ which leads to the coupled radial equations

$$\left[\frac{1}{r^2} \frac{\partial}{\partial r} r^2 \frac{\partial}{\partial r} - \frac{\ell(\ell+1)}{r^2} \right] R_L = \sum_K W_{LK} R_K - \epsilon R_L. \quad (3.28)$$

The functions $W_{KL}(r)$ are made from the potential V_I using Clebsch-Gordan coefficients*:

$$\begin{aligned} \text{with } V_I(r) &= \sum_L V_L(r) Y_L(r) \\ W_{KL}(r) &= \sum_M C_{KLM} V_M(r) = \sum_{n=0}^{\infty} W_{KL,n} r^n. \end{aligned} \quad (3.29)$$

By substituting the power series (3.27) and (3.29) in (3.28), the recursion relation for the coefficients is determined:

* For real spherical harmonics, the C_{KLM} are symmetric in all three indices and real. The expansion theorem is: $Y_K Y_L = \sum_M C_{KLM} Y_M$. C_{KLM} is zero unless $|k+\ell| \geq m \geq |k-\ell|$ (triangle rule) and $k+\ell+m = \text{even integer}$.

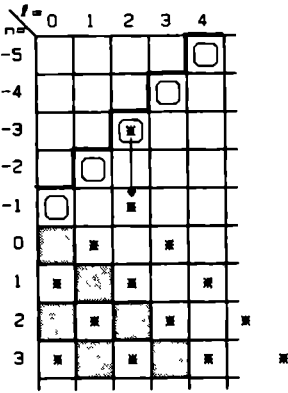


Figure 3.3. The coupling of terms in the L-dependent power series expansion eq. (3.27). All shaded terms can appear in the series, whereby light and dark squares denote singular and analytic terms, respectively. By choosing one of the circled terms non-zero, the singularity of the function is fixed. The recursion relation eq. (3.30) uses the potential to determine the other singular terms. The stars indicate the coefficients which come out non-zero in this way for a singularity with $\ell=2$. The absence of coupling between singular and analytic parts of the function reflects that an arbitrary solution of the homogeneous problem can be added.

$$[n(n+1) - \ell(\ell+1)]A_{Ln} = \sum_k \{ W_{LK,0} A_{K,n-2} + W_{LK,1} A_{K,n-3} + \dots \} - \varepsilon A_{L,n-2}. \quad (3.30)$$

Thus A_{Ln} can be calculated if the $A_{Kn'}$ for $n' < n$ are known. The only exceptions are the coefficients for $n=\ell$ or $n=-\ell-1$ for which the multiplier on the left-hand side is zero. Therefore the values of the coefficients $A_{L,\ell}$ and $A_{L,-\ell-1}$ are arbitrary. For every possible choice there results a unique function ϕ . Hereby the coefficients $A_{L,-\ell-1}$ determine the leading singular terms and therefore the linear combination of the D_L which stands on the right-hand side of the differential equation (3.23).

Many terms in (3.30) do not couple because V_1 is analytic and consequently many of the $W_{LK,n}$ disappear. The power series for $V_1(\mathbf{r})$ in eq. (3.29) only contains terms $r^\ell, r^{\ell+2}, r^{\ell+4}$ etc. From the properties of the Clebsch-Gordan coefficients it follows that $W_{LK}(\mathbf{r})$ only has terms of orders $|\ell-k|, |\ell-k|+2$ etc. This means that in (3.30) singular terms are coupled to each other only (light squares in Fig. 3.3) and the same for analytic terms (dark squares). Thus the singular and analytic parts of ϕ can be treated separately.

Now it is clear in principle how a function $\phi^{(0)}$ with the proper singular behaviour can be constructed. By choosing $A_{L_0, -\ell_0-1} \neq 0$ and all other $A_{L, -\ell-1}$ and $A_{L,\ell}$ zero, the leading (singular) term is determined correctly. Then all

other coefficients of the expansion (3.27) are fixed by the recursion relation. They are calculated up to some n_{\max} . The truncated series gives a function $\phi^{(0)}$ which has the same singular behaviour as the true solution up to the order n_{\max} (typically about 4). This function is a much better representation of the singularity than a single Hankel function, which only describes the first two terms correctly. The reason is that the coupling of the different angular momentum components by the non-constant potential V_l is included correctly by the recursion relation.

The problem with the power series expansion (3.27) is that it defines a function which diverges for large $|r|$. Also, a Bloch sum of this function over a lattice is not a useful object. Instead, a representation in energy derivatives of Hankel functions will be used:

$$\phi^{(0)} = \sum_L \sum_{p=0}^{p_{\max}} C_{Lp} H_L^{(p)} \quad (3.31)$$

where $H_L^{(p)}$ is the p -th energy derivative of H_L . The energy defining the $H_L^{(p)}$ (controlling their localization) can be different from the energy in the Schrödinger equation (3.23). The coefficients C_{Lp} can be chosen in such a way that all singular terms up to order $n=p_{\max}$ are correct. This is easy to do since the singular parts of the $H_L^{(p)}$ have successively higher leading orders as p is increased. For example, for $\epsilon=k^2>0$ the function $h(r)$ is equal to $\cos(kr)/r$ so

$$h = \frac{1}{r} - \epsilon \frac{r}{2!} + \epsilon^2 \frac{r^3}{4!} - \epsilon^3 \frac{r^5}{6!} \pm \dots$$

$$\frac{\partial h}{\partial \epsilon} = -\frac{r}{2!} + 2\epsilon \frac{r^3}{4!} - 3\epsilon^2 \frac{r^5}{6!} \pm \dots$$

$$\vdots$$

As a function in 3-space the series contains only singular terms. Taking the p -th energy derivative removes the first p of these. A general singular function of the form

$$f(r) = a \frac{1}{r} + br + cr^3 + dr^5 + \dots$$

can be written as a linear combination of the $h^{(p)}$ in a straightforward manner. The coefficients to $h, h^{(1)}, h^{(2)} \dots$ are determined recursively: first the coefficient of h is chosen to get the $1/r$ -term right, then the proper amount of $h^{(1)}$ is added

to correct the r -term etc. An expansion of this type is called a Neumann expansion. The calculation of the coefficients C_{Lp} in (3.31) is given in detail in Appendix B.

To summarize: the representation of the singularity of the multipole Green function in the form (3.31) has a number of positive features:

- (i) The singularity is reproduced exactly up to some prescribed order.
- (ii) The coefficients of the expansion are easy to calculate by recursion. Input is a Taylor expansion of the smooth potential at the atomic position τ .
- (iii) Expansion of the singular part around a different site is easy (by means of energy derivatives of the expansion theorem eq. (3.12)).
- (iv) For periodic systems, there are two extra advantages. First, Bloch sums of the functions can be calculated just as for the Hankel functions (Ewald method). Second, the C_{Lp} 's are independent of the Bloch vector.

At this point, a word is in order about the choice of the potential V_I inside the atomic spheres. In principle this is arbitrary; primarily the purpose is to remove the Coulomb singularities. This then makes tractable the calculation of the Green function for the 'medium' given by V_I . However, it is useful to choose the interpolation through the spheres as smooth as possible. The first reason is that oscillations in V_I induce corresponding variations in the functions $\phi_{L\tau}$. These must be resolvable by whatever representation is used for the smooth part of the functions. Second, the singular part $\phi_{L\tau}^{(0)}$ is a good approximation over a large part of space only if V_I is slowly varying in the neighborhood of τ . In practice only the first few Taylor terms of V_I are used to make $\phi_{L\tau}^{(0)}$. It is important that these terms describe V_I well in a large volume around τ . For example, in principle it is possible to take V_I constant inside the spheres. Then one Hankel function would describe the singularity perfectly. But because of the jump of V_I at the sphere surface, the remaining 'smooth' part χ would not be smooth in reality.

To summarize this chapter: In 3.1 it was shown how the definition of the solid Hankel functions (which are central to multiple scattering theory in muffin-tin potentials) can be reduced to one compact equation. In 3.2 the equation was generalized to a non-homogeneous 'medium' V_I , defined as a smooth extension of the interstitial potential into the atomic spheres. Finally, 3.3 showed how the functions can be calculated in practice by splitting them into a singular and a smooth part.

CHAPTER 4

Implementation for Periodic Systems

Part of the work in the course of this thesis was to implement the ideas which were presented in chapter 3 for periodic systems. This chapter describes the necessary steps in a more or less detailed manner. The first section is concerned with the calculation of the eigenstates for a given Bloch vector. Section 4.2 describes the representation for the total charge density and how the program is made self-consistent as well as the evaluation of the total energy (in the framework of local-density theory).

4.1 Calculation of eigenstates

The periodic crystal potential is given in the following form. Inside the atomic sphere centered at τ , the potential is a finite sum

$$V_{\tau}(\mathbf{r}) = \sum_{L=0}^{L_{\max}} V_{L\tau}(s) Y_L(s), \quad \mathbf{s} = \mathbf{r} - \tau. \quad (4.1)$$

The interstitial potential is a Fourier sum:

$$V_I(\mathbf{r}) = \sum_{\mathbf{G}} V_{\mathbf{G}} e^{i\mathbf{G} \cdot \mathbf{r}} \quad (4.2)$$

with \mathbf{G} running over a finite subset of the reciprocal lattice. The atomic spheres do not overlap so that the potential is defined uniquely for every point in space. Since V_I interpolates smoothly through the spheres, the Fourier series contains only a small number of plane waves. The aim is to calculate the eigenstates of the Hamiltonian for this potential, in some energy range of interest and for a given Bloch vector \mathbf{k} .

(A) SMOOTH PART OF THE MULTIPOLE GREEN FUNCTION

The 'generalized Hankel functions' or multipole Green functions $\phi_{L\tau}$ must be calculated for all atomic positions τ in the unit cell. The maximal angular momentum for each site follows more or less from chemistry, so that s,p,d functions are used for a transition metal while silicon uses s and p functions only.

The energy ϵ chosen for the functions is discussed in part (D) of this section. Before entering the loop over the Bloch vectors, the coefficients in expression (3.31) for the singular part $\phi_{L\tau}^{(0)}$ of each $\phi_{L\tau}$ are determined as was described in section 3.3. The required Taylor series for V_I around a site τ is made using the partial derivatives of V_I , which are straightforward sums over the reciprocal lattice. This is then rewritten in the L-expansion (eq. 3.29) using Clebsch-Gordan coefficients. The recursion relation is evaluated as described in Appendix B and the coefficients up to the desired order p_{\max} are stored. The next steps are done for each \mathbf{k} -vector separately. The residuum $R(\mathbf{r})$ (eq. 3.25) and the smooth part χ (eq. 3.26) are calculated in the plane wave representation. If for some pair $L_0\tau$ (suppressed in the notation) the singular part is

$$\phi^{(0)} = \frac{1}{\Omega} \sum_{\mathbf{G}} A_{\mathbf{G}}^{(0)} e^{i(\mathbf{k}+\mathbf{G})\cdot\mathbf{r}} \quad (4.3)$$

then, from the expansion (3.29) and the Fourier transform of the solid Hankel functions (eq. 3.18), the Fourier coefficients are

$$A_{\mathbf{G}}^{(0)} = \sum_{L_p} C_{L_p} i^{\ell_0-\ell} p! \frac{4\pi^{\ell} y_L(\mathbf{k}+\mathbf{G})}{[(\mathbf{k}+\mathbf{G})^2 - \epsilon_H]^{p+1}} e^{-i(\mathbf{k}+\mathbf{G})\cdot\tau}. \quad (4.4)$$

Here ϵ_H is the energy defining the Hankel functions (which can be different from ϵ). The L_0 dependence on the right-hand side enters only over the C_{L_p} which are different for each pair $L_0\tau$. The Fourier coefficients of the residuum are calculated from

$$R_{\mathbf{G}} = [\epsilon - (\mathbf{k}+\mathbf{G})^2] A_{\mathbf{G}}^{(0)} - \sum_{\mathbf{G}'} V_{\mathbf{G}-\mathbf{G}'} A_{\mathbf{G}'}^{(0)} + 4\pi^{\ell} y_{L_0}(\mathbf{k}+\mathbf{G}) e^{-i(\mathbf{k}+\mathbf{G})\cdot\tau}. \quad (4.5)$$

Unfortunately, this involves doing a finite, but still troublesome convolution for the coefficients of the product $V_I \phi^{(0)}$. If the $R_{\mathbf{G}}$ are needed for $|\mathbf{G}| < G_{\phi}$ and if the $V_{\mathbf{G}}$ are non-zero for $|\mathbf{G}| < G_V$, then $A_{\mathbf{G}}^{(0)}$ must be evaluated in a large sphere of radius $G_{\phi} + G_V$ when evaluating eq. (4.5). Done the way it stands, this in fact turns out to be the most time-consuming part of the program.

An effective way around the problem is the following. Including the \mathbf{k} -dependence explicitly, the convolution in (4.5) is equal to $e^{-i(\mathbf{k}+\mathbf{G})\cdot\tau} S(\mathbf{k}+\mathbf{G})$ with

$$S(\mathbf{q}) := \sum_{\mathbf{G}} V_{\mathbf{G}} e^{i\mathbf{G}\cdot\tau} A^{(0)}(\mathbf{q}-\mathbf{G}). \quad (4.6)$$

Here $A^{(0)}(\mathbf{q})$ is the Fourier transform of $\phi_{L\tau}^{(0)}$ without the phase, that is, (4.4) for $\mathbf{k}+\mathbf{G} \rightarrow \mathbf{q}$ and $\tau \rightarrow 0$. Thus $S(\mathbf{q})$ is a linear combination of $A^{(0)}$ centered on the reciprocal lattice vectors with different amplitudes. This is a strongly varying

function of \mathbf{q} since in general the amplitudes $V_{\mathbf{G}'} e^{i\mathbf{G}' \cdot \mathbf{r}}$ have different signs. However, when evaluating $S(\mathbf{k}+\mathbf{G})$ with \mathbf{k} varying through the first Brillouin zone, the oscillations come from terms with \mathbf{G}' close to \mathbf{G} only. The much larger number of terms with \mathbf{G}' far away from \mathbf{G} add up to something which is effectively \mathbf{k} -independent. This part of the sum is calculated once for $\mathbf{k}=0$. Inside the loop over \mathbf{k} -vectors, only the short sum over the remaining terms must be done.

Once the residua for all functions have been determined, the inverse of the plane wave Hamiltonian is applied to them, yielding the Fourier coefficients of the corresponding smooth functions χ . Most of the work in the inversion can be done with the efficient Cholesky factorization [97], since a large lower block of the Hamiltonian is definite due to the dominating diagonal elements. The matrix equation giving (3.26) in the plane wave basis is blocked as

$$\begin{bmatrix} \mathbf{H}_0 & \mathbf{H}_2^+ \\ \mathbf{H}_2 & \mathbf{H}_1 \end{bmatrix} \begin{bmatrix} \chi_0 \\ \chi_1 \end{bmatrix} = \begin{bmatrix} -\mathbf{R}_0 \\ -\mathbf{R}_1 \end{bmatrix}$$

with \mathbf{H}_1 definite and as large as possible. The solution is given by

$$\begin{aligned} \chi_0 &= [\mathbf{H}_0 - \mathbf{H}_2^+ \mathbf{H}_1^{-1} \mathbf{H}_2]^{-1} (-\mathbf{R}_0 + \mathbf{H}_2^+ \mathbf{H}_1^{-1} \mathbf{R}_1) \\ \chi_1 &= -\mathbf{H}_1^{-1} (\mathbf{R}_1 + \mathbf{H}_2 \chi_0). \end{aligned}$$

\mathbf{H}_1^{-1} is calculated using Cholesky factorization while the small matrix in the expression for χ_0 is inverted by a general method. Thus the overall effort connected with the plane wave Hamiltonian is basically that of a Cholesky factorization, which is much less than that of a diagonalization.

(B) AUGMENTATION AND MATRIX ELEMENTS

To get a Rayleigh-Ritz basis set, each function $\phi_{L\tau}$ is augmented inside all atomic spheres. Inside the sphere at τ , the function is replaced by a linear combination of solutions of the Schrödinger equation to the true atomic potential eq. (4.1) (cf. section 2.2(E)). This is done in such a way that the final basis function is once-differentiable at the sphere surface. For this it is necessary to know value and slope on the sphere surface, that is, the numbers $u_L(\mathbf{R})$ and $u'_L(\mathbf{R}) = du_L(\mathbf{R})/dr$ where \mathbf{R} is the sphere radius and

$$\phi_{L\epsilon, \tau_0}(\mathbf{r}) = \sum_L \frac{u_L(s)}{s} Y_L(s) \quad , \quad s = \mathbf{r} - \tau. \quad (4.7)$$

In fact, the $u_L(\epsilon, \mathbf{R})$ and $u'_L(\epsilon, \mathbf{R})$ in the relevant energy range are the only

information needed about the interstitial potential. They are the sum of contributions from the singular and smooth parts of ϕ_{L_0, κ_0} . The singular contribution is evaluated using energy derivatives of the Hankel function expansion theorem (eq. 3.19). The smooth contribution is made by summing over the plane wave expansion of χ using eq. (2.4).

The non-spherical potential terms inside the atomic spheres are so small that they are treated adequately by perturbation theory [51]. This is a great simplification for augmentation (but even more so when making the charge density, section 4.2). For every L , two independent solutions $u_{L1}(s)$, $u_{L2}(s)$ of the radial Schrödinger equation in the spherical atomic potential are chosen. Of these there is a unique linear combination which matches in value and slope to the $u_L(R)$ and $u'_L(R)$ of the multipole Green function. The choice of u_{L1} and u_{L2} is not especially critical as long as they more or less span the range from zero-value to zero-slope boundary conditions. For historical reasons, they were taken to satisfy Hankel function and Bessel function logarithmic derivatives for a small negative energy for low values of ℓ . For $\ell \geq 3$, however, the Hankel boundary conditions push the energy too far up so it is better to define the functions with two logarithmic derivatives close to that of the Bessel function.

In many methods using atom-centered basis functions, the calculation of the Hamiltonian and overlap matrix elements is very involved. Examples are the discrete variational method [25,76] and the cluster methods of Gunnarsson, Harris, and Jones [34] and of Harris and Painter [40]. The problem is the potential integral over the complicatedly shaped interstitial region. An advantage of using the augmented multipole Green functions as basis set is that all interstitial integrals are easy to evaluate, due to the fact that the functions solve the Schrödinger equation. Thus, assume that in the interstitial the functions ϕ_1 , ϕ_2 satisfy

$$\begin{aligned}\Delta\phi_1 &= (V_1 - \epsilon_1)\phi_1 \\ \Delta\phi_2 &= (V_1 - \epsilon_2)\phi_2.\end{aligned}$$

Then

$$\begin{aligned}\nabla \cdot [\phi_1^* \nabla \phi_2 - \phi_2 \nabla \phi_1^*] &= \phi_1^* \Delta \phi_2 - \phi_2 \Delta \phi_1^* \\ &= (\epsilon_2 - \epsilon_1) \phi_1^* \phi_2.\end{aligned}\tag{4.8}$$

By integrating over the interstitial region I and using Gauss' theorem, a surface integral results. The term from the surface of the cell gives zero. Since the surface ∂I is the union of the sphere surfaces but with outward normal vectors pointing in opposite directions, one has

$$\int_I \dot{\phi}_1^* \dot{\phi}_2 d\mathbf{r} = \frac{1}{\epsilon_2 - \epsilon_1} \sum_{\tau} \oint_{\partial S_{\tau}} [\phi_2 \nabla \dot{\phi}_1^* - \dot{\phi}_1^* \nabla \phi_2] \cdot d\mathbf{a}. \quad (4.9)$$

The right-hand side is straightforward to express using the values $u_L(\mathbf{R})$ and the slopes $u'_L(\mathbf{R})$, which are needed for augmentation anyway. To get the corresponding expression for $\epsilon_1 = \epsilon_2$, the limit of (4.9) is taken. This leads to energy derivatives of the functions (denotes by $\dot{\phi}$):

$$\begin{aligned} \int_I \dot{\phi}_1^* \dot{\phi}_2 &= + \sum_{\tau} \oint_{\partial S_{\tau}} [\dot{\phi}_2 \nabla \dot{\phi}_1^* - \dot{\phi}_1^* \nabla \dot{\phi}_2] \cdot d\mathbf{a} \\ &= - \sum_{\tau} \oint_{\partial S_{\tau}} [\phi_2 \nabla \dot{\phi}_1^* - \dot{\phi}_1^* \nabla \phi_2] \cdot d\mathbf{a}. \end{aligned} \quad (4.10)$$

Finally, interstitial contributions to the Hamiltonian matrix elements in both cases are simply

$$\int_I \dot{\phi}_1^* H \dot{\phi}_2 d\mathbf{r} = \int_I \dot{\phi}_1^* (-\Delta + V_I) \dot{\phi}_2 d\mathbf{r} = \epsilon_2 \int_I \dot{\phi}_1^* \dot{\phi}_2 d\mathbf{r}. \quad (4.11)$$

Of course, the integrals are easy to evaluate only because there has already been an investment of work when making the functions ϕ_1 and ϕ_2 . Note that the Hamiltonian matrix is not hermitian before the contribution from the atomic spheres is added.

Because of the diagonal matrix elements, some integrals of the energy-derivative type (4.10) must always be calculated. This means that the energy derivative $\dot{\phi}_{L\tau}$ must be calculated for every function in the basis. The defining equation is, analogous to eq. (3.23),

$$(\Delta - V_I(\mathbf{r}) + \epsilon) \dot{\phi}_{L\tau} = -\phi_{L\tau}. \quad (4.12)$$

The singularity of $\dot{\phi}_{L\tau}$ is weaker than that of $\phi_{L\tau}$ (because energy differentiation eliminates the leading singular term) but a separate treatment of the singular part is nonetheless necessary. The calculation then is very similar to that of $\phi_{L\tau}$ and reduces to taking the energy derivatives of the steps described here and in the preceding sections.

Next, the contribution of the atomic spheres to the matrix elements is considered. After augmentation, each function is given inside the sphere S_{τ} as a linear combination of the functions

$$U_{Li}(s) = \frac{u_{Li}(s)}{s} Y_L(s), \quad s = \mathbf{r} - \boldsymbol{\tau}, \quad i=1,2. \quad (4.13)$$

The overlap integrals are done by direct integration:

$$\int_{S_r} U_{L_i}(s)U_{K_j}(s)ds = \delta_{LK} \int_0^R u_{L_i}(s)u_{K_j}(s)ds.$$

For the Hamiltonian matrix elements, the potential inside the sphere is written as the sum of a spherical and a non-spherical part $V_{\text{sph}} + V_{\text{nsph}}$. By construction U_{L_i} is an eigenfunction of $-\Delta + V_{\text{sph}}$. Thus the major contribution is given as in eq. (4.11) for the interstitial part. Finally, the effect of V_{nsph} is introduced as a perturbation correction to the Hamiltonian matrix elements. To this aim the integrals

$$\int_{S_r} U_{L_i} V_{\text{nsph}} U_{K_j} ds$$

are calculated using Clebsch-Gordan coefficients and radial integrations. These k -independent numbers are only evaluated once outside of the k -loop.

(C) L-TRUNCATION OF AUGMENTATION SUMS

In the description above, the sums over the angular momenta were assumed to go to infinity. In practice, however, augmentation can only be done for a finite set of L 's, say for $L < L'_{\text{max},\tau}$ in the sphere at τ . In the following the effect of the truncation of the sums is considered. It will turn out that the truncated expressions are correct if augmentation is defined in the following way: Inside a sphere, the components for $L \leq L'_{\text{max}}$ are *replaced* by numerical functions of the same value and slope; for $L > L'_{\text{max}}$, the components are *left the way they are**.

First, we return to the case of a zero interstitial potential, so that the $\phi_{L\tau}$ are solid Hankel functions and the method is similar to ASW or LMTO. In the sphere with center τ , the functions ϕ_1 and ϕ_2 of eq. (4.8) can be written in a Y_L -representation:

$$\phi_i(\mathbf{r}) = \sum_L \frac{u_{iL}(s)}{s} Y_L(s), \quad s = \mathbf{r} - \tau. \quad (4.14)$$

The logic of eqs. (4.8) and (4.9) is repeated for the sphere in place of the interstitial, starting from the radial Schrödinger equation:

* I am indebted to F Springelkamp for pointing this out. A different interpretation can be found in ref. [98]. See also the definition of the 'combined correction term' in the LMTO method [4] and ref. [90].

$$u_{iL}^*(s) = \left[\frac{\ell(\ell+1)}{s^2} - \epsilon_1 \right] u_{iL}(s)$$

$$\frac{d}{ds} [u_{iL}^* u'_{2L} - u_{2L} u'_{iL}] = (\epsilon_1 - \epsilon_2) u_{iL}^* u_{2L} \quad (4.15)$$

$$\int_0^R u_{iL}^* u_{2L} ds = \frac{1}{\epsilon_1 - \epsilon_2} [u_{iL}^*(R) u'_{2L}(R) - u_{2L}(R) u'_{iL}(R)].$$

The last equation is valid for the case that neither ϕ_1 nor ϕ_2 are singular in the sphere. When summed over ℓ , the right-hand side gives exactly the negative of the contribution from this sphere to the interstitial overlap integral eq. (4.9). Thus, the truncation of the sum in eq. (4.9) is the same as adding the terms for $L > L'_{\max}$ from the integral over the sphere. Expressed differently: adding a term in the τ, L -sum in eq. (4.9) is equivalent to removing the L -component from ϕ_1 and ϕ_2 inside the sphere around τ . Next, if ϕ_1 or ϕ_2 has its singularity at τ , the same thing happens except that an extra term arises from the lower limit of the radial integration. This cancels the term which comes from the corresponding δ -function if the volume of integration in eq. (4.9) is defined to include the sphere. In the same way the infinity in the integral is cancelled if both functions are singular at the atomic site. The final conclusion is that without any approximation,

$$\int_{\text{unit cell}} \bar{\phi}_1^* \bar{\phi}_2 d\mathbf{r} = \frac{1}{\epsilon_2 - \epsilon_1} \sum_L [\dots] \quad (4.16)$$

with the contents of $[\dots]$ as in the last equation and where $\bar{\phi}_1$ and $\bar{\phi}_2$ are defined as the functions ϕ_1 and ϕ_2 with only the lowest $L'_{\max, \tau}$ terms removed in each sphere. After the augmentation contributions are added, the resulting overlap matrix elements are exact for functions which are made from ϕ_1 and ϕ_2 by replacing only the low L -components by the numerical functions.

The interpretation of augmentation as the replacement of the low L -components (rather than as the representation of the function as a finite sum) is related to the reduced scattering of the atoms at high angular momenta. For large values of ℓ , the radial equation (eq. 4.15) is dominated by the $\ell(\ell+1)/s^2$ term. The regular solution (with or without a potential) is similar to the Bessel function which is practically equal to a constant times r^ℓ inside the sphere. Thus, augmentation for high values of ℓ comes down to replacing the L -component of ϕ_1 by a numerical function which is almost the same. This is equivalent to saying that the potential does not scatter in the L -channel.

However, it is still important to include the high L-components in some way since they become negligible only if L is very large. In practice the regular solutions are Bessel functions for $\ell \geq 4$ while components can be left away only for about $\ell > 8$.

At the same time, the r^ℓ character of the radial solutions explains why only small errors are introduced when making the Hamiltonian matrix elements as in eq. (4.11). The 'interstitial functions' $\hat{\phi}_i$ are not zero inside the spheres, therefore it is not strictly true that they solve the Schrödinger equation for the real crystal potential. However, the high- ℓ terms which are left inside the spheres feel little of the shielded Coulomb potential near the center, because a high power of r concentrates the charge near the sphere surface. This makes it permissible to replace the Hamiltonian by the interstitial energy when calculating the interstitial part of the matrix elements (eq. 4.11).

Turning now to a varying interstitial potential and the functions $\phi_{L\pm}$, the situation is almost the same. The difference is that V_I is not spherically symmetric inside the spheres so that the u_{iL} are coupled. As a result the cancellation of the potential terms to get the second equation of (4.15) is complete only if an infinite sum over L is taken. The extra error in the matrix elements is given by terms such as

$$\sum_{L \leq L_{\max}} \sum_{K > L_{\max}} \int_0^R u_{iL}^* W_{LK} u_{2K} ds$$

with W_{LK} given in eq. (3.29). However, if ℓ is high enough for scattering a potential inside the sphere to be negligible, then the coupling to low angular momenta can safely be ignored.

(D) CHOICE OF ENERGY PARAMETERS

Up to now, the choice of the energy in the definition of the multipole Green functions was left open. Since this is the eigenvalue of the Schrödinger equation in the interstitial region, it must in some way be permitted to vary over the energy range of the bands in question. An exception to this are the ASW and LMTO methods, which eliminate the interstitial by using overlapping atomic spheres. This makes it possible to use one fixed interstitial energy which is considered as a parameter (in ASW) or simply set to zero (in LMTO). The error introduced hereby is small because every point of space lies in some sphere, where the wave function is built up out of numerical solutions. For a muffin-tin geometry with a finite interstitial, however, a single energy parameter means insufficient degrees of freedom because otherwise the curvature of the interstitial wave function is fixed. The result is that the minimal-basis band structure is

almost independent of the energy parameter, but the errors are too large to be acceptable

The easiest solution is to work with a double basis by including all functions for two different interstitial energies, ϵ_1 and ϵ_2 . As is demonstrated in chapter 5, the calculated eigenvalues are correct. In fact, since a single basis for either energy gives almost the right eigenvalues, the problem is rather that the double basis is close to degenerate (see Appendix C). Care must be taken that the energy parameters avoid the singularities in the multipole Green functions. The latter are the energies for which an eigenstate exists for the interstitial potential alone. For a muffin-tin potential, these are of course the free electron bands. If the true interstitial potential V_1 is used, the corresponding condition is that the energy parameters must avoid the energy bands calculated for V_1 . At each atomic site the interstitial potential is a rounded well with the result that there is a wide gap in the bands for V_1 (Fig. 4.1). Furthermore, the gap lies near the middle of the true bands. Therefore the first energy parameter can be put into the gap and the second at some sufficiently negative energy.

Because the multipole Green functions are calculated numerically, the matrix elements have a somewhat larger error than in the ASW and LMTO methods (where the functions are known analytically). Together with the almost-degenerate double basis this can lead to numerical difficulties. The basis functions for the two energy parameters are similar which means that they are almost linear dependent. This can become worse at certain k -points. Consequently the overlap matrix will have some small but positive eigenvalues. A small error in the matrix elements can then result in small *negative* eigenvalues so that the overlap matrix is no longer positive definite. This problem is discussed in Appendix C.

4.2 Charge density and self-consistency

The difficult problem of the interaction between the electrons is treated by means of the local density approximation. In this model every electron moves in an effective potential which is determined by the distribution of all other electrons. Because the effective potential is a function of the charge density, the system must be made self-consistent iteratively. The interstitial potential will not be approximated in any way so that it is necessary to solve the Poisson equation properly in the interstitial region.

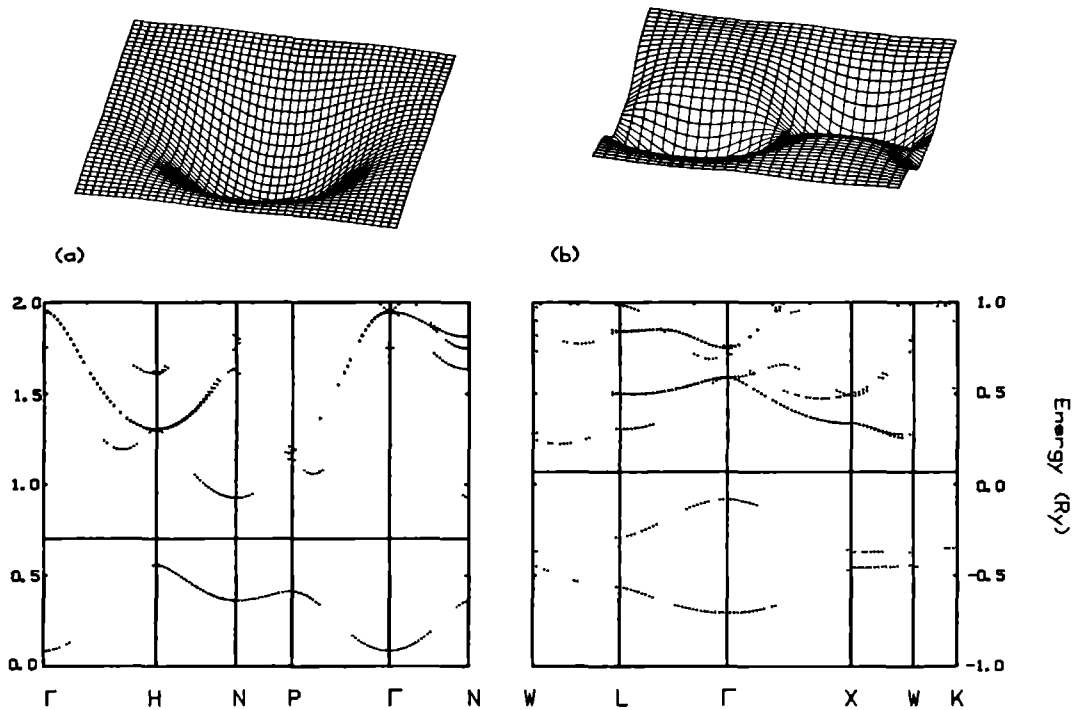


Figure 4.1. The energy bands for the interstitial potential V_I (which correspond to the free-electron bands in muffin-tin methods) for (a) bcc Nb and (b) Si. The interstitial potential is displayed above in the (100), respectively (110) plane. Because of the rounded wells at the atomic sites, one state is split off for

each atom in the unit cell, making it possible to use a constant energy parameter (horizontal line) without encountering 'free electron' singularities. The occupied states of the true bands extend from 1 to 1.5 Ry for Nb and from -0.4 to 0.5 Ry for Si.

(A) LOCAL-DENSITY APPROXIMATION

Density-functional theory has shown that the ground state of a system of interacting electrons is known in principle if the charge density is given [43]. This has led to efficient new approaches to the problem of interacting electrons, in which emphasis is placed on the charge density rather than on the many-particle wave function. The main result is that, for a given external potential V , there exists an energy functional $E_V[\rho]$ which is minimal at the true ground-state charge density. The value of the functional at the minimum is then the true ground-state total energy. Thus the obvious approach is to vary a test charge density in some suitable space until the minimum is found. However, there is an important difficulty because, whereas the existence of the energy functional has been proven, its explicit form is not known. Therefore a practical utilization of the approach was not possible before the local-density approximation to the energy functional was introduced [55,41]. The functional is written as

$$E_V[\rho] = T_S[\rho] + U_{\text{ext}}[\rho] + E_H[\rho] + E_{\text{xc}}[\rho] \quad (4.21)$$

where T_S is the kinetic energy of a system of non-interacting electrons with the same charge density, U_{ext} is the potential energy of the electrons in the external potential, E_H is the electrostatic (Hartree) energy, and E_{xc} is called the exchange-correlation energy. In effect, one has included as many terms as possible which are expected to be important and at the same time possible to calculate. These are the terms T_S , U_{ext} and E_H . The last term E_{xc} is defined to be everything else. The hope is that the functional is represented well enough if a suitable approximation is found for E_{xc} . In practice, E_{xc} is defined in such a way that the approximate functional gives the proper results for a homogeneous electron gas. E_{xc} is written as

$$E_{\text{xc}}[\rho] = \int \rho \epsilon_{\text{xc}}(\rho) dr \quad (4.22)$$

where ϵ_{xc} is a local function of ρ given numerically. For crystals, the additional nucleus-nucleus term in the total energy is usually taken together with U_{ext} and E_H to make the total electrostatic energy U :

$$U = \int \frac{\rho(\mathbf{r})\rho(\mathbf{r}')}{|\mathbf{r}-\mathbf{r}'|} d\mathbf{r}d\mathbf{r}' - 2 \sum_{\nu} \int \frac{\rho(\mathbf{r})Z_{\nu}}{|\mathbf{r}-\mathbf{R}_{\nu}|} d\mathbf{r} + \sum_{\nu \neq \nu'} \frac{Z_{\nu}Z_{\nu'}}{|\mathbf{R}_{\nu}-\mathbf{R}_{\nu'}|} \quad (4.23)$$

where Z_{ν} is the atomic number of the atom at \mathbf{R}_{ν} . This expression is a little tricky because each of the three terms is divergent; for example, the last term is the energy of an infinite lattice of positive charges. Therefore it is better to

rewrite the energy as

$$U = \frac{1}{2} \int \rho(\mathbf{r}) V_{es}(\mathbf{r}) d\mathbf{r} + \frac{1}{2} \sum_{\nu} Z_{\nu} V_{\nu} \quad (4.24)$$

where $V_{es}(\mathbf{r})$ and V_{ν} are the total electrostatic potentials seen by an electron and a nucleus, respectively:

$$V_{es}(\mathbf{r}) = 2 \int \frac{\rho(\mathbf{r}')}{|\mathbf{r}-\mathbf{r}'|} d\mathbf{r}' - 2 \sum_{\nu} \frac{Z_{\nu}}{|\mathbf{r}-\mathbf{R}_{\nu}|}$$

$$V_{\nu} = 2 \sum_{\nu' \neq \nu} \frac{Z_{\nu'}}{|\mathbf{R}_{\nu}-\mathbf{R}_{\nu'}|} - 2 \int \frac{\rho(\mathbf{r})}{|\mathbf{R}_{\nu}-\mathbf{r}|} d\mathbf{r}. \quad (4.25)$$

In this way, the total electrostatic energy of the crystal decomposes into a sum over equal finite contributions from the unit cells.

If the local-density expression for the energy functional is used, the minimalization is readily done. It is assumed that the charge density can be written as a sum over N wave functions as $\rho = \sum_i \phi_i^* \phi_i$. The Euler-Lagrange variation leads to one equation for each wave function:

$$(-\Delta + V_{eff})\phi_i = \epsilon_i \phi_i$$

$$\text{with } V_{eff} = V_{es} + \frac{d}{d\rho}(\rho\epsilon_{xc}(\rho)) =: V_{es} + \mu_{xc}(\rho) \quad (4.26)$$

which is recognized to be the single-particle Schrödinger equation in an effective ρ -dependent potential. The 'eigenvalue' ϵ_i is in principle only a Lagrange multiplier associated with the auxiliary condition that the total number of electrons is N . However, the total energy can be related to the sum of the single particle energies by using eq. (4.26) to rewrite it as

$$E = \sum_i \epsilon_i + \int \rho(\epsilon_{xc} - \mu_{xc}) d\mathbf{r} - \frac{1}{2} \int \rho V_{es} d\mathbf{r} + \frac{1}{2} \sum_{\nu} Z_{\nu} V_{\nu}. \quad (4.27)$$

In addition, there are theorems which relate ϵ_i to the total energy change for changes in the occupation numbers [46]. The electrostatic part of the 'double counting' term which correct the sum of the eigenvalues is just the difference of the two terms which were added to make U . The additional exchange-correlation μ_{xc} part of the effective potential models the effect of an 'exchange-correlation hole' around every electron. Because of the Coulomb repulsion and the Pauli principle, the other electrons will tend to stay away from a given

electron. Thus the electrostatic potential V_{es} alone will overcount the energy cost of the Coulomb repulsion between the electrons. The variation of μ_{xc} with ρ describes the change in the size of the hole as the density of the surrounding electrons varies. It can be shown that the local-density approximation is equivalent to the assumption that only the size but not the shape of the hole changes [33]. The dependence of μ_{xc} on ρ is only given numerically but the most important part is ρ to the power of one-third. This is similar to the Slater $X\alpha$ method [85].

Since the effective potential is a function of ρ the equations can only be solved iteratively. After an initial guess for V_{eff} is made, one proceeds by alternately solving the Schrödinger equation to make ρ and calculating a new potential. This is repeated until input and output charge density are equal. The following points must be considered when implementing the scheme:

- (i) For a metal, the total charge density is an integral over the Brillouin zone with a cutoff at the Fermi energy. However, the Fermi energy can only be determined after the eigenvalues at all k -points have been calculated to make the density of states.
- (ii) To make the charge density, the wave functions should be absolutely squared which is unfortunately a troublesome operation in every representation except a point-wise one. This part must be efficient since it must be done at all k -points and for all bands.
- (iii) The representation chosen for ρ must make it possible to solve the Poisson equation for V_{es} and to evaluate the exchange-correlation potential.

(B) REPRESENTATION OF THE CHARGE DENSITY

Suitable representations for the charge density must be found both inside the atomic spheres and in the interstitial region. Inside a sphere, all wave functions are given as sums over L -components. This makes it straightforward to derive ρ by means of Clebsch-Gordan coefficients. Thus the real problem is to calculate and accumulate the square of the interstitial wave function. For a periodic system, the first approach which comes to mind is to write the interstitial charge density as a Fourier series. The coefficients are obtained by convoluting the series for the interstitial wave function with itself. Despite the fact that this is a time-consuming process, this is what is done in full-potential LAPW methods [100]. An alternative is to accumulate ρ on some set of points and then to fit to these values with suitable functions.

For the multipole Green function basis, the convolution for the Fourier coefficients of ρ is made difficult because the series for the singular parts of the wave functions are very slowly convergent (eq. 4.4). This problem can be solved by smoothing each solid Hankel function inside the sphere where it is centered as described in section 3.1(D). In this way the function is modified only inside the sphere so that the interstitial charge density is not affected. The Fourier coefficients then have Gaussian convergence and the convolution can be done. This scheme is then more or less equivalent to the FLAPW way of calculating the charge density.

However, the method is still not really satisfactory due to the large number of plane waves needed to get a good representation of ρ . The time for accumulating ρ takes up a large part of the total computer time per k-point. On the other hand, the motivation for the atom centered description for the wave function was that the desired solutions have an atom-centered character. The same is true for the square of the wave function and the charge density. Therefore it is sensible to represent ρ using the Bloch-sums of Hankel functions from section 3.1(C). These functions are periodic and atom centered, smooth outside the atomic spheres, and complete if their defining energy is allowed to vary. Furthermore, the Poisson equation is very easy to solve in this basis (see part C). Since the charge density is not expected to have wild oscillations in the interstitial, it is probably adequate to use two functions per angular momentum. In this way the localization of the functions is variable. For molecules, a similar kind of basis has been used successfully by Harris [40].

Next the question arises as to what the best method is to find the proper linear combination in the Hankel function basis. This will be done by some kind of fit to data which is accumulated over the Brillouin zone. A first approach is to make a least-squares fit of the Hankel functions to the Fourier series for ρ in the interstitial. To do this one must calculate integrals over the interstitial such as

$$\int_V \mathcal{H}_L e^{i\mathbf{G} \cdot \mathbf{r}} d\mathbf{r} , \int_V \mathcal{H}_L \mathcal{H}_K d\mathbf{r}.$$

where \mathbf{G} is a vector of the reciprocal lattice. These are easily done in the same way as the overlap integrals for the multipole Green functions (eq. 4.9) since the integrands are all products of functions which satisfy the Schrödinger equation (to zero potential). However, the disadvantage of this method is that the fitted series will never be better than the Fourier series for ρ , which was seen to be bad. If this Fourier series was truncated at some point, then the fit will try to make a function for which the higher Fourier terms are zero. Consequently it is much better to use the coefficients of the Fourier expansion of ρ as *conditions*

for the least squares fit by the Bloch-Hankel functions. This means that the higher Fourier terms are not set to zero but rather left open. For best results one also includes Gaussians localized inside the spheres in the basis. Then there is enough freedom in the basis to describe the smoothed interstitial charge density throughout the whole cell. The coefficients in the fit are chosen so that the first Fourier terms of the linear combination reproduce the terms in ρ in the least squares sense. It turns out that the resulting fit describes the charge density much better than the input Fourier series unless very many terms are included in the latter. In other words, in this way the error in the truncated series is healed when the higher Fourier terms adjust themselves to yield a smooth function.

This method was seen to be a practical way to translate the truncated Fourier series for ρ into a basis of Bloch-Hankel functions. The disadvantage is that quite a few of the time-consuming convolutions must still be done to get the input data for the least-squares fit. The alternative method described next works without any Fourier expansion at all. One could try to fit the functions directly to the charge density at representative points in the interstitial region. This is not practical because many extra structure constants must be calculated to accumulate ρ at the points. However, one can exploit the fact that everything about the charge density is known on the surfaces of the spheres. Also it is known that ρ is smoothly varying in the interstitial. Thus it can be expected that a fit which reproduces both the value and the slope of the true charge density on all sphere surfaces will be a good enough representation. If necessary, this can be improved by adding a few special points in the interstitial. For these, ρ is accumulated directly and included in the fit. The major advantage of this method is that the time spent to accumulate the charge density is very small. The calculations in chapter 5 were done in this way. The basis for ρ consisted of Bloch-Hankel functions and their first energy derivative up to the maximum angular momentum $\ell=4$. For close-packed metals, the interstitial charge from the fit was calculated and the fit was then scaled to make the cell neutral. The correction hereby was always less than 4%. For the semiconductor calculations it was found better to use the total interstitial charge as a constraint on the fit. The resulting mismatch of value and slope on the spheres was no larger than 3%.

All together, ρ is made in the following way. First the charge density inside the spheres is calculated. Hereby it is useful that the non-spherical potential terms in the spheres are treated as a perturbation. In that case every wave function is a linear combination of the few functions given in eq (4.13), making it easy to calculate the charge density by summing over Clebsch-Gordan coefficients. During the scan over the irreducible part of the Brillouin zone, only the coefficients in front of the products of the functions must be accumulated. Later these coefficients are symmetrized and combined with the recalculated radial

solutions to get

$$\varrho_{\tau}(\mathbf{r}) = \sum_L \frac{\varrho_L(s)}{s^2} Y_L(s), \quad \mathbf{s}=\mathbf{r}-\boldsymbol{\tau} \quad (4.28)$$

in the sphere at $\boldsymbol{\tau}$. The summation goes up to (yet another) cutoff $L_{\max,\tau}^*$. The values and derivatives $\varrho_L(R)$ and $\partial\varrho_L(R)/\partial s$ at the sphere radii are known and are used to fit the linear combination of the Bloch-Hankel functions for the interstitial charge density in the form

$$\varrho_I(\mathbf{r}) = \sum_{L\tau} \{ C_{0L\tau} \mathcal{H}_L(\mathbf{r}-\boldsymbol{\tau}) + C_{1L\tau} \dot{\mathcal{H}}_L(\mathbf{r}-\boldsymbol{\tau}) \} \quad (4.29)$$

To be precise, the interstitial charge density is chosen in such a way that it gives the same values and slopes for the low L 's on the sphere surface when expressed in an expansion as (4.28). The *higher* angular momentum components are not small; formally, they are determined by the condition that ϱ must be expandable as a sum of the Bloch-Hankel functions. Thus, the expressions (4.28) and (4.29) for ϱ must be interpreted just as was the case for augmentation of the wave function: the true charge density inside a sphere is defined as ϱ_I with the lowest angular momentum terms *replaced* by the expansion (4.28). By construction, ϱ is then smooth throughout the whole cell and contains all L -components up to infinity in each sphere.

(C) HARTREE AND EXCHANGE-CORRELATION POTENTIALS

A major advantage of the Hankel-function representation for the interstitial charge density ϱ_I is that the Hartree potential $V_H(\mathbf{r})$ is easy to calculate. The aim is to solve the Poisson equation

$$\Delta V_H = -8\pi\varrho \quad (4.30)$$

where ϱ is the true electron charge density, given in the mixed representation eqs. (4.28) and (4.29). The principle when doing this is the same as in the method presented by Weinert [93] but the realization here is much simpler. The starting point is that the multipole moments of a charge distribution inside a sphere completely determine the electrostatic potential at any point outside it [45]. One therefore constructs a 'pseudocharge density' $\tilde{\varrho}(\mathbf{r})$ in such a way that $\tilde{\varrho}$ is equal to ϱ_I in the interstitial region and has the same multipole moments as ϱ in all spheres. If the Poisson equation can be solved for $\tilde{\varrho}$, then it is known that the resulting potential \tilde{V}_H is equal to the true electrostatic potential in the interstitial. \tilde{V}_H then gives the boundary conditions for a well-defined Dirichlet

problem in each sphere. This is solved using the numerical charge density in the Y_L -representation.

In the method of Weinert, both the interstitial charge density ϱ_I and the pseudocharge density $\bar{\varrho}$ are written as Fourier series. ϱ_I is made into $\bar{\varrho}$ by distorting it inside the spheres to reproduce the prescribed multipole moments while keeping the function as smooth as possible. This leads to some involved mathematics. In the atom-centered Hankel function basis, the equivalent effect can be obtained by simply adding point multipoles at the atomic sites. In the following the general case is treated that energy derivatives up to some cutoff p_{max} are used to represent ϱ_I . For simplicity it is assumed that there is one atom per unit cell. Then the pseudocharge density is

$$\bar{\varrho} = \sum_{pL'} C_{pL} \mathcal{X}_L^{(p)} + \sum_L C_L D_L. \quad (4.31)$$

For charge densities and potentials it is simpler to work with real functions. Here and in the following the functions \mathcal{X}_L , \mathcal{F}_L and the distributions D_L are defined using $y_L(-\nabla)$ in place of $Y_L(-i\nabla)$. The functions here are $(-i)^\ell$ times those of section 3.1. The first term of eq. (4.31) is just ϱ_I of eq. (4.29) and the second represents the added point multipoles. $\bar{\varrho}$ is made by extending the interstitial charge density ϱ_I into the sphere and then correcting for the error in the multipole moments by choosing the amplitudes C_L properly. In the $\ell=0$ term, the charge of core and nucleus are included. These terms play the role of a Madelung potential. Similarly a core polarization could be included in the $\ell=1$ terms. The solutions of $\nabla^2 \bar{V}_H = -8\pi\bar{\varrho}$ can be written in the form

$$\bar{V}_H = \sum_{pL} A_{pL} \mathcal{X}_L^{(p)} + \sum_L A_L \mathcal{F}_L \quad (4.32)$$

where p goes up to the same maximal value p_{max} as in the sum for $\bar{\varrho}$. The function \mathcal{F}_L is the solution of the Poisson equation for a lattice of point multipoles (in a compensating background for the case $\ell=0$) so that $\mathcal{X}_L^{(p)}$ and \mathcal{F}_L satisfy the equations

$$\begin{aligned} (\Delta + \epsilon_0) \mathcal{X}_L &= -4\pi D_L \\ (\Delta + \epsilon_0) \mathcal{X}_L^{(p)} &= -p \mathcal{X}_L^{(p-1)} \quad \text{for } p > 0 \\ \Delta \mathcal{F}_L &= -4\pi D_L + 4\pi \delta_{L0} \bar{D}_0. \end{aligned} \quad (4.33)$$

ϵ_0 is the energy of the Hankel functions. The constant $\bar{D}_0 = Y_0/\Omega$ is the average of D_0 over the cell; this term describes the compensating background*. By ap-

plying Δ to \hat{V}_H and then comparing coefficients with $-8\pi\bar{q}$, the following relations for the A_{pL} and A_L result:

$$\begin{aligned}\epsilon_0 A_{p_{\max}L} &= 8\pi C_{p_{\max}L} \\ \epsilon_0 A_{pL} + (p+1)A_{p+1,L} &= 8\pi C_{pL} \quad \text{for } p=0, \dots, p_{\max}-1 \\ A_L + A_{0L} &= 2C_L.\end{aligned}\tag{4.34}$$

These are solved successively for A_{pL} , $p=p_{\max}, p_{\max}-1, \dots, 0$ and for A_L .

Before the pseudocharge density can be made, the multipole moments of both q_I and q_τ inside each sphere S_τ must be calculated. The moments are defined by

$$q_L = \int_{S_\tau} q(\mathbf{r}) y_L(\mathbf{r}) d\mathbf{r}.\tag{4.35}$$

Since this is equal to $(2\ell+1)!!/4\pi$ for a (real) point multipole $q=D_L=y_L(-\nabla)\delta(\mathbf{r})$ (eq. A23), the correcting charges $C_L D_L$ in eq. (4.31) are given by

$$C_L = \frac{4\pi}{(2\ell+1)!!} (q_L - q_L^{(0)})\tag{4.36}$$

where q_L and $q_L^{(0)}$ are the moments for q_τ and q_I in S_τ , respectively. The first of these is just

$$q_L = \int_0^R q_L(r) r^\ell dr.\tag{4.37}$$

from expression (4.28) for q_τ . To derive $q_L^{(0)}$, a structure-constant expansion is used to write the (real) Bloch-Hankel function \mathcal{X}_K as in eq. (3.19) so that

$$\begin{aligned}\int_{S_\tau} \mathcal{X}_K y_L d\mathbf{r} &= \int_{S_\tau} H_K y_L d\mathbf{r} + \sum_M \beta_{KM} \int_{S_\tau} J_M y_L d\mathbf{r} \\ &= \delta_{KL} \int_{S_\tau} H_L y_L d\mathbf{r} + \beta_{KL} \int_{S_\tau} J_L y_L d\mathbf{r}\end{aligned}\tag{4.38}$$

(or the same expression without the first term if \mathcal{X}_K is centered at $\tau \neq \tau$). As shown in Appendix A, the remaining integrals are transformed to surface

* For $\ell \neq 0$, \mathcal{H}_L is the limit of \mathcal{X}_L for $\epsilon_H \rightarrow 0$. For $\ell = 0$, the constant term must be subtracted from \mathcal{X}_0 before taking the limit.

integrals in the usual way, which then evaluate to

$$\int_{S_r} \mathcal{Y}_L Y_L d\tau = (R^{\ell+2} h_{\ell+1}(R) - (2\ell+1)!!) \epsilon^{-1}$$

$$\int_{S_r} J_L Y_L d\tau = R^{\ell+2} j_{\ell+1}(R) \epsilon^{-\ell-1}. \quad (4.39)$$

Here $\mathcal{Y}_L(\mathbf{r}) = h_\ell(r) Y_L(\mathbf{r})$ and $J_L(\mathbf{r}) = \epsilon^{-\ell} j_\ell(r) Y_L(\mathbf{r})$. h_ℓ and j_ℓ are similar but not the same as the spherical Hankel and Bessel functions (see Appendix A).

To solve the interior Dirichlet problem, the differential equation for each L-component of the Hartree potential is integrated separately. Note that this is again equivalent to replacing the corresponding components in \tilde{V}_1 without modifying the higher components. Defined in this way, the final Hartree potential solves the Poisson equation exactly for the similarly-defined charge density (eq. 4.28 and 4.29). In neither case is the sum over L truncated. Finally, a choice must be made for the arbitrary zero of the Hartree potential. In the interest of a unique definition it was fixed so that the average over the cell of the total electrostatic potential is zero.

Next, the exchange-correlation part of the potential is considered. Since μ_{xc} is given numerically it can only be evaluated point-by-point. Inside the spheres, a fit with Y_L 's is made to $\mu_{xc}(\mathbf{r})$ evaluated on an angular mesh. This must be done separately at every radial grid point. Once μ_{xc} has been represented in the Y_L -expansion in all the spheres, the values and slopes at the sphere surface are used to make an interstitial fit with periodic Hankel functions, exactly as in the case of the charge density. The function $\epsilon_{xc}(\rho)$, which is needed to evaluate the total energy, is treated in the same way.

The final step which must be done is to interpolate the calculated interstitial potential in a smooth way through the atomic spheres to make a suitable input V_1 for the next iteration. Since the incoming parts of the periodic Hankel functions are smooth already, it is enough to discuss a single H_L centered at zero. The first step is to eliminate the singularity by substituting the smoothed Hankel from (3.21) (here denoted by H_L^{sm}) for H_L , whereby a is chosen so that $e^{-a^2 r^2}$ is practically zero at the sphere radius. The second improvement is to add terms which are localized inside the sphere. A suitable set of functions is $G_L, \Delta G_L, \Delta^2 G_L, \dots$ with G_L given in eq. (A20). Thus the 'really smooth' function is given as

$$H_L^{sm} = H_L^{sm} + \sum_p C_p \Delta^p G_L.$$

The optimal coefficients C_p are determined by minimizing the quantity

$$X := \int H_L^{sm}(-\Delta)^m H_L^{sm} dr.$$

For $m=1$ this is just the 'kinetic energy' of H_L^{sm} . The minimalization tries to reduce the amplitudes of high Fourier terms since $(-\Delta)^m$ leads to a weight factor of q^{2m} in the Fourier integral expression for X . The integrals needed to do the minimalization can be expressed in closed form by the method shown in Appendix A. The smoothing parameters a, m influence the shape of the potential V_I inside the sphere. The value of a determines how far out the potential is modified. Increasing m makes the potential smoother while making the well at the atomic site deeper. This is not a problem since the ease in calculating the interstitial Green function depends mainly on the smoothness of the potential and not on how deep the wells are. In fact, deep wells are an advantage because they open up a wide gap in the bands for V_I (see section 4.1(D)). In practice, m must be adjusted until a gap of proper position and width opens up. Usually a value of $m=3$ is good, giving wells of about 1–2 Ry depth.

(D) SELF-CONSISTENCY CYCLE

In this part of section 4.2, some remaining particulars concerning the self-consistency loop are discussed.

The *core states* are permitted to relax as the atomic potential changes. By means of the good approximation that the core does not feel the non-spherical part of the potential, the states are easy to calculate by numerical integration of the radial Schrödinger equation. For a deep core state, the amplitude at the sphere radius is so small that the boundary conditions are not relevant. A high-lying core state is more sensitive. For these, the logarithmic derivative at the sphere radius is taken from the Hankel function to the energy $\epsilon_c - V_{av}$, which is a solution if the potential outside the sphere is taken equal to the average over the sphere surface V_{av} . In principle this is an iterative problem since the core eigenvalue ϵ_c depends on the boundary conditions, but one iteration is perfectly adequate in practice. The effect of the boundary conditions on the charge density is small but a proper treatment is needed to make the total energy independent of the sphere radii, since a small error in the charge density is weighted by the degeneracy of the core state.

In order to reduce the number of self-consistency iterations needed, it is useful to include an *internal loop* which makes one sphere self-consistent independently of the rest of the system. In the ASW method [98], there is a natural way to do this because an ASW 'compressed sphere' is described completely by only a few logarithmic derivatives and charges. This is a consequence of the method used to calculate the charge density. Each scan through the

Brillouin zone gives new values of these parameters and thus defines a new atomic potential. In a full-potential method where the charge density is calculated directly, it is not so clear which quantities should be invariant as the atomic potential relaxes. The following choice was used: (1) the value of the charge density over the sphere surface and (2) the decomposition of the total atomic valence charge into contributions from the different angular momenta. If augmentation is done with functions to pure value and slope boundary conditions, a suitable scaling of the pure slope function keeps these quantities fixed as the functions change with the potential.

The problem that the *Fermi energy* is not known before the scan through the Brillouin zone is completed was mentioned at the beginning of this chapter. In a more or less standard way, the problem is solved by accumulating the charge density for three energies [73]. These are ϵ_F^0 and $\epsilon_F^0 \pm \Delta\epsilon_F$ where ϵ_F^0 is the Fermi energy from the last iteration and the size of the window $\Delta\epsilon_F$ is reduced as the Fermi energy becomes stable. The three charge densities define a quadratic approximation for the dependence on the Fermi cutoff. Evaluating this for the new Fermi energy determines weights for combining the three densities. With increasing convergence the window becomes so small that the quadratic approximation does not introduce any error.

Finally, some kind of *mixing scheme* is needed to reach self-consistency at all. The aim is to find a fixed point of the functional $\rho_{\text{out}} = F[\rho_{\text{in}}]$, defined as one whole loop of the cycle. A number of sophisticated schemes exist [20,8] but the simplest method is to calculate a series of charge densities by the prescription $\rho_{n+1} = \beta F[\rho_n] + (1-\beta)\rho_n$. The mixing parameter β can be taken close to one for semiconductors but must be much smaller for metals ($\beta \approx 0.3$). Convergence can be speeded up by choosing $\beta=1$ once in 3 to 4 iterations. The difficult convergence for metals can be traced to the fact that long-wavelength components of the charge density error are weakly damped by one iteration loop. Taking $\beta=1$ from time to time speeds up the convergence of the short wavelengths without letting the long-range part diverge.

(E) TOTAL ENERGY

A large part of the usefulness of the local-density approach is that the total energy can be calculated. In fact, the charge density, the chemical potential, and quantities derived from the total energy are the only results which have unambiguous physical interpretations. By comparing total energies for related systems, it should be possible to predict cohesive energies, the configuration of atoms in space, lattice constants, and elastic properties. In addition, the Born-Oppenheimer approximation makes it possible to calculate vibrational and

phonon frequencies. The energy differences are usually very small so that care must be taken to evaluate the total energy to a high degree of precision, especially in an all-electron method where the core states lead to very large total energies.

The first step towards high precision is to make sure that exactly the functional $E[\rho]$ from eq. (4.21) is evaluated for the current charge density. At true self-consistency, there is no problem because all input and output quantities are the same. In practice this is almost never attained, but the current ρ will be close to the true self-consistent charge density ρ_{sc} that $E[\rho]$ is almost exactly equal to $E[\rho_{sc}]$. This way the minimal property of the functional is exploited to reduce the error. The contributions to $E[\rho]$ must be calculated as

$$T_S = \sum_i \epsilon_i - \int \rho V_{\text{eff}}^{(0)} \text{d}\mathbf{r}$$

$$U = \frac{1}{2} \int \rho V_{\text{es}} \text{d}\mathbf{r} + \frac{1}{2} \sum_{\nu} Z_{\nu} V_{\nu}$$
(4.41)

$$E_{\text{xc}} = \int \rho \epsilon_{\text{xc}}(\rho) \text{d}\mathbf{r}$$

where $V_{\text{eff}}^{(0)}$ is the potential *used to make* ρ and V_{es}, V_{ν} are *made using* ρ .

The quantities $\rho, \epsilon_{\text{xc}}, V_{\text{eff}}^{(0)}$ and V_{es} which appear under the integrals are all represented in the same way: as a linear combination of real periodic Hankel functions in which the low L -components have been replaced by numerical functions inside the atomic spheres. An advantage of the Hankel function representation is that the integrals over the interstitial region can all be expressed as simple surface integrals. The following types of products must be integrated:

$$\mathcal{H}_L \mathcal{H}_K, \quad \mathcal{H}_L \mathcal{H}_K, \quad \mathcal{H}_L \mathcal{H}_K, \quad \mathcal{H}_L \mathcal{F}_K, \quad \mathcal{H}_L \mathcal{F}_K.$$

where \mathcal{F}_K is the periodic Hankel function for energy $\epsilon=0$ and the point denotes the energy derivative. The simplest cases are those containing \mathcal{F}_K since for these the two functions have different energies. Thus:

$$\Delta \mathcal{F}_K = 0, \quad \Delta \mathcal{H}_L = -\epsilon_0 \mathcal{H}_L \text{ in } I$$

$$\int_I \mathcal{H}_L \mathcal{F}_K \text{d}\mathbf{r} = \frac{1}{\epsilon} \oint_{\partial I} [\mathcal{H}_L \nabla \mathcal{F}_K - \mathcal{F}_K \nabla \mathcal{H}_L] \cdot \text{d}\mathbf{a}$$

$$\int_I \mathcal{H}_L \mathcal{F}_K \text{d}\mathbf{r} = \frac{\partial}{\partial \epsilon_0} \int_I \mathcal{H}_L \mathcal{F}_K \text{d}\mathbf{r}.$$

The integrals over the sphere surfaces are done using structure-constant

expansions of the functions. The Hankel-Hankel integrals are done by the same principle but are slightly more complicated because all functions have the same energy. For any pair L,K (fixed in the following) define

$$S_{pq} := \int_{\Gamma} \partial_C^{(p)} \partial_C^{(q)} d^3r \quad (4.42)$$

$$J_{pq} := \oint_{\partial\Gamma} [\partial_C^{(p)} \nabla \partial_C^{(q)} - \partial_C^{(q)} \nabla \partial_C^{(p)}] \cdot d\mathbf{a}.$$

The superscripts denote energy derivatives. If $\partial_C^{(p)}$ and $\partial_C^{(q)}$ had been defined to the energies ϵ and ϵ' , respectively, then Gauss' theorem and the differential equations $(\Delta + \epsilon)\partial_C^{(p)} = -p\partial_C^{(p-1)}$ would lead to the recursion relation

$$(\epsilon - \epsilon')S_{pq} = qS_{p,q-1} - pS_{p-1,q} + J_{pq}.$$

In the limits $\epsilon \rightarrow \epsilon'$ and $\epsilon' \rightarrow \epsilon$ two relations result:

$$\begin{aligned} (1+p)S_{pq} &= qS_{p+1,q-1} + J_{p+1,q} \\ (1+q)S_{pq} &= pS_{p-1,q+1} - J_{p,q+1}. \end{aligned} \quad (4.43)$$

Using these, any desired S_{pq} can be calculated from the (easily evaluated) surface integrals. For the case that S_{00} , S_{10} , S_{01} and S_{11} are needed, the recursion makes it necessary to calculate up to the third derivative of the Hankel functions.

The contributions from the atomic spheres are obtained by numerical radial integration. The discussion of the L-truncation of the sums in section 4.1(C) is applicable here also. By including the same angular momenta in the sums for the surface integrals J_{pq} and in the numerical sphere contributions, the final results are *exact*. As before, this is because augmentation is defined as the replacement of the low L-components of a function. The higher components are not small but they are included properly in all integrals.

Applications

In the course of the last years, the covalent semiconductors C, Si and Ge have become standard test cases for general-potential methods. The largest amount of work, both theoretical and experimental, has been done on silicon. To a degree this is a matter of convention since the electronic structure is very similar for the three elements. The results are also typical for covalent systems such as graphite or GaAs. Most realistic calculations of the electronic structure for these systems either use a large plane wave basis (in LAPW or pseudopotential methods) or an equally large LCAO-type of basis. In section 5.1 it is demonstrated that the multipole Green functions make it possible to calculate results which are just as precise as those of the best of the existing methods in a much smaller basis set. Also, it is shown that the efficient Hankel-function plus energy-derivative representation of the interstitial charge density is good enough to calculate even such small effects as elastic energies and phonon frequencies. In section 5.2 the method is used to investigate non-muffin-tin effects in metals.

5.1 Covalent crystals

Results are presented for calculations for silicon and diamond, whereby most emphasis is on Si. The diamond-lattice structure in which silicon crystallizes consists of two interpenetrating fcc lattices, shifted against each other by the vector $a(1/4, 1/4, 1/4)$ where a is the edge of the conventional cubic cell. This results in a four-fold coordination where each atom is situated in the center of a regular tetrahedron of neighbouring atoms. Chemically, this comes from the hybridized sp-orbitals which are occupied by the four valence electrons. The tetrahedral coordination forces the structure to be loosely packed so that roughly speaking about one-half of space is filled by atoms. Characteristic is a very strong concentration of valence charge along bonds between neighbours. The charge density in the interstices is typically about a factor of 10 smaller than that in the center of the bond. The effective potential seen by an electron is very inhomogeneous: first of all, because the loosely-packed arrangement of the ions leads to a strong variation of the nuclear potential and, second, because the concentration of charge along the bonds leads to an inhomogeneous interaction potential. For a

band-structure method, the problems posed by this kind of potential are similar to those encountered when considering molecules.

(A) METHODS AND RESULTS TO DATE

A sign that the calculation of electronic structure for semiconductors is far from trivial is that methods based on several different concepts are in use. In comparison, the methods used for metals are much more closely related. The approaches to the semiconductor problem can be divided into pseudopotential methods, which transform to a smooth potential and usually work in a plane wave basis, and more elaborate and work-intensive methods which attempt to solve the Schrödinger equation exactly for the true potential. The method presented in chapter 5 is to be classified with the latter.

The principle of the pseudopotential is to eliminate the electronic core and the nucleus by defining a smooth potential which gives the proper valence functions outside the core. A true valence state must be orthogonal to all core functions, which leads to oscillations in the valence function and at the same time pushes up the valence state energy. Outside of the core, the oscillations are not noticeable. In a phase-shift description this is equivalent to stating that a phase shift of 2π has no effect. By defining the pseudopotential properly, the solution of the Schrödinger equation (the 'pseudowavefunction') can be made to be nodeless and equal to the true function outside the core. Within these restrictions one tries to construct the potential to be as well-behaved as possible.

The pseudopotential is an elegant way to deal with the core and the Coulomb singularity of the potential and it has been used in many successful calculations for crystals and molecules. The best results have been attained in the framework of local-density theory. There are, however, some problems. First is that the central variable of the local density description is the total electronic charge density and it is not clear that this can be replaced by the pseudocharge density. Since the calculated results are very good in spite of this the question is somewhat academic and possibly a sound theoretical footing can be found. A second point is that, since there is no obvious prescription for defining the pseudopotential, new potentials are being introduced continually. This gives the approach something of the character of a fit to experimental results. With time, three requirements for a good pseudopotential have become clear. First, it must be 'hard-core' that is, repulsive at short distances. Second, it must be non-local, which means (in this context) that different potentials must be used for the different ℓ -components of the pseudowavefunction. Third, it must be norm-conserving: the pseudocharge inside the core region, while permitted to be distorted from the true distribution, must give the proper value when integrated.

This is important for local-density applications where the interstitial charge determines the effective potential. A pseudopotential which fulfills these conditions is that of Hamann, Schluter, and Chiang [37] which has been applied with large success. It is calculated by fitting analytic functions to the results of a self-consistent all-electron calculation for a free atom. The sophisticated potentials which lead to the best results are complicated and tend to lose the elegant simplicity of the original empirical approaches. However, the effort is justified by the quality of the results such as calculated phonon frequencies which lie within a few percent of the measured values. For a thorough discussion and tables of pseudopotentials see [6].

Opposed to the pseudopotential approach there are a number of different methods which treat the region near the nucleus exactly. The LAPW method can easily be modified to include the effect of the general interstitial potential and these results have been presented by Hamann [38], while the similar FLAPW method has been applied to graphite [100]. Other calculations for the electronic structure of Si have used a linear combination of Gaussian orbital [92] or atomic orbital [39] basis. Finally, Jarlborg and Freeman [47] and Glotzel, Segall and Andersen [29] have demonstrated that good results can also be obtained with methods based on atomic spheres if extra empty spheres are added to reduce the size of the interstitial region. By adding two empty spheres centered on the interstices, the set of all sphere centers makes a bcc lattice and standard band-structure methods such as LMTO [4] or ASW [98] can be used. When made self-consistent, the results of all the approaches are in essential agreement except for those of 'soft core' empirical pseudopotentials.

Comparison with experiment is given for the calculated eigenvalues (with photoemission measurements) and for the charge density (by means of x-ray structure factors), among other quantities. Both come out well for most calculations except for the fact that local-density results systematically underestimate the band gap [78,107]. Local density theory also supplies the total energy so that energy-derived quantities can be compared: the cohesive energy, the equilibrium lattice constant and the bulk modulus, which generally agree to within a few percent. Finally, in recent times good results have been presented for elastic constants and phonon frequencies for pseudopotential [103] and a linear combination of atomic orbitals (LCAO) calculation [39].

(B) APPLICATION TO SILICON: EIGENVALUES AND BULK PROPERTIES

Before the method presented in chapters 3 and 4 can be applied, a number of parameters must be fixed. The number of terms in the expansions for the singular and smooth parts of the multipole Green functions must be chosen. Hereby extra singular terms are not expensive (they mean calculating some more structure constants) so the cutoff was arbitrarily and generously taken at $\ell=4$ and the fourth energy derivative. However, it is desirable to keep the number of plane waves in the expansion of the smooth part χ as small as possible, since the effort in setup of the right-hand side of eq. (3.26) and the inversion of the plane wave Hamiltonian go with the third power of the number of plane waves. The effect of truncating the expansion is to introduce numerical noise in the matrix elements which eventually leads to a non-definite eigenvalue problem even if the technique of Appendix C is used. This was studied by first making Si self-consistent using 113 plane waves in the expansion for χ and then examining the dependence of the eigenvalues on the number of plane waves.

The basis for solving the Schrödinger equation included s and p functions on each of the two atoms in the unit cell to two different energy parameters giving secular matrices of dimension 16. The energy parameters were chosen to lie below and in the gap of the 'free electron' bands as explained in section 4.1. At self-consistency, they are located at -1.2 and 0.1 Ry while the valence bands extend from -0.36 to 0.53 Ry so that one energy parameter lies nicely in the middle of the band. Augmentation inside the atomic spheres (of radius 2.1 a.u.) was done up to $\ell=4$. This was also the cutoff for the potential and charge density representations eq. (4.29) and (4.32), which used Hankel functions defined at the energy $\epsilon_0=-0.3$ Ry. The Brillouin zone integration was done using 10 regularly spaced points in the irreducible $1/48$ -th of the fcc Brillouin zone. It is well known that for semiconductors a small number of points is sufficient because there is not the problem of the Fermi cutoff [12].

Table 5.1 gives the bands energies at the symmetry points Γ , X and L as the number of plane waves in χ is varied from 113 to 283. For less than 113 waves, the matrix eigenvalue problem tends to become unstable, especially at the edge of the Brillouin zone, and for more than 283 there is no appreciable change. It can be seen that the states of low energy (specifically the valence band states) are almost constant over the considered range. This corresponds to the discussion of Appendix C that non-definiteness is associated with high energies whereas the lower states are relatively insensitive. A special effect of the numerical noise is that the X_1 states, which should be doubly degenerate by glide-plane symmetry, are split. This is especially pronounced for the upper state

	113	181	259	283	'KKR'	pseudop.	LCGO	LAPW	ASA
Γ_1	-12.04	-12.16	-12.11	-12.11	-12.09	-11.93	-12.20	-12.02	-11.87
Γ_{15}	2.49	2.42	2.46	2.45	2.46	2.53	2.66	2.49	2.59
$\Gamma_{2'}$	3.25	3.20	3.26	3.26	3.22	3.29	3.05	3.18	3.11
X_1	-7.94	-7.98	-7.93	-7.93	-7.88	-7.78	-8.03	-7.84	-7.75
X_4	-3.07	-3.04	-3.02	-3.02	-2.96	-2.88	-3.11	-2.82	-2.72
X_1	0.04	0.46	0.73	0.73	0.37	0.61	0.79	0.55	0.62
X_4	10.27	10.27	10.29	10.30	10.33	9.97	10.11	10.32	10.10
$L_{2'}$	-9.64	-9.77	-9.73	-9.73	-9.68	-9.52	-9.86	-9.64	-9.53
L_1	-7.25	-7.25	-7.22	-7.22	-7.17	-7.00	-7.25	-7.06	-6.93
$L_{3'}$	-1.32	-1.30	-1.30	-1.30	-1.24	-1.20	-1.40	-1.16	-1.05
L_1	2.13	1.65	1.53	1.61	1.39	1.48	1.46	1.40	1.57
L_3	4.02	3.99	4.04	4.05	3.27	3.31	3.66	3.37	3.51

Table 5.1. Eigenvalues of Si at Γ, X , and L in eV calculated with different numbers of plane waves in the expansion of the smooth part of the multipole Green function, and comparison with results of other methods. The valence-band maximum $\Gamma_{25'}$ was set to zero.

	Lattice constant (a. u.)	Bulk modulus (Mbar)	Cohesive energy (eV/atom)
experiment	10.26	0.99	4.66
present result	10.20	0.97	5.4
pseudopotential	10.30	0.98	4.84
ASA	10.22	0.98	4.8

Table 5.2. Comparison of calculated and measured bulk properties of Si.

for which the splitting reaches $\approx 3\text{eV}$ for the 113 plane wave case. In spite of this uncomfortably large value, the occupied valence states all come out well. Since it is of interest to determine how efficient the method can be made while still giving good results, the following calculations were all done using the same number of 113 waves for the χ -expansion.

For comparison, the last four columns of Table 5.1 give the eigenvalues at the symmetry points for some representative self-consistent calculations with other methods. These are: the calculation using the Hamann-Schlüter-Chiang ab-initio pseudopotential done by Yin and Cohen [102], the linear combination of Gaussian orbitals method (LCGO) [92], the full-potential LAPW calculation [38], and the LMTO calculation of Glötzel, Segal and Andersen [29]. In the latter, overlapping atomic and empty spheres are used and the Γ_2 level includes the so-called combined correction term [4]. It is seen that the present calculation compares well with the other results. To determine the effect of using only two fixed energies in the interstitial, more precise eigenvalues were determined by varying the upper energy parameter until it was equal to the eigenvalue for one state at a time. These energies are given in the column labeled 'KKR'. The shifts in this process are small and it is concluded that the double basis is adequate to describe the energy dependence of the interstitial wave function. As in the ASW method, the effect of a restricted energy basis is to pull the bands apart by a small amount. The overall effect of the shifts is to move the eigenvalues very close to the LAPW result. The notable exception is again the X_1 level at 0.55 eV which comes out too low by about 0.2 eV. This will be discussed later in connection with the charge density. The good agreement with the other calculations shows that it is indeed adequate to use the small number of 113 plane waves in the χ -expansion when making the potential self-consistent.

Next, the total energy and derived bulk quantities are considered. The bulk properties of Si are determined by performing a number of calculations at slightly different lattice constants. The position and depth of the minimum in the total energy give the theoretical lattice constant and cohesive energy, respectively, while the curvature predicts the bulk modulus. These values are compared with experiment [32] as well as with the pseudopotential and ASA results in Table 5.2. For the other self-consistent methods these numbers come out very well also: for Si the agreement is in general even better than for most other materials. In the present calculation the equilibrium lattice constant and the bulk modulus are predicted to within 2% but the crystal seems to be too strongly bound. However, this deviation of about 15% is not larger than what is found for many other elements as can be seen from the systematic calculations by Moruzzi, Janak and Williams for the metallic elements [73]. These are also consistent with the present result in that the theoretical cohesive energy always

comes out too large. As is suggested by them, there is a strong probability that the deviations are caused by errors in the total energy calculated for the free atom. For an isolated Si atom the ground state is spin-polarized whereby the two p electrons have parallel spins and are in the same angular momentum state. Consequently, it is possible that the spherical approximation to the charge density and potential, used when making the atom self-consistent, result in noticeable errors. Similar related arguments are given by Wimmer et al. [100], who calculated a cohesive energy too large by about 1.3 eV/atom for a graphite monolayer using the FLAPW method. They attribute the discrepancy to the neglect of correlation with low-lying atomic states in the atomic calculation. Also, they report that the cohesive energy is much more sensitive to the quality of the basis than other calculated quantities such as lattice parameters or force constants. This was also observed for the present calculation. When the number of terms in the expansion of χ was increased, the cohesive energy stabilized at about 5.4 eV, which is 0.7 eV larger than the experimental value and 0.3 eV larger than the value calculated using 113 terms. The bulk modulus and the lattice constant were essentially unchanged and the total energy *changes* are predicted correctly using 113 terms (see part (D)).

Another possible explanation for the discrepancy is that the representation for the charge density, using only a few atom-centered Hankel functions and their energy derivatives, is not good enough. Because of the large Hartree term in the total energy, small errors in the charge distribution could have a large effect on the total energy. To check this, the energy of the Hankel functions was varied from -0.15 to -0.60 Ry, corresponding to a factor two change in the localization. The total energy changed by only 8 mRy and was minimal for a Hankel energy of about -0.25 Ry. This was also the value for which the mismatch between the fitted interstitial charge density and the charge density inside the spheres was smallest (less than 2%). Thus, the charge density representation used here is not responsible for the calculated overbinding. In summary, the results presented here strengthen the conclusion of Wimmer et al.: that agreement in the cohesive energy is not necessarily a useful criterium for the quality of a calculation.

(C) CHARGE DENSITY

In Fig. 5.1a, the calculated charge density for Si is presented. Analogous calculations were done for carbon in the diamond structure at the experimental lattice constant 6.75 a.u. and these are shown in Fig. 5.1b. It is interesting to see that the total charge densities for Si and C are much more alike than the valence contributions alone. For both materials, the results in Fig. 5.1 are very similar

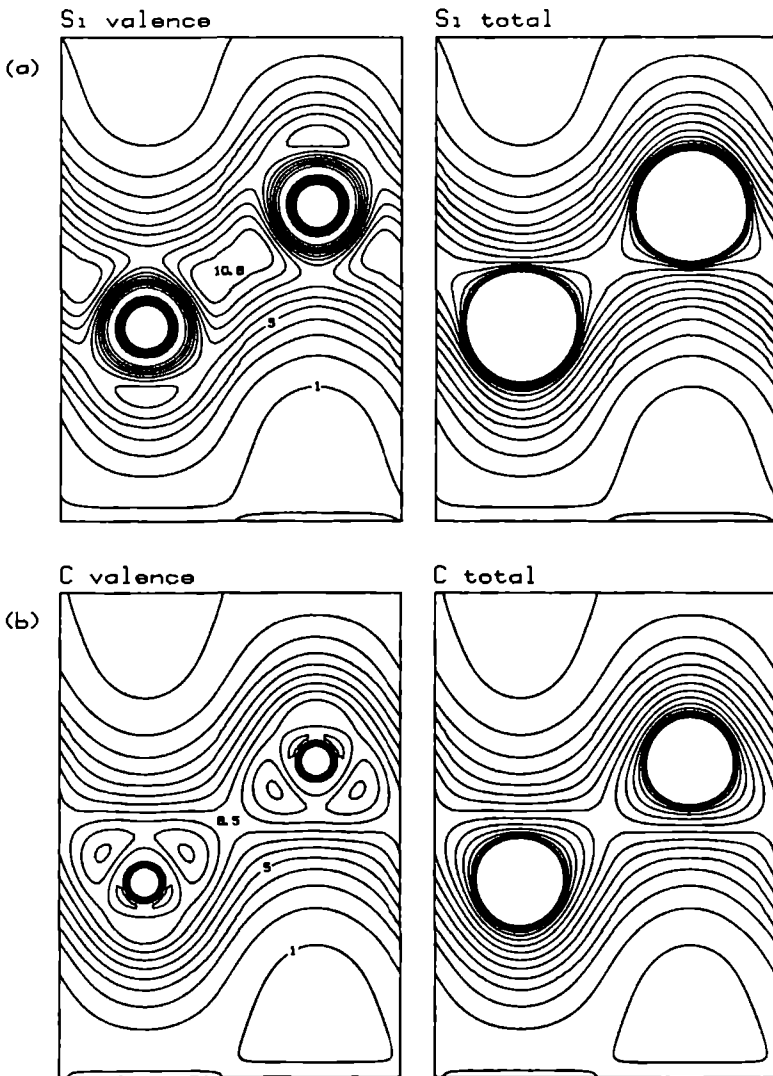


Figure 5.1a,b. Contour plots of the calculated charge density for (a) Si and (b) C in the $(1\bar{1}0)$ plane of the diamond structure. The contour interval is one electron/atomic volume. Both the valence and the total charge density are presented. Note that the total densities of Si and C are very similar while the valence densities show large differences.

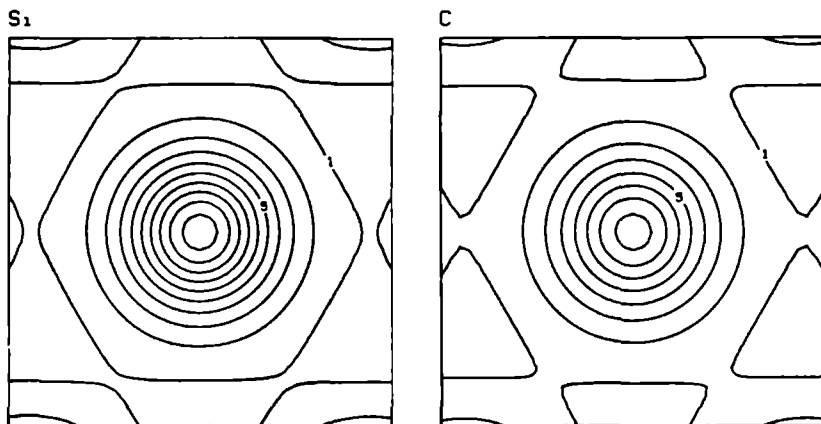


Figure 5.1c. Cross-sections through the total charge density for Si and C.

	exp	MPGF	LCGO	pseudop.	valence	core
000	(28)	(28)	(28)	(28)	(8.0)	(20)
111	15.19	15.09	15.11	15.13	1.718	13.374
220	17.30	17.30	17.26	17.23	0.006	17.298
331	11.35	11.40	11.37	11.28	-0.219	11.618
222	0.38	0.34	0.25	0.34	0.338	0.000
400	14.89	14.96	14.92	14.76	-0.174	15.131
331	10.25	10.21	10.17	10.11	0.005	10.203
422	13.42	13.38	13.37	13.22	0.005	13.372
333	9.09	9.06	9.07	8.92	0.015	9.049
511	9.11	9.07	9.08	8.96	0.021	9.049
440	12.08	12.03	12.04	11.88	0.100	11.928
Q_{bond} (el/at.vol.)	13.8	10.7	10.65	11.7	-	-

Table 5.3. Comparison of calculated and measured x-ray structure factors. The last two columns separate the present result (under the heading MPGF) into valence and core contributions.

to those of pseudopotential calculations using Hamann-Schluter-Chiang potentials [102,21] The valence charge density for C shows the double hump along the bond which is also found by pseudopotential methods [44] Note that close inspection of the contour plots reveals the small mismatch at the sphere surfaces Calculations of this type are usually compared with similar plots of the valence charge density for Si which were generated from the measured x-ray data by Yang and Coppen [101] Since they estimate an error of only 0.15 electron/cell, corresponding to about 1% of the value at the band maximum, the comparison is of obvious interest Alternatively, one can calculate the x-ray structure factors (the Fourier coefficients of the charge density) and compare these with experimental values [2,80] The calculated and measured structure factors are listed in Table 5.3 together with some other theoretical results For either way of comparison, the core states must be taken into account in some way, since the x-ray data includes (and in fact is dominated by) the core contributions This can be seen from the last two columns in Table 5.3 which separate the total calculated structure factors into valence and core parts Yang and Coppen used the results of Hartree-Fock calculations to subtract off the core before synthesizing the experimental valence charge density In complement to this, the structure factors of the valence charge density from the pseudopotential calculation were added to those of the cores from an isolated atom by Yin and Cohen to obtain the figures quoted in the second column

Contour plots of the valence charge density can be found for most calculations on Si, for example, also in refs [21,109] in addition to the pseudopotential, LAPW and LCGO papers In general the overall shape of the distribution agrees well with the experimental result as is also the case for the distributions shown in Fig. 5.1 The only exceptions are charge densities derived from empirical 'soft-core' pseudopotentials which tend to spread out charge too much perpendicular to the bond This was demonstrated in detail by Hamann [38]

When absolute values of the charge density are compared, however, the deviation between theory and experiment is somewhat larger The values ρ_{bond} for the maximum in the bond in the last row of Table 5.3 together with the LAPW result ($\rho_{\text{bond}}=11$) show that theory consistently lies too low by about 10-20% Of course, the systematic deviation between calculated and measured band-maximum charge density has led to suggestions that maybe the error in the experimentally derived value is larger than stated after all [108] The present result is close to those of the LAPW and LCGO, all of which are smaller than the pseudopotential value While pseudopotential seems to be doing best in this context, the situation is different when the x-ray structure factors in the top part of Table 5.3 are compared Considering the small magnitude of the valence part for most terms, it is seen that the pseudovalence contribution calculated by Yin

and Cohen must be off by a substantial amount for a number of reflections; for example, for the cases (220) and (440). The best values are from the LCGO calculation which are close to the present results. Note that both methods include the effect of the valence states on the core properly. Unfortunately the structure factors for the LAPW calculation are not available. It is somewhat surprising that the 'forbidden' (222) reflection, which is described well by the present and the pseudopotential methods, comes out wrong for the LCGO approach. The (222) reflection comes about through the charge density in the bond and this lies close to other theoretical values for the LCGO method.

From the discussion above, it is concluded that the charge density in the interstitial region is well described by the simple Hankel function representation used here. This is an interesting result for a number of reasons. First, there is practically no work per k-point associated with the accumulation of the charge density. Opposed to this, the plane wave representation used for example by full-potential LAPW methods requires a large amount of the computing time. Second, as was described in chapter 4, the expansion in periodic Hankel functions makes it simple to solve the Poisson equation and to evaluate the interstitial integrals for the total energy. There is one problem, however, in that the value of the charge density at the interstices will not necessarily come out exactly right by the fit to value and slope on the sphere surfaces. This is the origin of the 0.2 eV shift of the X_1 level discussed under (B). As was shown by Rompa et al. [81], this state is especially sensitive to potential perturbations at the interstices. The values in column labeled 'KKR' of Table 5.1 were calculated using an energy of $\epsilon_0 = -0.3$ for the Hankel functions charge density basis which led to a value of $\rho_0 = 0.4$ el/atomic volume at the interstices. Using the energy $\epsilon_0 = -0.6$ instead, one finds that ρ_0 is now equal to 0.6, which is close to the value of 0.7 given by the pseudopotential calculation, and that the X_1 eigenvalue now comes out to 0.58 eV. This is in agreement with the LAPW result. This deficiency of the charge-density representation could easily be solved by using the exact accumulated charge density at the interstice as an extra constraint when fitting the Hankel functions. The extra work hereby would be is no more than the calculation of a few more reduced structure constants at every k-point.

(D) DISTORTION ENERGIES

Once a band structure method has been shown to describe the ground state properly, further information can be extracted by determining the response of the total energy to perturbations of the atomic positions. Of special interest are so-called 'frozen phonon' calculations. The total energy is determined for the system with the atoms shifted slightly from their equilibrium positions according

to some prescribed phonon mode. Because of their smaller mass, the electrons in a real crystal can be assumed to follow the motion of the nuclei instantaneously so that the electron system is always in the ground state (Born-Oppenheimer approximation [10]). Thus the static calculation of the perturbed crystal describes realistically the instantaneous state of a crystal oscillating with the phonon mode. From the total energy as a function of the atomic displacement, the phonon frequency as well as anharmonic terms can be derived. A different but related approach is to use the Hellmann-Feynman theorem to find the forces on the other atoms caused by the perturbation of one atom [60]. A special frozen phonon case is the limit as the wave vector approaches zero; then the wavelength of the phonon becomes much longer than the size of the unit cell and the acoustical phonon frequencies can be derived from the elastic constants of the crystal. For all calculations of this type the energy differences under consideration are at most a few mRy so that a precise treatment of all energy contributions is necessary. Specifically any kind of straightforward muffin-tin approach will fail since the important effect of the unsymmetric charge distribution around the perturbed atom is ignored*. In the following it is shown that the multipole Green function basis properly describes phonon and shear modes in *ab-initio* all electron calculations.

To calculate the elastic shear constants, the unit cell is distorted at constant volume. For tetragonal distortion the z axis is stretched by a factor $(1+\alpha)$ and the x,y axes are scaled by $(1+\alpha)^{-1/2}$. To first order in α , the distortion is given as

$$\begin{bmatrix} x' \\ y' \\ z' \end{bmatrix} = \begin{bmatrix} x \\ y \\ z \end{bmatrix} + \alpha \begin{bmatrix} -1/2 & 0 & 0 \\ 0 & -1/2 & 0 \\ 0 & 0 & 1 \end{bmatrix} \begin{bmatrix} x \\ y \\ z \end{bmatrix}. \quad (5.1)$$

The leading (quadratic) term in the total energy charge per unit cell is given by elasticity theory [5] as

$$W_{\text{tet}} = \frac{3}{4} \Omega (C_{11} - C_{12}) \alpha^2. \quad (5.2)$$

Ω is the volume of the cell. The corresponding expressions for a trigonal distortion are

* Good results have been obtained in the framework of LMTO-ASA for the elastic constants of metals if the electrostatic energy terms are evaluated carefully (Christensen [15]).

$$\begin{bmatrix} x' \\ y' \\ z' \end{bmatrix} = \begin{bmatrix} x \\ y \\ z \end{bmatrix} + \alpha \begin{bmatrix} 0 & \frac{1}{2} & \frac{1}{2} \\ \frac{1}{2} & 0 & \frac{1}{2} \\ \frac{1}{2} & \frac{1}{2} & 0 \end{bmatrix} \begin{bmatrix} x \\ y \\ z \end{bmatrix} \quad (5.3)$$

$$W_{\text{trig}} = \frac{3}{2} \Omega C_{44} \alpha^2 \quad (5.4)$$

where the (111) direction is scaled by $(1+\alpha)$ and the two orthogonal directions are scaled by $(1+\alpha)^{-1/2}$. By using the calculated bulk modulus and the relation $B=(C_{11}+2C_{12})/3$, one can now predict all three elastic constants. The distortion reduces the symmetry so that twice, respectively three times the number of k-points must be calculated. It is important to keep the set of points for the Brillouin zone integration fixed, that is, to transform them reciprocally to the distortion in real space. The distorted crystals were made self-consistent for values of $\alpha=0, \pm 0.02, \pm 0.04$ and a least-squares fit of a third-order polynomial was made to the five calculated total energies. From the coefficient of the quadratic term, the shear constants $C' = C_{11} - C_{12}$ and C_{44} are determined.

For the tetragonal distortion, the result calculated in this way is $C_{11} - C_{12} = 0.98$ Mbar which compares well with the experimental value of 1.02 Mbar [5]. The pseudopotential result (1.07 Mbar) is about equally good [102]. The case of the trigonal distortion is slightly more complicated due the fact that the symmetry between the four bonds around a site is broken. A stress along the [111] direction gives rise to an internal strain which corresponds to an extra shift of the two sublattices against each other [39]. The equilibrium state of the strained crystal can be reached by way of a linear homogeneous distortion of the unit cell plus a further relaxation of the atoms along the [111] direction. Physically, the effect is that the energy cost of the distortion is reduced if the lengths of the two types of bonds remain approximately equal. The internal strain is described by a parameter ζ which is equal to zero for a linear distortion (no further relaxation) and equal to one if all bond lengths are equal. A calculation which did not take into account the internal strain led to a result of 0.85 Mbar for C_{44} , which is slightly larger than the experimental value (0.80 Mbar). One could expect the additional relaxation to reduce this error since the total energy of the distorted crystal is lowered. This was investigated by mapping out the total energy as a function of the internal strain parameter for each of the five trigonal distortions. However, the value of $C_{44} = 0.57$ found this way is $\approx 30\%$ too small whereas the calculated internal strain parameter (0.55) is in reasonable agreement with experiment ($\zeta = 0.62$). The relaxation correction to C_{44} can also be estimated by using the measured values of ζ and the frequency of the TO(Γ) phonon (see below), leading to about the same

result as calculated. Thus, the error already lies in the total energy calculated for the homogeneously distorted crystal: this might indicate the limits of the straightforward charge-density representation used here. Note that the very involved representation in the LCAO calculation [39] obtains a better value of 0.61 for ζ . Unfortunately and somewhat surprisingly, no predictions for C_{44} from comparable calculations (either all-electron or pseudopotential) are available.

At Γ , there is one triply-degenerate optical phonon mode in Si. For this $\text{TO}(\Gamma)$ mode the two atoms in the fcc unit cell move against each other. The pseudopotential calculation [103] as well as the LCAO all-electron method [39] were able to calculate the frequency and first anharmonic term properly. Similar results were obtained by Chelikowsky and Louie [14] for diamond. To reproduce this, five self-consistent calculations were done for Si with the atoms situated at $\pm a(\xi, \xi, \xi)$ where ξ ranged from 0.120 to 0.130 in steps of 0.0025. This corresponds to shifting the atoms by ± 0.0444 and 0.0889 a.u. from their equilibrium positions. The resulting total energies and the least-squares fit with a second plus a third-order term is shown in Fig. 5.2. The coefficients of the fit give the phonon frequency and an experimentally measured cubic force constant denoted by k_{xyz} as is described in ref. [103]. The comparison of the values for the present, the pseudopotential, and the LCAO calculations with the experiment is as follows:

	exper- iment	present result	pseudo- potential	LCAO	
f	15.53	15.12	15.16	15.0	THz
k_{xyz}	-35.1	-36.9	-32.8	-34.8	ev/Å ³

The agreement is in all cases about equally good.

From the sign of the anharmonic term it follows that it costs more energy to compress the bond than to expand it. It is of interest to find the cause for this in the way in which the charge density is distorted. If $\delta q(u)$ is the change in the charge distribution for a displacement u of the atoms towards each other, then to second order in u ,

$$\delta q(r) = u f_1(r) + \frac{1}{2} u^2 f_2(r). \quad (5.5)$$

In the harmonic regime, the second term is negligible. The two terms can be separated by adding and subtracting the changes for $+u$ and $-u$:

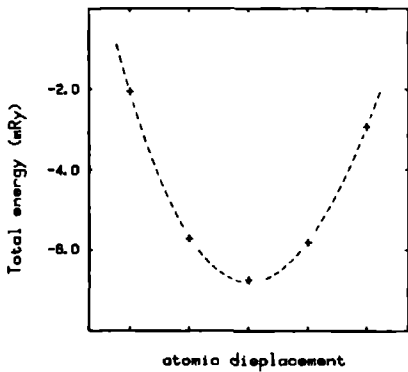
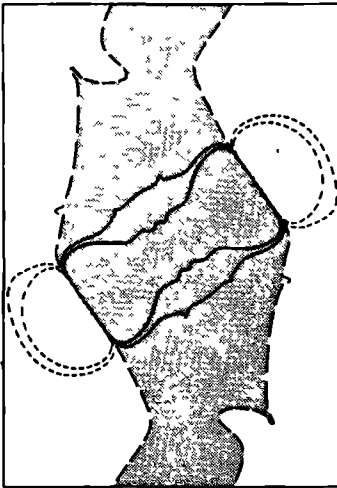


Figure 5.2. The mRy-part of the calculated total energies per fcc unit cell for five frozen phonons corresponding to the optical mode at Γ in Si (crosses). The total energy for unperturbed Si is -1153.6368 Ry. The atomic displacements were ± 0.0444 and ± 0.0889 a.u. The dashed line is least-squares fit by a polynomial with a zeroth, second and third-order term.

(a)



(b)



Figure 5.3. The linear term (a) and the quadratic term (b) in the change of the total charge density for frozen phonons with $u = \pm 0.0899$ a.u. The positive parts are shaded. The contour interval is 0.5 e/atomic volume for the linear term and 0.025 e/atomic volume for the quadratic (see eq. 5.5).

$$\begin{aligned}
 uf_1(\mathbf{r}) &= \frac{1}{2} \{ \delta\rho(\mathbf{u}) - \delta\rho(-\mathbf{u}) \} \\
 \frac{1}{2} u^2 f_2(\mathbf{r}) &= \frac{1}{2} \{ \delta\rho(\mathbf{u}) + \delta\rho(-\mathbf{u}) \}.
 \end{aligned}
 \tag{5.6}$$

Since $\delta\rho(-\mathbf{u}) \approx -\delta\rho(\mathbf{u})$, the first function is made by averaging two similar distributions while the second is their difference. The functions are shown in Fig. 5.3a and b. The contour plots for $\delta\rho(\mathbf{u})$ and $\delta\rho(-\mathbf{u})$ are both very similar to that of uf_1 . Of course, the small mismatch on the surfaces of the spheres is amplified by the higher-order differencing, resulting in the small spikes in Fig. 5.3a and in some obvious distortion in Fig. 5.3b. However, this is unimportant for the linear term and qualitative information can still be won from the plot of the quadratic term. The first and second-order shifts of the atomic positions lead to charge density variations of dipole and quadrupole character, respectively, near the atoms. This is similar to the generation of the distributions D_L used in section 3.1. In the linear term (Fig. 5.3a), the dipoles connect together to an island between the atoms; the positive contours describe the charge which is added by a compression and removed by an expansion of the bond. This is the expected result that charge piles up in the bond when the atoms are moved closer together. The next-higher term (Fig. 5.3b) shows the function which is positive at those points where the amount of charge added on compression is larger than that which is removed on expansion. As can be seen from the 0.05 electron/atomic volume contour, this is also a quite localized patch between the atoms. Therefore the anharmonic extra energy cost for a bond compression comes about through an increasing localization of electrons which must be paid for by higher kinetic and electrostatic energies.

A contour plot of the distortion of the pseudocharge density similar to Fig. 5.3a is shown by Yin and Cohen. They find patches of negative charge distortion between the positive maximum at the bond center of and the atoms. These are also seen if a plot similar to Fig. 5.3a is made without the core contributions (Fig. 5.4). The subtraction of valence charge near the atoms when the atoms are moved closer together arises because the valence electrons move away as the core is pushed into the bond. It is interesting that the pseudopotential can describe this effect properly; this is only possible because it is hard-core. Use of a soft-core potential would lead to a smaller value of the charge distortion at the bond center and presumably to a wrong phonon frequency. However, even for the good pseudopotential results of Yin and Cohen and the all-electron results presented here there is some deviation. For the charge buildup at the bond center, they get a value of about 17 electron/atomic volume per 1 a.u. of atomic displacement while the present result is about 20% smaller. It is surprising that in spite of this discrepancy, the frequency and anharmonic term come out

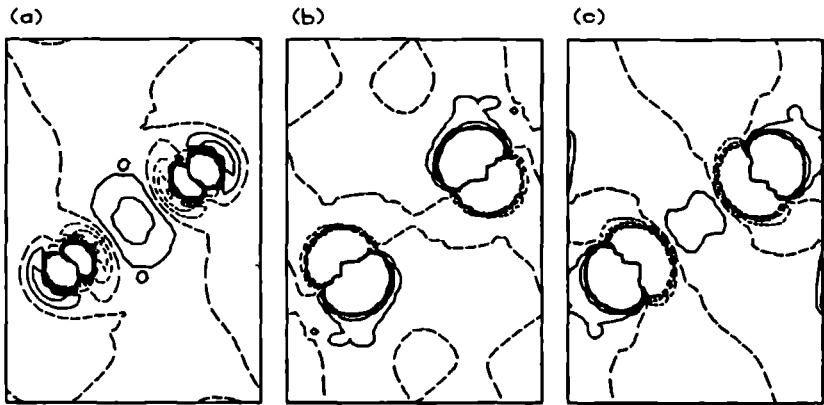


Figure 5.4. (a) Change in the valence charge density for a frozen phonon with a compression of 0.0899 a.u. along the bond (contour interval 0.025 e/atomic volume). (b) Distortion of the valence charge density for the tetragonal shear mode. (c) The same for the trigonal shear mode.

properly in both cases, indicating that perhaps details of the charge distortion are less important for correct frozen phonon energies than expected.

To conclude this section: It was shown that all results obtainable by other methods for silicon can be reproduced using the compact 16-function basis set of multipole Green functions. This is relevant because Si is the standard example of a system for which the muffin-tin approximation fails. The results which were calculated correctly included the energy bands, the static bulk properties, the charge density, and the change in the total energy for perturbations of the atomic positions.

5.2 Metals

The close-packed metals are the systems for which the muffin-tin approximation has been used with the greatest success. The interstitial region contains only a small part of the total volume and the potential is relatively flat there, since points in the interstitial region are about equidistant from the neighboring Coulomb singularities. The effect of non-muffin-tin terms on the eigenvalues has been estimated to be in the order of a few mRy, for example by use of the KKR discrete-variational method [77]. In general the bulk properties come out well within the muffin-tin approximation but calculated frozen-phonon or shear

energies do not. To determine the error made by the flat interstitial potential, the transition metal rhodium was made self-consistent at the experimental lattice constant for both the full potential and with a flat interstitial potential. The effects can be expected to be largest for transition metals because of the partly-filled d bands. Fig. 5.5 compares the energy bands for the two types of potential. It is seen that the eigenvalues are very similar. However, the small differences in the eigenstates add up to a larger deviation in the total charge density as can be seen from Fig. 5.6. The net effect of the uniform interstitial potential is to reduce the difference between the maximal and minimal charge density; these are at the octahedral and tetrahedral interstices, respectively. At the points where the distance between neighboring spheres becomes the smallest the charge density is unchanged. Fig. 5.6 shows that the uniform potential flattens out variations of about 200 mRy between the two types of interstices. Consequently there is an artificial transfer of charge from the tetrahedral site (where the true potential is low) to the octahedral site. The total error made in this way is about 10% which is smaller than would be expected from the size of the potential deviation. One can conclude that the muffin-tin approximation works, not so much because the true potential is flat in the interstitial region, but because of the insensitivity of the wave function to perturbations of the interstitial potential. As a consequence of the cubic symmetry, the non-flat potential terms are either of a high-order angular momentum or vary in the radial direction (relative to the center of the cell). In both cases the variation is of a short-wavelength type which has a small influence on the wave function where the kinetic energy is low (see section 3.2(B)).

5.3 Conclusions

The calculations in this chapter have demonstrated the usefulness of an atom-centered description for an exact treatment of the interstitial region in two connections. First, it was shown that the multipole Green function basis correctly solves the Schrödinger equation for the true crystal potential. This is not surprising since the functions were constructed to be solutions in the interstitial. While there is some work in setting up the functions, this is compensated by the conceptual simplicity and by the small basis size. In the same way as in KKR the basis can be tailored to include exactly the needed degrees of freedom; first, by choosing the energy parameters to lie in the proper range and second, by choosing the angular momentum cutoff properly. Thus, in the same way as in the ASW or LMTO methods, s and p functions alone make an adequate basis for Si

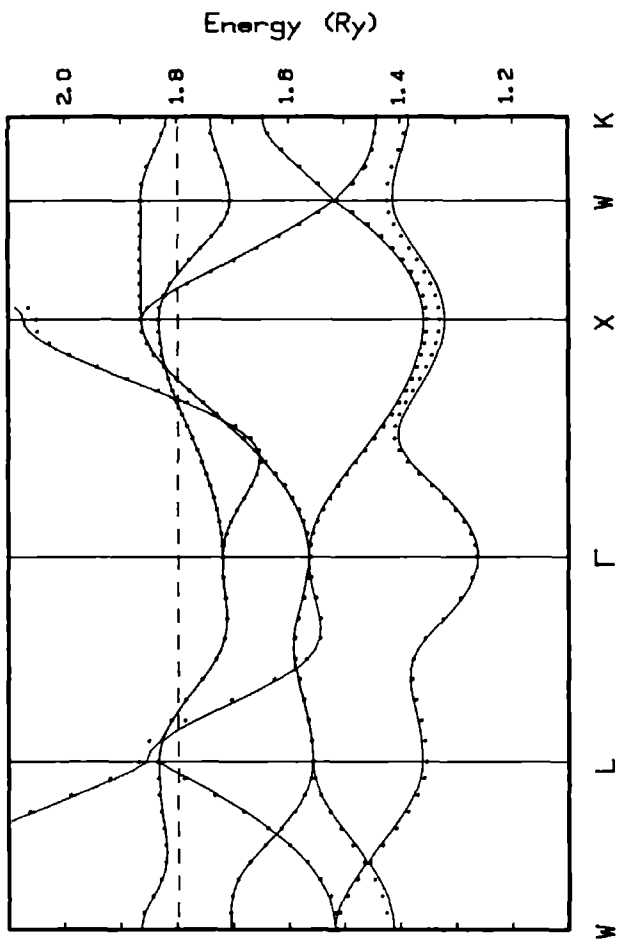


Figure 5.5. Comparison of the energy bands of Rh for self-consistent calculations using a flat interstitial potential (connected line) and the full potential (dots).

while d functions are included for a transition metal. The second point which demonstrates the utility of the atom-centered description is the unexpected fact that the interstitial charge density is well described by a simple scheme in which the behaviour on the sphere surfaces is fitted by atom-centered Hankel functions in the interstitial. The description is good enough to lead to the correct values for subtle energy differences such as frozen phonon energies. At the same time it is very efficient and permits an easy evaluation of the electrostatic potential and total energy integrals.

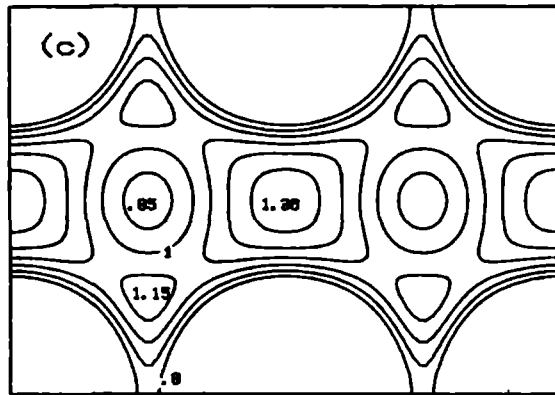
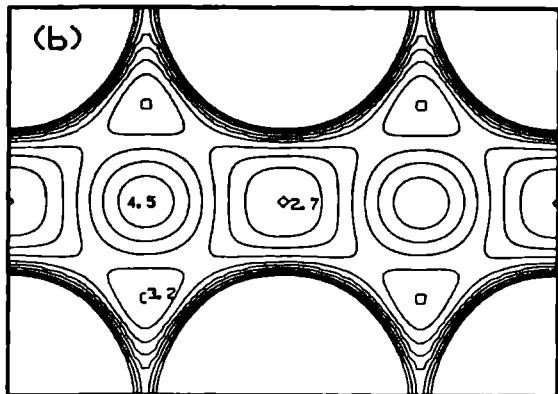
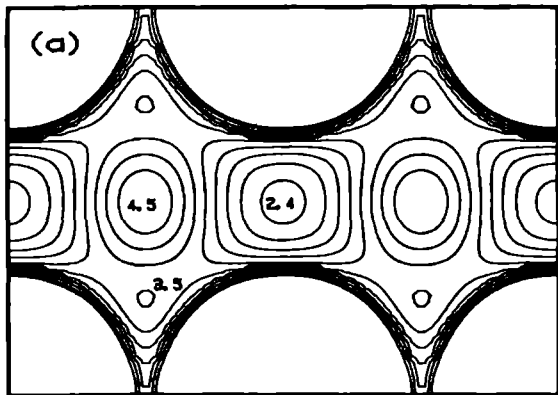


Figure 5.6. Calculated self-consistent charge density of Rh in the (110) plane for a constant interstitial potential (a) and the full potential (b). The true potential in the interstitial is shown in (c) with a contour interval of 0.1 Ry. The value for the constant potential in the muffin-tin case is 1.07 Ry.

The Analytic-Quadratic Integration Method

A second independent topic which is treated in this thesis is the numerical evaluation of singular Brillouin-zone integrals. These are of the general form

$$F(\epsilon) = \int_{\text{BZ}} u(\mathbf{k})\delta[\epsilon - E(\mathbf{k})]d\mathbf{k}$$

where $u(\mathbf{k})$ is some well-behaved function and $E(\mathbf{k})$ is an energy band. The most common example is the density of states but integrals of this type must be calculated for many other quantities of interest such as, for example, susceptibilities. The input data consists of the values of $u(\mathbf{k})$ and $E(\mathbf{k})$ over some mesh of points through the Brillouin zone. A frequently used method of the type which to be considered in this chapter was developed by Jepsen and Andersen [48] and Lehmann and Taut [61]. They divide space into small tetrahedra and use a linear interpolation of $E(\mathbf{k})$ throughout each tetrahedron. This approach has the disadvantage that it fails near Van Hove singularities, which are integrable singularities in $F(\epsilon)$ caused by points in \mathbf{k} -space for which the gradient of the energy band vanishes. The contributions calculated for close-by tetrahedra become unpredictable since the linear term alone does not describe the band adequately. The result is spurious oscillatory 'noise' in the calculated quantity $F(\epsilon)$ as ϵ approaches the singularity energy. This effect was the motivation for developing a tetrahedral integration technique which expands $u(\mathbf{k})$ to linear and $E(\mathbf{k})$ to quadratic order. The first part of this chapter presents the method for the density of states, that is, for the case that u is constant. The second part then extends the method to include general functions $u(\mathbf{k})$.

LETTER TO THE EDITOR

Analytic-quadratic method of calculating the density of states

M S Methfessel, M H Boon and F M Mueller

Research Institute for Materials and Faculty of Science, Toernooiveld, Nijmegen, 6525 ED, The Netherlands

Received 4 July 1983

Abstract. A new analytic method of calculating the density of states based on local quadratic expansions is given. Results are presented for the tight binding s band and for the valence bands of silicon. These show that the new technique properly treats van Hove singularities, where the commonly applied method using local linear expansions fails.

The density of states is defined as

$$D(\epsilon) = \int \frac{dS}{|\nabla E(\mathbf{k})|} \tag{1}$$

where the integral is taken over the constant energy surface $E(\mathbf{k}) = \epsilon$ in the Brillouin zone and $E(\mathbf{k})$ is a band energy. Two methods have been used in practical calculations: constructing a histogram by sampling on a large number of points in the Brillouin zone and the linear integration method of Lehmann and Taut (1972). In the latter method, the Brillouin zone is divided into a large number of small tetrahedra and the energy band is interpolated linearly within each tetrahedron. In our method, the Brillouin zone is again divided into tetrahedra but $E(\mathbf{k})$ is expanded to quadratic order as

$$E(\mathbf{k}) = \mathbf{k}^T A \mathbf{k} + B^T \mathbf{k} + C \tag{2}$$

where A is a (non-singular) symmetric (3×3) matrix, B is a vector and C is a constant. We have derived expressions for the density of states contribution as determined by A , B , C and the geometry of the tetrahedron. While it is not necessary to use tetrahedra as basic space-filling volume elements, the choice is natural because the ten constants in the interpolation (2) can be fixed uniquely by prescribing the values at the corners and mid-edges of the tetrahedron.

In every tetrahedron, we can shift the origin of energy by adding a constant and shift the origin of the coordinate system in reciprocal space. Such shifts remove both the linear and the constant terms in equation (2). Therefore, in the following we assume the reduced dispersion relation

$$E(\mathbf{k}) = \mathbf{k}^T A \mathbf{k} \tag{3}$$

holds. From the matrix A we define a scalar product and generalised angles. The density of states is a function of generalised angles and consists of a series of piecewise analytic functions

Letter to the Editor

To construct the density of states contribution, our prescription is the following. For a given energy ϵ one determines the curved polygon formed by the intersection of the tetrahedron faces with the constant energy surface. Such a polygon consists of a closed connected series of curved lines. The energy derivative of the density of states is governed by the sum of the generalised angles at the vertices of the intersection polygon

$$\frac{dD(\epsilon)}{d\epsilon} = \frac{1}{4} |\det A|^{-1/2} |\epsilon|^{-1/2} \{\sum \alpha_i(\epsilon) - m\pi\} \quad (4)$$

where m is an integer and the $\alpha_i(\epsilon)$ are generalised angles. The above expression is a generalisation of the well-known formula expressing the area of a spherical triangle as the sum of the three vertex angles minus π . Since the polygon changes with energy, both the angles and the number of vertices are energy dependent. As an example, consider the simplest possible case where (3) is a spherical dispersion relation and where the corners of the tetrahedron are $(0, 0, 0)$, $(1, 0, 0)$, $(1, 1, 0)$ and $(1, 1, 1)$ with energies 0, 1, 2 and 3 respectively. The intersection polygon is first a curved triangle in the energy range from 0 to 1, then a curved quadrilateral from 1 to 2, and finally a curved triangle again as the constant energy sphere passes over the tetrahedron. More complicated cases occur if the origin of the quadratic form lies inside the tetrahedron or if an edge is reached before the corresponding vertices. Our formalism applies to all cases in the same way.

The generalised angles are derived from the scalar product

$$[x, y] = x^T A y \quad (5)$$

which is positive or negative definite for ellipsoidal cases and indefinite for hyperboloidal cases. The metric is Euclidian only when A is the unit matrix but all cases can be treated by the same formalism. The constant energy surface is given by the condition $[k, k] = \epsilon$ and is a sphere in the sense of the A metric but is an ellipsoid or a hyperboloid in the normal sense. To obtain α_i , the angles in the vertices of the polygon are calculated by using the scalar product between normalised vectors which lie simultaneously in the face of the tetrahedron and in the plane tangent to the surface of energy ϵ . There are six functions $\alpha_i(\epsilon)$, each one corresponding to one edge of the tetrahedron. For the ellipsoidal cases, each one is of the form

$$\alpha(\epsilon) = \tan^{-1}[T_1(1 - \epsilon_0/\epsilon)^{1/2}] + \tan^{-1}[T_2(1 - \epsilon_0/\epsilon)^{1/2}] \quad (6)$$

The parameters T_1 , T_2 and ϵ_0 are calculated from the geometry of the tetrahedron using the scalar product (5). T_1 and T_2 are the tangents of two angles whose sum is the dihedral angle between the faces meeting at the given edge and ϵ_0 is the energy at which the edge is first touched by the constant energy surface. For the hyperboloid cases a similar expression holds but with hyperbolic functions taking the place of trigonometric functions. The expressions may be derived from (6) by analytic continuation. A practical realisation of the method consists of two steps. First, one calculates all the necessary parameters entering in (6), and second, the functions $\alpha_i(\epsilon)$ are assembled to yield $dD(\epsilon)/d\epsilon$. The integer m depends on the signature of the quadratic form and on the number of vertices of the polygon and is most easily calculated from continuity requirements. The density of states is determined by integrating (4) analytically. A FORTRAN program working along these lines is available on request.

The proof of equation (4) follows from differential geometry. The central result is an expression for the area of a polygon on ellipsoidal and hyperboloidal surfaces,

again in the sense of the metric defined in equation (5). This is derived from the Gauss–Bonnet theorem and related formulae (Eisenhart 1947). The proofs and details of the method will be presented in a subsequent paper.

As a first application we consider the simple cubic s band:

$$E(\mathbf{k}) = -(\cos \pi k_x + \cos \pi k_y + \cos \pi k_z)/3. \quad (7)$$

The structure is well known and contains four van Hove singularities. In figure 1(a) we compare the density of states using both the analytic–quadratic as well as the linear method. Figure 1(b) shows the deviation from the exact result on a larger scale and figure 1(c) shows the energy derivative $dD(\epsilon)/d\epsilon$. In order to make a fair comparison

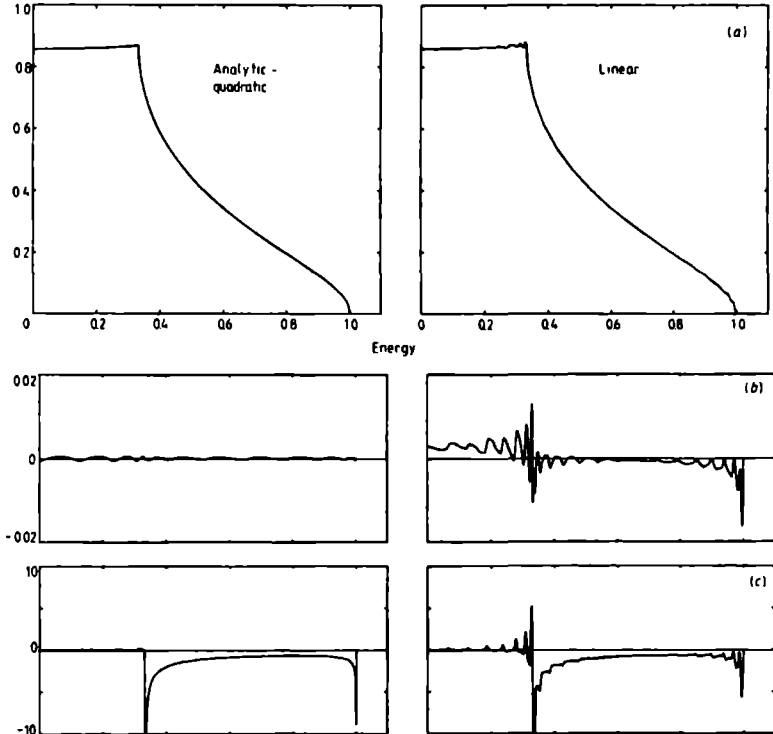


Figure 1. The density of states for the cubic tight-binding s band (a) Full density of states. (b) Deviation from exact result (Morita and Horiguchi 1971) (c) Derivative As discussed in the text, eight times more tetrahedra were used in the linear case, so that 1000 and 8000 tetrahedra were used respectively. Only the positive energy range is presented.

between the methods, we have used eight times more tetrahedra for the linear case since the interpolation is determined by the four corner energies alone, whereas the quadratic interpolation uses the six midpoints also. Thus both methods done this way use the same density of k points.

At first sight, it seems as if both methods describe the density of states adequately. However, the close-up views and the derivatives show that there is a basic difference. The inadequacy of the linear scheme is evident in the oscillations at energies approaching the singularity; furthermore, we have found that the amplitude of the oscillations decreases only slowly as the number of tetrahedra is increased. One can understand this by noting that, in the linear method, the contribution of each tetrahedron is always a piecewise quadratic, once-differentiable function of energy. A convergence towards a function having infinite slope or with a jump in derivative is only possible

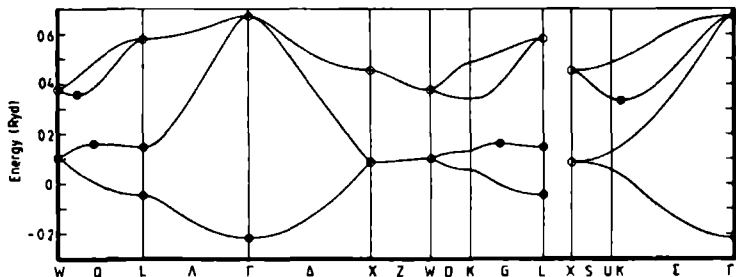


Figure 2. The valence band of silicon. The critical points are marked as full circles (analytic) and open circles (fluted)

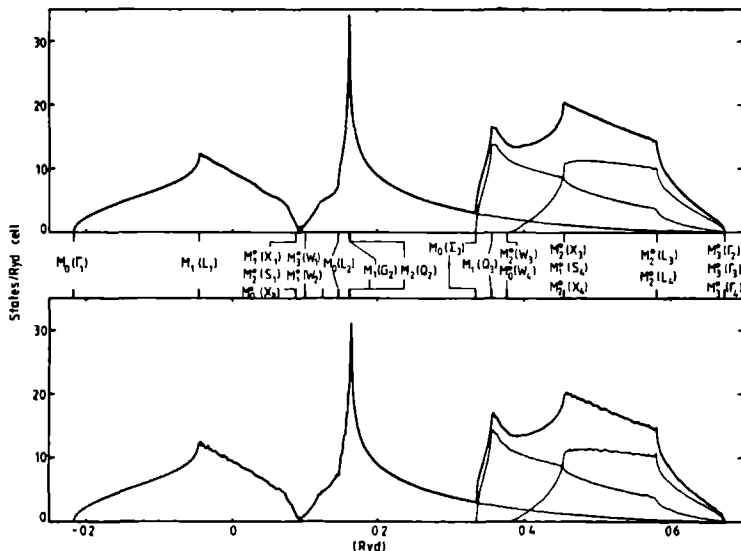


Figure 3. The density of states of the valence bands of silicon (a) Analytic quadratic for 500 tetrahedra (b) Linear for 4000 tetrahedra. All the van Hove singularities are marked on a band-by-band basis

by overshooting strongly, exactly as with the Gibbs phenomenon in the convergence of Fourier series at jump discontinuities. Thus the oscillations must appear since a function with singularities is being approximated by unsuitably smooth functions. The contributions derived from the quadratic interpolation, on the other hand, are flexible enough to describe such singularities exactly.

A second, unexpected conclusion from the comparison of the two methods is that the oscillations in the linear result are not random but systematically in error. The linear-method density of states lies too high near the centre of the band and too low near the ends. Spectral weight is being shifted even though the contribution of every tetrahedron extends only over a small energy range (the total weight being of course invariant). The effect arises because the centre of mass of the contribution for each tetrahedron is moved slightly in a direction which depends on the character of the band. These shifts add up to an error which is not restricted only to energies near critical points.

We have determined the rates of convergence for both the root mean square (RMS) and the maximal error for the two methods. Expressing the results with the mesh size h , both RMS and maximal error converge as h^1 for the quadratic method (equivalently, as the reciprocal of the number of tetrahedra). For the linear method, however, the

Table 1 The van Hove singularities for the valence bands of silicon. The Morse relations are fulfilled (Phillips 1976). The complex fluted critical points at X are described as superpositions of two neighbouring analytic critical points. The types marked with an asterisk are all fluted critical points.

En(k)	k	Type	Degeneracy
Band 1			
-0.217	Γ	M	1
-0.046	L	M_1	4
0.087	S	M^*	12
0.087	X	M_1^*	3
0.100	W	M_1^*	6
Band 2			
0.087	X	M^*	3
0.100	W	M_1^*	6
0.147	L	M	4
0.161	G	M_1	24
0.162	O	M	24
0.674	Γ	M_1^*	1
Band 3			
0.334	Σ	M	12
0.356	Q	M_1	24
0.377	W	M^*	6
0.455	X	M^*	3
0.581	L	M^*	4
0.674	Γ	M_1^*	1
Band 4			
0.377	W	M^*	6
0.455	S	M_1^*	12
0.455	X	M	3
0.581	L	M^*	4
0.674	Γ	M_1^*	1

maximal error converges more slowly than the RMS error the rates are h^1 and h^2 respectively This is again similar to the least-squares types of convergence of Fourier series The slow reduction of numerical noise with increasing number of tetrahedra was already observed by Lehmann and Taut (1972)

As a second application, we have applied the method to the realistic case of the silicon valence bands (figure 2) In figure 3, we compare the densities of states for the two methods We see that in the silicon case the same two phenomena of oscillations and shift of spectral weight occur In table 1 we list all the van Hove singularities These are also given in figure 2 as the full and open circles A comparison of figure 2, table 1 and figure 3 shows the central role which the singularities play in the structure of the density of states

We feel that the results presented above are strong arguments in favour of the analytic-quadratic method when calculating densities of states The slightly larger effort in programming and running is more than offset by the proper analytical structure of the resulting density of states near van Hove singularities smaller error and faster convergence rates This can never be attained using the linear method since a singular function cannot be represented as a finite sum of smooth functions (Mueller *et al* 1971) The quadratic method makes possible an efficient use of the information contained in a given number of k point energies and is therefore of considerable use wherever the calculation of band energies is connected with large effort per k point

We wish to thank Dr B Rompa for the silicon valence bands Dr R A de Groot and Dr H J F Jansen for helpful discussion, and the Stichting Fundamenteel Onderzoek der Materie for financial support

References

- Eisenhart L P 1947 *Introduction to Differential Geometry* (Princeton NJ Van Nostrand)
Lehmann G and Taut M 1972 *Phys Status Solidi* **54** 469
Morita T and Horiguchi T 1971 *J Math Phys* **12** 981
Mueller F M Garland J W Cohen M H and Bennemann K H 1972 *Ann Phys Lp*: **67** 19
Phillips J C 1956 *Phys Rev* **104** 1263

Singular Integrals over the Brillouin Zone: The Analytic-Quadratic Method for the Density of States*

M.H. Boon, M.S. Methfessel, F.M. Muellert

Research Institute for Materials and Faculty of Science,
Toernooiveld, 6525 ED Nijmegen, The Netherlands

Abstract

A new and simple scheme for evaluating analytically singular integrals over the Brillouin zone and which uses a local quadratic expansion is described. It is shown that the commonly used linear scheme converges only slowly in the vicinity of Van Hove singularities. Several examples are discussed. It is concluded that the new, quadratic, analytic scheme is at least an order of magnitude more efficient and is as simple to apply in practice as the linear scheme. The special case of the density of states is given in detail in this paper, the extension to general singular integrals is treated in the following article.

I. Introduction

The properties of condensed matter may be understood to a large extent in terms of thermodynamical averages. For regular solids these averages devolve for zero temperature into integrals of generalized or singular functions over an appropriate Brillouin zone (BZ) of the reciprocal space. In principle the evaluation of these integrals is straightforward, for example in the simple case of the density of states of the free electron gas, one finds the well-known square root density of states

$$D(E) = \int \delta(E(\mathbf{k}) - E) d^3k = \int_S dS / |\nabla E|$$

* Shortened version of a paper appearing in Journal of Physics C

† Present address: Center for Materials Science, Los Alamos National Laboratory,
Los Alamos, New Mexico 87545 U.S.A.

$$= \begin{cases} c\sqrt{E-E_c} & E \geq E_c \\ 0 & E \leq E_c \end{cases}$$

where c is a constant, and E_c is a critical energy. It is clear that if the dispersion relation $E(\mathbf{k})$ is generalized so that the local band mass-tensor is positive definite, but not necessarily diagonal, that a similar density of states shape would result, but with modified constants. The essential element is the square-root singularity and the fact that $D(E)$ is continuous as a function of E , but has singular or discontinuous first derivatives. (We restrict the discussion here and below to the case of three dimensions.) In the case of a general band, it is clear that other density of states shapes are possible. This was first investigated in some detail by Van Hove, who considered expansion about the points in \mathbf{k} space at which $|\nabla E(\mathbf{k})|=0$ was fulfilled. He identified 4 types of singularities now denoted by M_0 , M_1 , M_2 and M_3 depending on the number of *negative* elements of the local 3 dimensional mass tensor. The four cases are then positive spheroidal, hyperboloidal of one sheet, hyperboloidal of two sheets and negative spheroidal respectively, and where it is assumed that a local, analytic expansion of the dispersion relation existed [91]. Van Hove also discussed the rarer non-analytic critical points. Later the subject was generalized and extended by Phillips [79], who classified the non-analytic critical points into fluted (where different bands join at a symmetry point) and singular (at band crossings). At these points it is not possible in general to expand the dispersion relation in a Taylor series since the secular matrix introduces roots. However, Phillips showed that such critical points give rise to density of state singularities that are similar to or weaker than those due to the analytic ones. These results have been reviewed and extended by Maradudin, Montroll and Weiss [65].

In this paper we consider a new scheme, based on a local expansion of the dispersion relation to quadratic order, to evaluate singular Brillouin zone integrals such as the density of states. It is clear that only in a few special cases - for example in the case of a single s-band in the nearest neighbour, tight-binding approximation - may such integrals be performed analytically over the BZ directly. In most cases one must be satisfied with a piecewise continuous expansion over some neighbourhood: One divides up the zone into regions, evaluates the singular integral over each separate region and sums over all the regions. Such methods are practical, and are widely applied. A number of schemes for dividing \mathbf{k} -space are possible: 1) the root-sampling or Monte-Carlo technique chooses random or regularly spaced points, and stores results in histograms. For the density of states, this technique converges as $1/N$ on the average and $1/\sqrt{N}$

point-wise where N is the number of points. For a global picture this method is quite useful for results accurate on the scale of a few per cent and is arguably the most efficient scheme for low precision. A second scheme is that of Jepsen and Andersen [48] and Lehmann and Taut [61] in which one expands the dispersion relation to linear order over a neighbourhood and integrates the resulting structure analytically. In this case the density of states is a piecewise continuous function of quadratic order in the energy: there are 4 breaks at the corner energies of the tetrahedron. This linear technique is, because of its simplicity, perhaps the one currently in greatest use by researchers today. Its difficulty lies in the fact that since it does not make any provision for a Van Hove-like expansion (which necessitates an expansion to *quadratic* order) the method does not reproduce or develop structure such as Van Hove singularities, except as the limit of a series. As we have demonstrated [69], this series itself converges only as $1/N^{1/3}$, where N the number of sub-regions of the BZ. Hence in effect the linear scheme has actually a slower convergence rate than the Monte-Carlo. This was remarked upon implicitly by Lehmann and Taut in their publication.

The idea of using a higher-order, quadratic expansion is not new, but previous methods used either a Monte-Carlo sampling in sub-regions (Mueller et al. [74], Cooke et al. [17]) or a Lehmann and Taut-like procedure. The direct analytic integration of singular integrals of quadratic forms is somewhat complicated (Lehmann and Taut use the language 'impossible'), and is the subject of this article. We wish to emphasize that although the proofs of our results are quite detailed and involved, the scheme itself is rather simple. In fact, the algorithms and computer codes are as simple to *use* as the program of the linear scheme, but with a result which *explicitly preserves* the structure of the Van Hove singularities at the analytic critical points. In effect what is done in applying the quadratic scheme is to replace the piecewise-quadratic energy function of the density of states of the linear scheme by much more flexible functions. Basically, these are the arc-tangents of the square-root of the energy. This permits accurate representation of the discontinuous behaviour in energy around a Van Hove singularity, as discussed by Van Hove, Phillips, and Maradudin, Montroll and Weiss. At non-analytic critical points, the quadratic method is also superior (cf. our test with silicon) except for the case of band crossings. For these, there is no reason to assume that the new method is any worse. Moreover, a variety of direct comparisons show that the new algorithm is approximately one order of magnitude more efficient in the worst cases and substantially better in most.

The analytic-quadratic method was introduced and briefly described in ref. [69]. In this paper, we give a thorough discussion and derive the mathematical formulae but restrict ourselves to the calculation of the density of states. The extension to general singular integrals is treated in the following paper. The

plan of this paper is as follows: In section II we review and structure the main problem; in section III we describe the implementation of the new method, and in section IV several examples are discussed. Some proofs of the formulae used are omitted in this report (they can be found in an Appendix in the paper to be published).

II. Description of the method

In this section we outline the derivation of the basic formulae of the analytic-quadratic method as applied to the calculation of the density of states.

As in the linear method of Lehmann and Taut, the Brillouin zone is divided into space-filling tetrahedra, but here the energy band is approximated up to quadratic order from the numerical data in each tetrahedron. At a point $\mathbf{k}=(k^1, k^2, k^3)$ within a given tetrahedron, we have for the energy throughout the volume of that tetrahedron:

$$E(\mathbf{k}) = \sum_{i,j=1}^3 \beta_{ij}(k^i - k_j^0)(k^j - k_j^0) + E_0 \quad (\beta_{ij} = \beta_{ji}) \quad (1)$$

where the inverse local mass tensor β_{ij} , the local-origin coordinates k_j^0 , and the energy at the origin E_0 are determined by the ten values of the energy at the apexes and mid-points of the edges of the tetrahedron. (We omit a label identifying the individual tetrahedron to avoid complicating the notation.) The energies on common faces and edges of neighbouring tetrahedra will automatically agree, though not in general their \mathbf{k} -derivatives normal to the faces.

The density of states will be a sum of contributions (one from each tetrahedron) of the form:

$$D(E) = \int_V d^3\mathbf{k} \delta(E - E(\mathbf{k})) \quad (2)$$

integrated over the volume V of the tetrahedron. (A constant factor due to normalization and/or spin has been omitted from (2) for simplicity.) For a simple description of the method it is convenient to make an affine transformation so that the inverse local mass tensor in (1) is in diagonal form. We emphasize that this is not a necessary step in the practical application of the new method. The actual technique, to be discussed below, works in the original non-diagonal form and saves the necessity of diagonalizing the 3×3 inverse mass tensor matrix. Thus, we introduce new coordinates $\mathbf{r}=(x,y,z)$ here for the purpose of clarity, so that $E(\mathbf{k})=E_0+\epsilon(\mathbf{r})$ where:

$$\epsilon(\mathbf{r}) = \lambda_1 x^2 + \lambda_2 y^2 + \lambda_3 z^2 \quad (3)$$

and the signature $(\lambda_1, \lambda_2, \lambda_3)$ is, apart from rearrangement, one of the four:

$$(1,1,1) ; (-1,-1,-1) ; (-1,-1,1) ; (1,1,-1) \quad (4)$$

which correspond to the four Van Hove singularities M_0 , M_3 , M_2 and M_1 , respectively. (We have ignored the possible degenerate cases where the determinant of the quadratic form vanishes exactly, as occurring with negligible probability.) Explicitly, the transformation of coordinates is given by:

$$\mathbf{k} = \mathbf{S} \mathbf{r} + \mathbf{k}_0 \quad ; \quad \tilde{\mathbf{S}} \mathbf{B} \mathbf{S} = \Lambda, \quad (5)$$

where $\mathbf{B}=[\beta_{ij}]$ is the symmetric matrix of the form in (1) and \mathbf{S} is a matrix (transpose $\tilde{\mathbf{S}}$), which transforms \mathbf{B} to the diagonal matrix Λ , with diagonal elements $\lambda_1, \lambda_2, \lambda_3$. Then (2) becomes, using (3):

$$D(E_0 + \epsilon) = |\det \mathbf{B}|^{-1/2} \int_v d^3\mathbf{r} \delta(\epsilon - \epsilon(\mathbf{r})) \quad (6)$$

where $\epsilon = E - E_0$ is the energy measured from its value E_0 at the origin \mathbf{O} ($\mathbf{r} = \mathbf{O}$, i.e. $\mathbf{k} = \mathbf{k}_0$ in (1)), v is the volume of the tetrahedron in the new coordinates and $|\det \mathbf{B}|^{-1/2} = |\det \mathbf{S}|$ ($\neq 0$ by supposition) is the Jacobean of the transformation \mathbf{S} in (5).

Under the affine transformation the structure of the region of integration remains tetrahedral, but of course with a modified shape. In the following, we will consider the transformed tetrahedron and the dispersion relation (3). The new local origin \mathbf{O} may be inside, outside or on the tetrahedron. A Van Hove singularity, which occurs for $\nabla_{\mathbf{k}} E(\mathbf{k}) = \mathbf{O}$, corresponds from (1) to $\mathbf{k} = \mathbf{k}_0$, or $\mathbf{r} = \mathbf{O}$. Thus if \mathbf{O} is *inside* the tetrahedron, the contribution from this tetrahedron will have a Van Hove singularity. When \mathbf{O} is *on* the tetrahedron surface the strength of the singularity is shared with the neighbouring tetrahedron. This limiting situation occurs so infrequently, however, that we shall not discuss it in this article. All other singularities in the density of states are caused by the intersection of the quadratic form with the sides, planes or edges. They are artificial in the sense that they are caused by the partition of the Brillouin zone, and cancel to a large extent when the contributions from neighbouring tetrahedra are added.

We now note that the constant energy surfaces (CES) $\epsilon = \epsilon(\mathbf{r})$ in (6) are *spheres* for the first two signatures in (4), and either *1-sheet or 2-sheet hyperboloids of revolution* for the last two. For each signature we shall use an appropriate set of coordinates (R, θ, ϕ) , wherein the CES are described by $R = \text{constant}$. The transformations and some of their properties for the three

different cases (spherical, 1-sheet hyperboloidal and 2-sheet hyperboloidal) are summarized in Table I. In all cases we have by construction $\epsilon(r)=\pm R^2$; by transforming to the new coordinates and using

$$\delta(|\epsilon|-R^2) = \frac{1}{2|\epsilon|^{1/2}} [\delta(|\epsilon|^{1/2}-R) + \delta(|\epsilon|^{1/2}+R)]$$

in (6), we immediately obtain an expression for the density of states in the form:

$$D(E_0+\epsilon) = \frac{1}{2} |\det B|^{-1/2} |\epsilon|^{-1/2} A(\epsilon). \quad (7)$$

The quantity $A(\epsilon)$ is just the *area of that part* Σ *of the CES* $R^2=|\epsilon|$ *inside the tetrahedron*. It may be a single piece or consist of several disconnected pieces. It is important to remark, however, that $A(\epsilon)$ is an area *calculated in terms of a metric appropriate to the geometry of the CES*. Explicitly:

$$A(\epsilon) = |\epsilon| \int_{\Sigma} f(\theta) d\theta d\phi \quad (8)$$

where the element of area is taken from Table I and $f(\theta)$ depends on the type of energy surface. Of the four signatures (4), it is enough to consider henceforth only (1,1,1) and (-1,-1,1) since the density of states for the other two differ from these only by a reversal of the energy scale $\epsilon \rightarrow -\epsilon$. For (1,1,1), the CES are *spheres* for $\epsilon > 0$ and do not exist for $\epsilon < 0$ (Fig. 1). This is the familiar form of singularity for a free-electron band. For (-1,-1,1) the CES are *hyperboloids* of 2 sheets for $\epsilon > 0$ and of 1 sheet for $\epsilon < 0$ (Fig. 2). The situation is summarized by the supplementary specification to use in (8):

$$(1,1,1) : f(\theta) = \{\sin\theta, \epsilon > 0; \text{ no CES for } \epsilon < 0\} \quad (9a)$$

$$(-1,-1,1): f(\theta) = \{\sinh\theta, \epsilon > 0; \cosh\theta, \epsilon < 0\} \quad (9b)$$

For signature (1,1,1) the spheres are centered on O and the energy range for which $D(E_0+\epsilon) \neq 0$ is determined by the radii of the largest and smallest spheres that touch the tetrahedron. For signature (-1,-1,1), the CES pass from 1-sheet hyperboloids for $\epsilon < 0$ to 2-sheet hyperboloids for $\epsilon > 0$ (Fig. 2). At the dividing energy $\epsilon=0$, the surface is a double cone, with vertex O; but it is *not* necessary to treat this case separately as the behaviour of $A(\epsilon)$ across $\epsilon=0$ is correctly obtained by taking the limit from both sides. The range of energies in the hyperboloidal cases for which $D(E_0+\epsilon) \neq 0$ again lies between values determined by the two extremal surfaces touching the tetrahedron. The extremal surfaces may be hyperboloids of different or of the same sort (according to whether

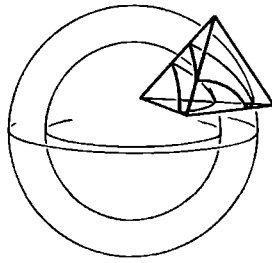


Figure 1. Tetrahedron intersecting spherical energy surfaces $R^2=\epsilon$ for two different energies The density of states is proportional to the intersected area (shaded)

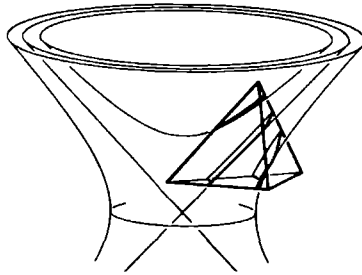


Figure 2. Tetrahedron intersecting hyperboloidal energy surfaces $R^2=|\epsilon|$ for positive and negative energies as well as for $\epsilon=0$ This tetrahedron cuts the cone (where $\epsilon=0$), in general it could lie entirely in either the 1-sheet ($\epsilon<0$) or 2-sheet ($\epsilon>0$) region The density of states is again proportional to the intersected area, provided this is calculated using a Minkowski metric

	x	y	z	range of θ	$f(\theta)$	$g(\theta)$
S	$R\sin\theta\cos\phi$	$R\sin\theta\sin\phi$	$R\cos\theta$	$0\leq\theta\leq\pi$	$\sin\theta$	$\cos\theta$
H1	$R\cosh\theta\cos\phi$	$R\cosh\theta\sin\phi$	$R\sinh\theta$	$-\infty<\theta<\infty$	$\cosh\theta$	$\sinh\theta$
H2	$R\sinh\theta\cos\phi$	$R\sinh\theta\sin\phi$	$R\cosh\theta$	$0\leq\theta<\infty$	$\sinh\theta$	$\cosh\theta$

Table I. The appropriate coordinates for the sphere (S) and the hyperboloids of 1-sheet (H1) and of 2-sheets (H2, only the upper half is given) In all cases $0\leq R\leq\infty$ and $0\leq\phi\leq 2\pi$ Here $f(\theta)$ is the surface area element (cf (8)) and $g(\theta)$ is the line element on the energy surface

the tetrahedron cuts the cone – as in Fig 2 – or not) and thus the (always finite) energy range can be anywhere in $-\infty < \epsilon < \infty$

It is worth re-emphasising that the area $A(\epsilon)$ in (8)-(9) is defined in terms of a surface metric which is ultimately derived from the quadratic term in $E(\mathbf{k})$ which is considered to provide the metric for the 3-dimensional space in which the surface is embedded. Thus for the spheres the surface metric is induced from the familiar *Euclidean* one, for the hyperboloids it is induced from one of *Minkowski* type $ds^2 = -dx^2 - dy^2 + dz^2$. Thus in the latter case x and y can be viewed as space-like coordinates and z as a time-like coordinate. In this picture the surface $\epsilon=0$ is the light cone through O .

It is clear from (7)-(9), and from geometrical considerations, that $D(E_0+\epsilon)$ is a continuous function of ϵ . Suppose O lies inside the tetrahedron, so that it is a critical point. For the *spherical signature* (9a), the spheres of radius $|\epsilon|^{1/2}$ lie *entirely inside the tetrahedron* beyond a certain value of energy as $\epsilon \rightarrow 0$, so that

$$A(\epsilon) \rightarrow 4\pi |\epsilon| \Rightarrow D(E_0+\epsilon) \approx 2\pi |\det B|^{-1/2} |\epsilon|^{1/2} \quad (\epsilon \rightarrow 0^+) \quad (10a)$$

as we expect. For the *hyperboloidal signature* (9b), the behaviour of the density of states across $\epsilon=0$ in the presence of a Van Hove singularity is given by

$$D(E_0+\epsilon) - D(E_0-\epsilon) \approx -2\pi |\det B|^{-1/2} |\epsilon|^{1/2} \quad (\epsilon \rightarrow 0^+) \quad (10b)$$

(see further below)

The area $A(\epsilon)$ in (7)-(9) will, in general, be the sum of the areas of a number of disconnected polygons inscribed on the CES, where the polygon sides are formed from the intersection of the planes of the tetrahedron with the surface. Included in this description are polygons of 'one' side and no vertices, which can occur for spherical or 2-sheet hyperboloidal CES where a single plane slices through the surface, forming a 'boss'. Also included are polygons with one or more 'holes', caused by the CES projecting out of tetrahedron faces, holes likewise contribute no vertices. Figs 3-6 show several examples of the situations that can occur.

We now discuss the problem of calculating $A(\epsilon)$ as a function of ϵ . Consider the spherical case (Fig 1) if it so happened that all lines of the polygon lay on great circles, the area would be expressible in terms of the spherical angles, from the well-known formula of Gauss. A similar relation would also hold in the hyperboloidal case (Fig 2), because planes through the origin O cut the hyperboloids in curves geodesic in the Minkowski metric. But, in general of course, the planes do *not* pass through O , and the area will depend on the geodesic curvature [24] of the sides as well. Remarkably, however, it turns out that the *derivative* of the density of states (7) depends essentially on the polygon

angles only. For the moment, suppose the origin O lies outside the tetrahedron. Then

$$\frac{d}{d\epsilon} [|\epsilon|^{-1/2} A(\epsilon)] = \frac{1}{2} |\epsilon|^{-1/2} \Gamma(\epsilon) \quad (11)$$

where:

$$\Gamma(\epsilon) = \begin{cases} 2\pi N(\epsilon) - \sum_{i=1}^n \gamma_i(\epsilon); & 0 \leq \gamma_i \leq \pi & \text{sphere} & (\epsilon > 0) \\ \sum_{i=1}^n \gamma_i(\epsilon) - 2\pi N(\epsilon); & 0 \leq \gamma_i \leq \pi & \text{2-sheet hyperboloid} & (\epsilon > 0) \\ - \sum_{i=1}^n \gamma_i(\epsilon); & -\infty < \gamma_i < \infty & \text{1-sheet hyperboloid} & (\epsilon < 0). \end{cases} \quad (12)$$

Here $\gamma_i(\epsilon)$ is the *external* surface angle of a polygon at vertex i (see Fig. 3) and the sum goes over *all* vertices of *all* the disconnected polygons making up the area $A(\epsilon)$. There are no vertices associated with bosses or holes. $N(\epsilon)$ is a step function taking integral values:

$$N(\epsilon) = [\text{Total number of disconnected polygons (including bosses)} \\ - \text{Total number of holes}]. \quad (13a)$$

If the origin O lies inside the tetrahedron, as happens at a Van Hove singularity, a new situation can occur when the signature is (1,1,1). For sufficiently small values of ϵ , the energy surface inside the tetrahedron will be the complete sphere or the sphere with holes cut out by one or more faces (see Fig. 5). Elementary calculation of the area $A(\epsilon)$ then shows that eqs. (11)-(12) hold, on the understanding that there are *no vertices* and with (13a) substituted by

$$N(\epsilon) = [2 - \text{Number of holes}] \quad (\text{for signature } (1,1,1)). \quad (13b)$$

Equation (13a) takes over as soon as the sphere grows large enough to touch an edge. At Van Hove singularities of signature $(-1,-1,1)$, eq. (13a) applies as it stands.

The important expression (11) is only valid if the angles in (12) are defined in terms of the relevant metric, as are all other geometrical quantities. There is a difference in kind between the angles on a sphere and on the 2-sheet hyperboloid on the one hand, and on the 1-sheet hyperboloid on the other. In the first two cases, the surface metric on the CES $R^2 = |\epsilon|$ is *definite*. It is a standard result of curvilinear geometry that the angles are then quantities periodic in

2π , and because of the convexity of the tetrahedron all angles in (12) lie in $[0, \pi]$. On the 1-sheet hyperboloid the surface metric is *indefinite* with consequence that polygon sides may be 'spacelike' curves (negative length), 'timelike' curves (positive length) or null (zero length). The angles between such curves are hyperbolic with range $(-\infty, \infty)$. (If one or both of the sides forming the angle γ is null, then $\gamma = \pm\infty$; however the frequency with which this exact situation happens in the computation is negligible. In any case it can be shown that the *sum* of the angles of any polygon where such angles occur is always strictly finite.)

To implement the method, it is necessary to find an analytic expression for the $\gamma_i(\epsilon)$ as function of ϵ . Geometrically, $\gamma_i(\epsilon)$ is an angle formed between two faces of the tetrahedron where they meet at an edge, projected onto the tangent plane of the CES (Fig. 3). It is therefore apt to give the general expression for the surface angles formed at the line of intersection of two arbitrary planes. The two distinct cases that arise are distinguished by specifying whether the angle (or its opposite) is formed in the sector containing the origin O or not, and are denoted by $\gamma^+(\epsilon)$ and $\gamma^-(\epsilon)$ respectively. They are given by

$$\gamma^\pm(\epsilon) = \arctn \pm \left[\frac{\sqrt{|1 - \epsilon_0/\epsilon|} \operatorname{sn} \gamma_0}{\operatorname{cs} \gamma_0 + \sigma \sqrt{|\epsilon_1 \epsilon_2 / \epsilon^2|}} \right] \quad (14a)$$

where:

$$\sigma = \begin{cases} 1 & \text{signature } (1,1,1) \\ -\operatorname{sgn}(\epsilon) \operatorname{sgn}(\epsilon - \epsilon_0) & \text{signature } (-1,-1,1). \end{cases}$$

Here ϵ_1 , ϵ_2 and ϵ_0 are the energies at which the CES are tangent to the two planes and to the line of intersection, respectively. They are extrema of $\epsilon(\mathbf{r})$ as \mathbf{r} ranges over the geometrical entity in question. Formula (14a) is valid in the energy range $\infty > \epsilon \geq \epsilon_0$ in the spherical case or in one of the energy ranges $\infty > \epsilon \geq \epsilon_0$, $-\infty < \epsilon \leq \epsilon_0$ in the hyperboloidal case according as the line of intersection is 'timelike' or 'spacelike' (i.e. is asymptotically inside or outside the cone in Fig. 2, respectively). The notation sn , cs and $\operatorname{tn} = \operatorname{sn}/\operatorname{cs}$ is convenient shorthand for trigonometric or hyperbolic functions. In fact the $\gamma^\pm(\epsilon)$ are *trigonometric* for $\epsilon > 0$ with $\gamma^-(\epsilon) = \pi - \gamma^+(\epsilon)$ and *hyperbolic* for $\epsilon < 0$ with $\gamma^-(\epsilon) = -\gamma^+(\epsilon)$. As $|\epsilon| \rightarrow \infty$ along the line of intersection, $\gamma^+(\epsilon) \rightarrow \gamma_0$, where γ_0 is the true dihedral angle between the planes in the sector containing O. It is trigonometric or hyperbolic according as $\epsilon \rightarrow +\infty$ or $\epsilon \rightarrow -\infty$, respectively, in accord with the above rule. Explicit expressions for the quantities ϵ_0 , ϵ_1 , ϵ_2 , $\operatorname{sn} \gamma_0$, and $\operatorname{cs} \gamma_0$ in terms of the parameters of the intersecting planes are given in the

Appendix of the paper to be published.

A second more convenient form for $\gamma^\pm(\epsilon)$, which corresponds geometrically to splitting the angles into two parts, is

$$\gamma^\pm(\epsilon) = \sum_{j=1}^2 \arctan \left[\sqrt{|1-\epsilon_0/\epsilon|} T_j \right] ; \quad T_j = (\pm 1)^j \tan \gamma_0^{(j)} \quad (14b)$$

where $\gamma_0^{(j)}$ ($j=1,2$) are the near dihedral angles between the given planes and the dividing plane that passes through O. The angles in (14b) are special cases of (14a) with ϵ_1 or $\epsilon_2 \rightarrow 0$. Again, all angles in (14b) are trigonometric and in $[0, \pi]$ for $\epsilon > 0$ and are hyperbolic for $\epsilon < 0$.

The derivative of the density of states is from (7) and (11):

$$\frac{d}{d\epsilon} D(E_0+\epsilon) = \frac{1}{4} |\det B|^{-1/2} |\epsilon|^{-1/2} \Gamma(\epsilon) \quad (15)$$

where $\Gamma(\epsilon)$ is specified by (12)-(13). The part of $\Gamma(\epsilon)$ that is the most difficult to calculate directly is the step-function $N(\epsilon)$, so we determine it in practice from the continuity properties of $\Gamma(\epsilon)$. A study of (11)-(14) shows that $\Gamma(\epsilon)$ is piecewise analytic, on intervals separated by values of ϵ where $\Gamma(\epsilon)$ or its derivatives are discontinuous. We classify these singularities into different kinds, naming them according to their geometrical origin.

Volume singularities: When O is *inside* the tetrahedron, $\Gamma(\epsilon)$ jumps by 4π (signature (1,1,1)) or by -4π (signature (-1,-1,1)) at $\epsilon=0$, ϵ increasing. The former can be seen directly from (12) and (13b); the latter occurs when the CES crosses the double-cone $\epsilon=0$ from the 1-sheet to the 2-sheet hyperboloids. These jumps correspond to the presence of a Van Hove singularity, at which the behaviour of (15) is therefore

$$\frac{d}{d\epsilon} D(E_0+\epsilon) \approx \pi |\det B|^{-1/2} |\epsilon|^{-1/2} \quad (\epsilon \rightarrow 0^+) \quad (16a)$$

for signature (1,1,1), in agreement with (10a), and

$$\frac{d}{d\epsilon} [D(E_0+\epsilon) - D(E_0-\epsilon)] \approx -\pi |\det B|^{-1/2} |\epsilon|^{-1/2} \quad (\epsilon \rightarrow 0^+) \quad (16b)$$

for signature (-1,-1,1), in agreement with (10b).

If O is *outside* the tetrahedron (no Van Hove singularity), then we can show that both $\Gamma(\epsilon)$ and $dD(E_0+\epsilon)/d\epsilon$ in (15) are continuous at $\epsilon=0$. For signature (1,1,1) this is obvious, since $\Gamma(\epsilon)$ is identically zero in the $\epsilon=0$ region. For signature (-1,-1,1), it can be shown that $\Gamma(\epsilon) \rightarrow 0$ as $|\epsilon| \rightarrow 0$ in such a way that $|\epsilon|^{-1/2} \Gamma(\epsilon)$ is continuous across the double-cone. Although $\epsilon=0$ is not a point

of analyticity, the functions are sufficiently smooth there that it is not counted as a singularity in this case

Face singularities In the positive energy region, as ϵ increases $\Gamma(\epsilon)$ jumps by 2π at energies where ‘bosses’ appear (signature (1,1,1)) or ‘holes’ disappear (signature (-1,-1,1)), and by -2π where ‘holes’ appear (signature (1,1,1)) or ‘bosses’ disappear (signature (-1,-1,1)) This occurs at values of ϵ at which the spheres or 2-sheet hyperboloids are tangent at the tetrahedron face, causing $N(\epsilon)$ in (12) to change by ± 1 while adding no vertices In contrast to the jumps at volume singularities, these jumps are artificial in the sense that they are due to the dividing up of the Brillouin zone They cancel to first order when contributions from tetrahedra sharing the same face are added to become the total density of state, since the jumps will be of opposite sign However cancellation is not complete, a circumstance traceable to the fact that the slopes of $E(\mathbf{k})$ normal to the common face do not match exactly in the two tetrahedra

Edge and apex singularities At values of ϵ where the CES is tangent at a tetrahedron edge or passes through an apex, $\Gamma(\epsilon)$ is itself *continuous*, but its derivative is not, because the angle sum in (12) changes abruptly there These singularities, while less strong than the face singularities, have the same ‘artificial’ origin the discretization of the BZ into tetrahedra

A minimum of 4 and a maximum of 15 of the four kinds of singularity will be present The apex singularities are always present Consider the edges and faces of the tetrahedron as parts of the corresponding infinite lines and planes The (maximal 6) edge and (maximal 4) face singularities occur only for those lines and planes whose tangent CES touch on the tetrahedron itself, and then, in the case of face singularities, only when the tangent CES energy is positive (i.e. tangent CES not a 1-sheet hyperbola) Finally the volume singularity for $\epsilon=0$ is present only when the origin is inside the tetrahedron

At the edge and apex singularities, the number of angles changes, and it is convenient to register this explicitly by re-expressing the angle sum in $\Gamma(\epsilon)$ as a sum of contributions from the 6 edges of the tetrahedron We observe that an edge may intersect the CES twice, once, or not at all over different energy ranges In the first case, which occurs if and only if the CES tangent to the line touches on the edge itself, the two surface angles formed are equal Hence we can write

$$\sum_{i=1}^n \gamma_i(\epsilon) = \sum_{\alpha=1}^6 n_{\alpha}(\epsilon) \gamma_{\alpha}(\epsilon) \quad (17)$$

where the $n_{\alpha}(\epsilon)$ are step functions taking values 2,1 or 0 where appropriate, and $\gamma_{\alpha}(\epsilon)$ is whichever of $\gamma^{\pm}(\epsilon)$ of (14) is internal to the tetrahedron at edge α

The determination of $\Gamma(\epsilon)$ is the pivotal step in the method. After calculating the parameters for the $\gamma_\alpha(\epsilon)$, and $n_\alpha(\epsilon)$, $\Gamma(\epsilon)$ is constructed from (12) and (17) using its known continuity behaviour at the singularities. The density of states then is a piecewise analytic and *continuous* function

$$D(E_0 + \epsilon) = \frac{1}{4} |\det \mathbf{B}|^{-1/2} \int_{-\infty}^{\epsilon} |\epsilon'|^{-1/2} \Gamma(\epsilon') d\epsilon' \quad (18)$$

obtained from (15) and (12) by analytic integration, and expressed in terms of analytic primitives of $\text{sgn} \epsilon |\epsilon|^{-1/2} \gamma_\alpha(\epsilon)$. (The expression for the primitives is given in the next section.) The integration constants in (18) are obtained by using continuity to give matching conditions at the singularities.

In the preceding, it was shown how to treat a general $\mathbf{E}(\mathbf{k})$ by transforming the local inverse mass tensor β_{ij} to a diagonal matrix with either (1,1,1) or (-1,-1,1) on the diagonal. We close this section with the demonstration that the transformation does not need to be done explicitly. In an implementation of the method, only simple geometric quantities must be calculated as, for instance, the distance of a line from the origin, or the tangent of an angle, etc. Further, as will be seen in the next section, these quantities are all expressed in terms of *scalar products*. In terms of the transformed coordinates used in the theory above these scalar products are defined by

$$(\mathbf{r}, \mathbf{r}') = \pm x x' \pm y y' + z z' \quad (19)$$

for signatures (1,1,1) and (-1,-1,1), respectively (corresponding to space with a Euclidean, respectively Minkowski metric). If now we introduce a scalar product

$$[\mathbf{x}, \mathbf{x}'] = \sum_{ij} \beta_{ij} x_i x'_j \quad (\mathbf{x} = \mathbf{k} - \mathbf{k}_0) \quad (20)$$

for the original coordinates, defined in terms of the undiagonalized mass tensor, then by definition of the transformation (5), the scalar products (19) and (20) are numerically equal:

$$[\mathbf{x}, \mathbf{x}'] = (\mathbf{r}, \mathbf{r}')$$

Hence all expressions can be, and are, calculated directly in terms of the scalar product (20). Indeed, the whole theory can be developed throughout in terms of the metric β_{ij} ; the standard diagonalized form (19) is only used for the convenience of simpler formulas in the exposition.

III. Implementation of the method

The method has been described in section II and here we set out the steps in its practical implementation. The initial data consists of an energy band $E(\mathbf{k})$ given on a sufficiently fine grid over the Brillouin zone. The zone is divided into space-filling tetrahedra, and the central task will be the calculation of $D(E)$ for each tetrahedron using eq. (18). The total density of states is then obtained by accumulation of the results over all tetrahedra.

The *input* of the program to calculate (18) consists of the 10 values of energy at the apexes and mid-points of the edges of the tetrahedron, and the 4 \mathbf{k} -vectors at the apexes. We perform the following steps (A)-(D).

(A) Determine the 10 quantities $\beta_{ij}, \mathbf{k}_0, E_0$ of eq. (1) from the input. The way this is done is described at the end of the section. If $\det B < 0$, invert the energy grid $\epsilon \rightarrow -\epsilon$ and continue with the matrix $-B$ in place of B . Decide whether this matrix is equivalent to signature (1,1,1) or $(-1,-1,1)$. For the rest of the calculation, the matrix enters only through the scalar product (20). Finally, shift the tetrahedron by $-\mathbf{k}_0$. In the following, we consider the tetrahedron with apexes $\mathbf{q}_i = \mathbf{p}_i - \mathbf{k}_0$, $i=1, \dots, 4$.

(B) Set up a list of the singularity energies and sort by energy. The list will always contain the four apex energies $\epsilon_i^A = [\mathbf{q}_i, \mathbf{q}_i]$. The volume singularity ($\epsilon^V = 0$) is included if the origin lies inside the tetrahedron. For each face, it must be decided whether the point of tangency of the CES on the corresponding infinite plane lies within the face or not. One constructs the vector \mathbf{z} which connects the origin with the point of tangency by elementary vector algebra, using the scalar product (20); thus, take one of the three corner vectors of the face and find its projection orthogonal to the plane. Orthogonality is understood to be defined with respect to the scalar product (20). Writing \mathbf{z} as a linear combination of the three corner vectors, a face singularity is found if all coefficients are positive. In fact, this criterion also automatically excludes cases when the tangent CES is a 1-sheet hyperboloid, wherever the point of tangency is. The singularity energy is then $\epsilon^F = [\mathbf{z}, \mathbf{z}]$. Edge singularities are treated in an analogous way by constructing a vector \mathbf{w} joining the origin to the edge and orthogonal to it; the singularity energy is then $\epsilon^E = [\mathbf{w}, \mathbf{w}]$.

Also in this step, one determines the jumps which $\Gamma(\epsilon)$ should have at the various singularity energies, according to the discussion in the last section. For a volume singularity, the jump is simply 4π and -4π , for the spherical and hyperboloidal cases, respectively. To fix the sign of the jump $\pm 2\pi$ at face singularities, it must be decided whether the origin lies on the same side of the face as the fourth corner of the tetrahedron. This defines a sign σ_{ijk} for each face

$(\mathbf{e}_i, \mathbf{e}_j, \mathbf{e}_k)$, which is also used in step (C). In addition, the σ_{ijk} decide whether a volume singularity is present: this is the case if all four of them are positive.

(C) This step is done for the six edges one at a time. For edge α , do the following:

- (i) Determine the parameters T_1, T_2, ϵ_0 which enter in the expression (14b) for whichever of $\gamma^\pm(\epsilon)$ is the $\gamma_\alpha(\epsilon)$ of eq. (17). ϵ_0 is the edge singularity ϵ^E calculated in step (B). The T_j are (modulo a sign) the tangents or hyperbolic tangents of the angles between the vector \mathbf{w} of step (B) and vectors $\mathbf{x}^{(j)}$ orthogonal to the edge, which lie, respectively, in the two faces meeting at the edge (see Fig. 4). One then has

$$T_j = \pm \frac{\sqrt{|[\mathbf{x}^{(j)}, \mathbf{x}^{(j)}][\mathbf{w}, \mathbf{w}] - [\mathbf{x}^{(j)}, \mathbf{w}]^2|}}{[\mathbf{x}^{(j)}, \mathbf{w}]}$$

The sign to be chosen depends on which of γ^\pm in (14b) is the appropriate one. The rule is: the sign for T_j is $\text{sgn}([\mathbf{u}, \mathbf{u}])\sigma_{klm}$, where face $(\mathbf{e}_k, \mathbf{e}_l, \mathbf{e}_m)$ contains the vector $\mathbf{x}^{(j)}$, and \mathbf{u} points along the edge.

- (ii) Set $n_\alpha(\epsilon)=1$ in the energy interval bounded by the two apex energies. If there is an edge singularity for this edge, set $n_\alpha(\epsilon)=2$ in the interval bounded by ϵ_0 and the closer of the two apex energies. Otherwise, $n_\alpha(\epsilon)=0$.
- (iii) Next, add the primitives of $\frac{1}{4} |\det B \epsilon|^{-1/2} \gamma_\alpha(\epsilon)$ for $\alpha=1, \dots, 6$ (see below for analytic form) with weights 1, 2 or 0 in the appropriate energy intervals *without* worrying about the behaviour of $\Gamma(\epsilon)$ and $D(\epsilon)$ at the singularity energies. However, while looping over the edges, accumulate the heights of the jumps introduced in this way for both $\Gamma(\epsilon)$ and $D(\epsilon)$.

(D) After step (C), the resulting function $\bar{D}(\epsilon)$ satisfies $d\bar{D}/d\epsilon = \frac{1}{4} |\det B \epsilon|^{-1/2} \Gamma(\epsilon)$ but does not yet have the right behaviour at the singularity energies. That is, the jumps in $\Gamma(\epsilon)$ will in general not have the proper values. Therefore,

$$D(\epsilon) = \bar{D}(\epsilon) + \int_{-\infty}^{\epsilon} S_1(\epsilon') \frac{1}{|\epsilon'|^{1/2}} d\epsilon' + S_2(\epsilon)$$

where $S_1(\epsilon)$, $S_2(\epsilon)$ are step functions with jumps at the singularity energies only. By comparing the behaviour of $\bar{D}(\epsilon)$ (as accumulated in step (C)) with the desired behaviour of $D(\epsilon)$, it is straightforward to determine $S_1(\epsilon)$ and $S_2(\epsilon)$. Adding the correction to $\bar{D}(\epsilon)$ as in the above equation yields $D(\epsilon)$.

The analytic primitives for the functions $\text{sgn}\epsilon|\epsilon|^{-1/2}\gamma_a(\epsilon)$, needed in step (C), are given by the following. From eq. (14b), each function can be expressed as a sum of two terms, each of which has the form

$$f(\epsilon) = \text{sgn}\epsilon|\epsilon|^{-1/2}\arctn T\sqrt{|1-\epsilon_0/\epsilon|} \quad (T=\pm T_1)$$

where \arctn is as in eq.(A10) with $e_1=\text{sgn}\epsilon$. The primitive $g(\epsilon)$ of $f(\epsilon)$ is

$$g(\epsilon) = 2|\epsilon|^{1/2}f(\epsilon) - 2\left|\frac{\epsilon_0}{X}\right|TF(\sqrt{|X(\epsilon/\epsilon_0-1)|});$$

$$X = T^2 + \text{sgn}(\epsilon-\epsilon_0);$$

$$F(y) = \arctn(y) \text{ as in (A10) with } e_1 = \text{sgn}(\epsilon_0 X).$$

Finally, we show how to calculate the quantities β_{ij} , k_1^0 , and E_0 in eq. (1) from the energy values at the apexes and mid-edges. We determine the matrix $B=(\beta_{ij})$ together with a vector \mathbf{b} and a constant C such that $E(\mathbf{k})=\mathbf{k}^T B \mathbf{k} + \mathbf{b} \cdot \mathbf{k} + C$; then $\mathbf{k}_0 = -1/2 B \mathbf{b}$ and $E_0 = C - \mathbf{k}_0^T B \mathbf{k}_0$. It is useful to introduce the symmetric coordinates (x_1, x_2, x_3, x_4) of a given point \mathbf{k} by

$$\mathbf{k} = x_1 \mathbf{p}_1 + x_2 \mathbf{p}_2 + x_3 \mathbf{p}_3 + x_4 \mathbf{p}_4$$

with $1=x_1+x_2+x_3+x_4$ and where the \mathbf{p}_i are the tetrahedron corners. The symmetric coordinates of corner \mathbf{p}_1 are $(1,0,0,0)$ and the center of edge $\mathbf{p}_1-\mathbf{p}_2$ has coordinates $(1/2, 1/2, 0, 0)$ etc. The quadratic form as a function of the x_i can be determined by inspection to be:

$$2 \sum_{ij} g_{ij} x_i x_j - \sum_j g_{1j} x_j$$

with g_{ii} = corner values, $g_{ij} = g_{ji}$ = mid-edge values. To express the quadratic form as a function of the normal coordinates $\mathbf{k}=(k_1, k_2, k_3)$, one uses the transformation from normal to symmetric coordinates. This is given by

$$x_i = \mathbf{v}_i \cdot \mathbf{k} + C_i$$

$$\mathbf{v}_1 = (\mathbf{p}_2 \times \mathbf{p}_3 + \mathbf{p}_3 \times \mathbf{p}_4 + \mathbf{p}_4 \times \mathbf{p}_2)/T$$

$$\mathbf{v}_2 = (\mathbf{p}_3 \times \mathbf{p}_1 + \mathbf{p}_1 \times \mathbf{p}_4 + \mathbf{p}_4 \times \mathbf{p}_3)/T$$

$$\mathbf{v}_3 = (\mathbf{p}_1 \times \mathbf{p}_2 + \mathbf{p}_2 \times \mathbf{p}_4 + \mathbf{p}_4 \times \mathbf{p}_1)/T$$

$$\mathbf{v}_4 = (\mathbf{p}_3 \times \mathbf{p}_2 + \mathbf{p}_2 \times \mathbf{p}_1 + \mathbf{p}_1 \times \mathbf{p}_3)/T$$

$$C_1 = [P_2, P_4, P_3]/T$$

$$C_2 = [P_4, P_1, P_3]/T$$

$$C_3 = [P_2, P_1, P_4]/T$$

$$C_4 = [P_1, P_2, P_3]/T$$

$$T = 6(\text{volume of tetrahedron}).$$

Substituting for the x_i in (4) and collecting terms gives the result

$$A = 2 \sum_{ij} g_{ij} v_i v_j^t$$

$$b = 4 \sum_{ij} g_{ij} C_i v_j - \sum_i g_{ii} v_i$$

$$C = 2 \sum_{ij} g_{ij} C_i C_j - \sum_i g_{ii} C_i$$

IV. Results and discussion: Structures over one tetrahedron

Here we will focus on the practical application of the formulae of the preceding sections with a view toward examining the density of states of specific cases whose geometry is increasingly complex. See the previous paper for the results of applying the method to realistic energy bands.

(i) One tetrahedron hyperbolic dispersion relation (origin remote from tetrahedron) In figure 3 we consider the density of states $D(\epsilon)$ and the sum-of-the-angles $\Gamma(\epsilon)$ of eq (12) for a case in which the origin of the hyperbolic form lies far outside a chosen tetrahedron. The breaks or singularities in the density of states labeled V, P, E and A in this and the following Figs (4)-(6) represent singularities caused by volumetric, planar, edge and apex intersections respectively. In all cases the arrows mark energies of the CES shown in the tetrahedron at the right. In the present case only apex singularities occur. Such singularities are very weak and the density of states function has only jumps in its second derivative with respect to energy. This structure is similar to that found in the linear scheme, since in this limit the two schemes are identical. As the origin of the quadratic form becomes remote from the tetrahedron the spherically curved constant energy surfaces approach planes, or linear dispersion relations, and the resulting density of states approaches smoothly the piecewise quadratic density of states of the linear method. In a more typical case the constant energy surface has a shorter radius of curvature relative to the size of the tetrahedron. As soon as this radius becomes comparable with the size of the

tetrahedron, the linear approximation becomes rather bad: to make the linear approximation better, the zone must be further subdivided. The number of necessary subdivided tetrahedra grows as the cube of the ratio of the radius of curvature to the size of the tetrahedron. Hence the problem of treating Van Hove singularities by the linear expansion scheme is a problem of cubic order in the subdivision of the BZ, whereas treated by the analytic quadratic scheme as a quadratic expansion, it is a problem of linear order in the subdivision of the zone.

(ii) One tetrahedron: spherical dispersion relation (origin nearby to tetrahedron). In Fig. 4 we display the density of states $D(\epsilon)$ and also $\Gamma(\epsilon)$ for a spherical case where the quadratic energy surface shown has one planar and three edge singularities in addition to the four apex singularities. The nature of the planar singularity may be understood from Fig. 4; as the constant energy surface sweeps from below in energy, the surface breaks through the face shown – the rapid decrease in the density of states hardly resembles at all the ‘remote’ case considered in Fig. 3 and the preceding discussion. In particular the break in derivative of the planar singularity cannot be easily simulated by summing up smooth functions such as was given in Fig. 3. Note that now the origin of the quadratic form is closer to the tetrahedron, the curvature in the constant energy surfaces is larger so that a linear approximation would require substantial subdivision before a plane would be a good local approximation.

(iii) One tetrahedron: spherical dispersion relation (osculatory). In Fig. 5 we consider the ‘closest’ possible spherical case, in which the origin of the spherical quadratic form actually lies inside the given tetrahedron. This is signaled by the appearance of a V-singularity, which corresponds here to a Van Hove singularity of type M_0 . Of course, on a microscopic scale this singularity is the familiar square-root singularity of a free-electron metal near the minimum of the energy band. Comparing this case to the previous two cases, the structure is richer: now there are 1 volume, four planar and six edge singularities, in addition to the ubiquitous four apex singularities. This case has the maximum number 15 of singularities. Note the presence of a hole in the CES as well as disconnected pieces.

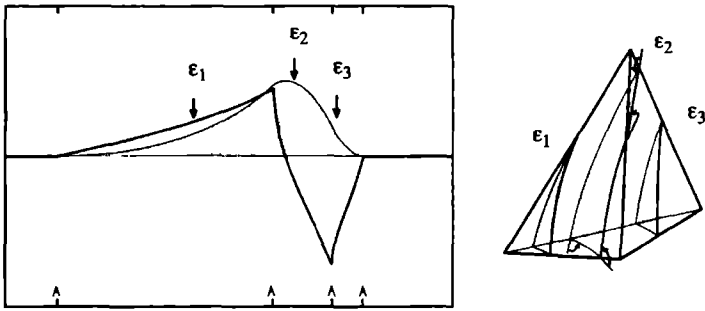


Figure 3. Figs 3 to 6 show the density of states (shaded) as calculated by the analytic-quadratic method for various single tetrahedra and quadratic dispersion relations. The angle sum $\Gamma(\epsilon)$ (Eq. (12)) is also shown (thick line) with a vertical scale in units of 2π . The arrows correspond to the energy surfaces shown in the tetrahedron. Apex (A), plane (P), edge (E) and volume (V) singularities are marked. Our method is based on the fact that the energy derivative of the density of states is related in a simple way to the sum of the exterior angles at each energy (Eq. (15)). The external surface angles are indicated here for energy ϵ_2 . This figure is for a hyperbolic dispersion relation with the origin far to the left of the tetrahedron.

(iv) One tetrahedron hyperboloidal dispersion relation (osculatory). Finally we show in Fig. 6 an hyperboloidal case whose origin is inside or is osculated by the selected tetrahedron. The reader perhaps may be initially skeptical that such unusual looking constant energy structures exist or occur very often in real materials. In fact searching critically for Van Hove structure in Pd (which we consider elsewhere) we have found that this last case is the most frequent of all. The sharp peak at the Van Hove singularity energy labeled V is at that energy for which the constant energy surface passes from one-sheeted to two-sheeted behaviour. Just at energy V, one is on the surface which for Minkowski geometry corresponds to the light cone. This is illustrated in Fig. 6 as the intersecting dashed lines near the center of the tetrahedron. (The unlabeled peaks in the function $\Gamma(\epsilon)$ are characteristic of hyperboloidal dispersion relations, and arise as integrable singularities in the derivative of the density of states due to the hyperbolic angle swinging through infinity.)

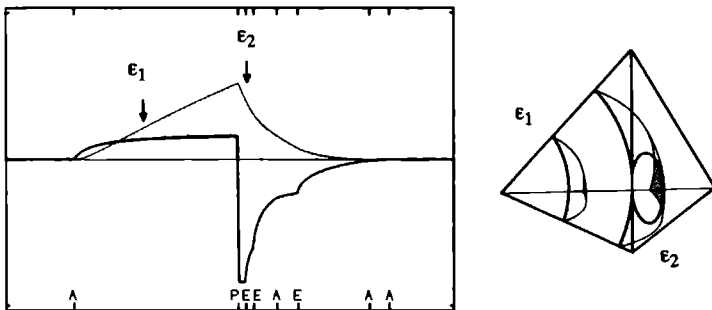


Figure 4. As for Fig. 3, but for a spherical dispersion relation with origin somewhat to the left of the tetrahedron.

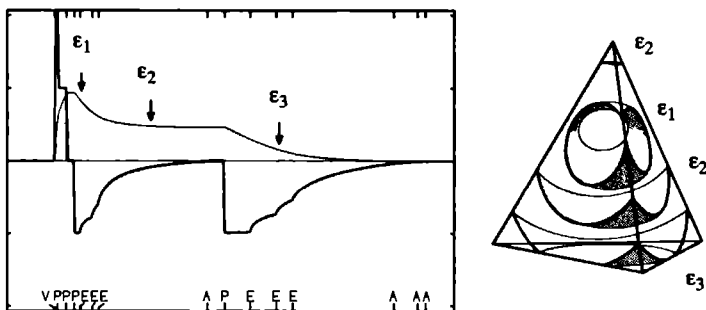


Figure 5. As for Fig. 3, but for a spherical dispersion relation with origin inside the tetrahedron. The density of states shows the free electron square-root Van Hove M_0 singularity at low energies.

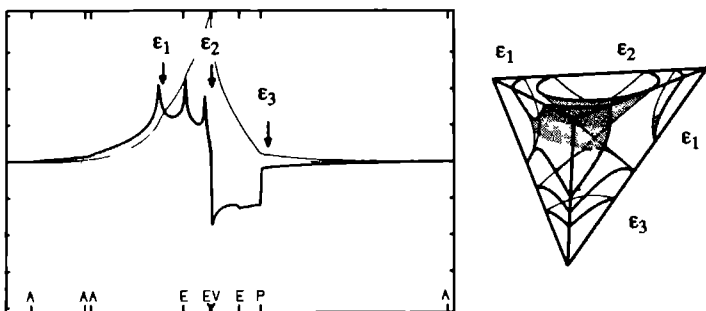


Figure 6. Same as Fig. 3, but for a hyperbolic dispersion relation with origin inside the tetrahedron. At energy $\epsilon_2=0$, the density of states has the proper analytic behaviour for a Van Hove M_1 singularity.

Research Institute for Materials and Faculty of Science,
Toernoorveld, 6525 ED Nijmegen, The Netherlands

Abstract

The analytic-quadratic method of integrating singular integrals such as the density of states over the Brillouin zone has been extended to include the effect of k -dependent matrix elements. The new general algorithm is not substantially slower than the version for the density of states while retaining the advantage over methods based on expansions to linear order only.

I. Introduction

Many quantities of interest in solid-state physics are given in the form of singular integrals over the Brillouin zone. Except for the few cases for which the integrals can be done analytically, the evaluation must be done by sampling over a set of points distributed through k -space. A number of methods have been developed in order to exploit this input data as efficiently as possible which are based on local linear expansions of the energy band. The methods of Jepsen and Andersen [48] and Lehmann and Taut [61] use tetrahedra as the basic volumes of integration. However, these methods share the disadvantage of not being able to resolve Van Hove singularities properly. This becomes noticeable in the form of spurious oscillations in the integrated result as the energy approaches the singularity. To eliminate this problem we have presented closed analytic expressions for the density of states combination derived from a general *quadratic* function for the bond energy over a tetrahedron in previous publications (Methfessel et al [69], Boon et al (1986), denoted by MBM and BMM)

* Submitted to Journal of Physics C

† Present address: Center for Materials Science, Los Alamos National Laboratory,
Los Alamos, New Mexico 87545 U S A

It was seen there that the new technique permitted a perfect representation of the Van Hove singularities as well as faster convergence rates as the number of sampling points is increased. In this paper, we extend the method to the general case that a well-behaved function $u(\mathbf{k})$ is included under the integral. For consistency in the orders of approximation, this makes it necessary to approximate $u(\mathbf{k})$ by a linear function. It is demonstrated that this does not make the method appreciably slower while retaining the advantages found for the density-of-states case.

In the following section, we show how the extra terms needed for the general case can be transformed to an integral over the surface of the tetrahedron. Evaluation of the surface integral turns out to be equivalent to calculating the densities of states for a quadratic function over a triangle in *two* dimensions and this will be discussed in section II(B). In section III we present a number of examples and in section IV we draw our conclusions.

II. Singular integrals and matrix elements

In this section we will consider the formal aspects of the analytic quadratic technique for matrix elements, as well as some technical details useful for the scheme's implementation.

(A) Reduction to $D(\epsilon)$ and $S(\epsilon)$

Assume that the energy of an electron or phonon band $E(\mathbf{k})$ is given as a function of \mathbf{k} in the Brillouin zone (BZ). We assume also a relatively slowly varying matrix element $u(\mathbf{k})$. The desired physical quantity is then given as the singular integral over the BZ as

$$F(\epsilon) = \int u(\mathbf{k})\delta[\epsilon - E(\mathbf{k})]d^3k. \quad (1)$$

This is equivalent to

$$F(\epsilon) = \int_{S_\epsilon} \frac{u(\mathbf{k})}{|\nabla E(\mathbf{k})|} d^2k \quad (2)$$

where ϵ varies throughout the energy range of the band. The symbol S_ϵ in the second expression denotes the constant energy surface $S_\epsilon = \{\mathbf{k}: E(\mathbf{k}) = \epsilon\}$. The integral for $F(\epsilon)$ is difficult to evaluate as is evident from the second, surface-integral expression. For certain values of \mathbf{k} , the denominator of the integrand vanishes. At these points, the integrand becomes singular but is still integrable. These 'critical points' are visible as Van Hove singularities in $F(\epsilon)$. An expansion to linear order in the vicinity of a critical point is inadequate since these

points are determined by the condition that the linear term, $\nabla E(\mathbf{k})$, disappears. Furthermore, every point in the Brillouin zone is more or less in the vicinity of some critical point because a minimal number of minima, maxima and saddle points must appear as a consequence of the connectivity of the bands induced by the periodic nature of $E(\mathbf{k})$ [72]. It is then not surprising that methods based on local linear expansions of $E(\mathbf{k})$ [48,61] only slowly converge (as $h^{1/3}$, where h gives the fineness of the \mathbf{k} -space mesh). Expanding E to quadratic order with a subsequent analytic integration improves the convergence rate and at the same time leads to a qualitative better result. Direct comparisons for the density of states have demonstrated that the linear result shows spurious oscillations near Van Hove singularities as well as a systematic shift of spectral weight from parts of the band with ellipsoidal mass tensor to parts with hyperbolic mass tensor (MBM, BMM).

Like most other Brillouin zone integration methods, the analytic quadratic method uses a partition of the Brillouin zone into a number of small tetrahedra and evaluates the integral (1) for one tetrahedron at a time. The difference to other methods lies in the order of the approximation to $E(\mathbf{k})$ and $u(\mathbf{k})$ taken throughout the tetrahedron. We expand $E(\mathbf{k})$ to quadratic order and $u(\mathbf{k})$ to linear order. The reason for limiting u to linear order is given by the following argument. Consider the desired integral in the form (2). Because of the gradient, the denominator is – in this representation – of linear order also. Formally expanding u to higher order would make little sense unless E were expanded to third order. But as we have argued before (MBM), since *quadratic* order preserves the structure of Van Hove singularities nothing substantial in this respect is gained by considering third and higher orders. Quadratic expansions of the energy bands are sufficient and necessary, and this is matched in precision by expanding matrix elements to linear order. Consequently, we have taken $u(\mathbf{k})$ as

$$u(\mathbf{k}) = u_0 + \mathbf{k} \cdot \mathbf{m}. \quad (3)$$

Placing this representation in (1) we find

$$\begin{aligned} F(\epsilon) &= u_0 \int \delta[\epsilon - E(\mathbf{k})] d^3\mathbf{k} + \mathbf{m} \cdot \int \mathbf{k} \delta[\epsilon - E(\mathbf{k})] d^3\mathbf{k} \\ &=: u_0 D(\epsilon) + \mathbf{m} \cdot \mathbf{S}(\epsilon). \end{aligned} \quad (4)$$

The volume of integration is now a single tetrahedron for which the expansions of $u(\mathbf{k})$ and $E(\mathbf{k})$ are valid and $F(\epsilon)$, $D(\epsilon)$, $\mathbf{S}(\epsilon)$ are the contributions from that tetrahedron. Of the two terms in (4), the first is just the density of states times a constant. Note that the separation (4) makes the method especially efficient if

integrals are to be calculated for many different functions $u(\mathbf{k})$ for the same $E(\mathbf{k})$, since $D(\epsilon)$ and $S(\epsilon)$ do not depend on u

The problem of calculating the density of states $D(\epsilon)$ for a quadratic dispersion relation and a tetrahedral volume has been solved in MBM and BMM and we briefly present the results. For a given energy ϵ , $D(\epsilon)$ is not equal to zero only if the constant energy surface S_ϵ intersects the tetrahedron. If this is the case, then the faces describe a polygon on S_ϵ . This polygon has vertices where the tetrahedron edges penetrate S_ϵ . The curved lines connecting the vertices are given by the intersections of the faces with S_ϵ . The central result is that the density of states at energy ϵ is related in a simple way to the angles in the vertices of the polygon. To be precise the energy derivative of the density of states is the sum of the angles, minus a constant and divided by $4\sqrt{|\det A(\epsilon - \epsilon_0)|}$. Here A is the symmetric matrix giving the quadratic term in $E(\mathbf{k})$ (i.e. the inverse mass tensor) and ϵ_0 is the energy at which $\nabla E(\mathbf{k})=0$. The only point which is subtle is that the angles must be defined in a way which takes into account the local shape of the band. This is done by using the inverse mass tensor to define a scalar product (the metric) and then using inverse trigonometric and inverse hyperbolic functions.

The reason for the unusual way of measuring the angles becomes clear when considering an example with an ellipsoidal dispersion relation. A linear transformation of \mathbf{k} -space exists which maps the ellipsoidal constant energy surfaces onto spheres. The density of states for the resulting spherical dispersion relation is equal to that of the original ellipsoidal dispersion relation times the determinant of the transformation. This leads to the factor $1/\sqrt{|\det A|}$. Assume that the formulation for the density of states using angles in the usual Euclidean sense is valid for the spherical case. Then these angles are just those which are measured in the original (ellipsoidal) system if the mass tensor is included in the way described above. In a similar way a hyperbolic case can be mapped onto the spherical dispersion relation by a complex linear transformation. Measuring the angles with the help of the (indefinite) hyperbolic scalar product and inverse hyperbolic functions can be seen as analytic continuation of the expressions for the ellipsoidal case. In sum, the definition of the scalar product using the inverse mass tensor is an elegant way to transform to a spherical dispersion relation implicitly.

(B) Evaluation of $S(\epsilon)$

We now turn to the evaluation of the vector $S(\epsilon)$. This term can easily be done by transforming it to a surface integral over the sides of the tetrahedron. As was explained in MBM and BMM, we can assume without loss of generality that $E(\mathbf{k}) = \mathbf{k}^T \mathbf{A} \mathbf{k}$ where the symmetric matrix \mathbf{A} is the inverse mass tensor. Let T denote the tetrahedron and $\chi_\epsilon(\mathbf{k}) = \theta[\epsilon - \mathbf{k}^T \mathbf{A} \mathbf{k}]$ the characteristic function which is equal to one inside the constant energy surface and equal to zero outside it. Then $\nabla \chi_\epsilon = -2\mathbf{A} \mathbf{k} \delta[\epsilon - \mathbf{k}^T \mathbf{A} \mathbf{k}]$ and

$$S(\epsilon) = \int_T \mathbf{k} \delta[\epsilon - \mathbf{k}^T \mathbf{A} \mathbf{k}] d^3 \mathbf{k} = -\frac{1}{2} \mathbf{A}^{-1} \int_T \nabla \chi_\epsilon(\mathbf{k}) d^3 \mathbf{k}. \quad (5)$$

Taking the scalar product of $S(\epsilon)$ with an arbitrary vector \mathbf{m} , one can pull the constant vector $\mathbf{A}^{-1} \mathbf{m}$ underneath the gradient operator, apply Gauss's theorem and take $\mathbf{A}^{-1} \mathbf{m}$ outside again, giving

$$\mathbf{m} \cdot S(\epsilon) = \mathbf{m} \cdot \left\{ -\frac{1}{2} \mathbf{A}^{-1} \int_{\partial T} \chi_\epsilon(\mathbf{k}) d\mathbf{a} \right\} \quad (6)$$

where $d\mathbf{a}$ is the element of area on the surface of the tetrahedron, ∂T . Since \mathbf{m} was arbitrary, $S(\epsilon)$ is equal to the quantity inside the curly brackets. We can split up the integration over the tetrahedron surface into a sum over the faces and use the fact that on each face F_i , $i=1..4$, the vector area element is parallel to the unit normal \mathbf{n}_i , giving

$$S(\epsilon) = -\frac{1}{2} \mathbf{A}^{-1} \sum_{i=1}^4 A_i(\epsilon) \mathbf{n}_i$$
$$A_i(\epsilon) = \int_{F_i} \chi_\epsilon(\mathbf{k}) d\mathbf{a}. \quad (7)$$

The quantity $A_i(\epsilon)$ is just the area of that part of the Face F_i which lies under the constant energy surface S_ϵ . *This is the integrated density of states in two dimensions for the dispersion relation which one obtains by restricting $E(\mathbf{k})$ to the face.* In this way, Gauss's theorem has been used to reduce the calculation of $S(\epsilon)$ to the problem of calculating the two-dimensional density of states. This problem is considerably simpler than the task of determining the three-dimensional density of states $D(\epsilon)$ and is solved by similar means.

(C) Analytic-quadratic method in two dimensions

In part (B) we have shown that a proper treatment of the linear term is equivalent to solving the density of states problem for a quadratic dispersion relation in two dimensions. For a given triangle and quadratic dispersion relation in the plane, the area of the part of the triangle which lies within the constant energy curve must be determined. This is then the integrated two-dimensional density of states $A(\epsilon)$. In this section, we derive the necessary expressions. The formalism is very similar to the three-dimensional case.

By shifting the origin in the plane and the energy scale, the dispersion relation is first brought to the form $E(\mathbf{k})=k^T B \mathbf{k}$ where B is a non-singular symmetric (2×2) matrix. The simple case $E=k^2$ is considered first. For an infinitesimal change in energy $d\epsilon$, one has (see Fig. 1a):

$$dA = \phi_{\text{tot}} k dk = \phi_{\text{tot}} \frac{1}{2} d\epsilon$$

$$\Rightarrow D_2(\epsilon) = \frac{dA}{d\epsilon} = \frac{1}{2} \phi_{\text{tot}}(\epsilon).$$

In this expression, $D_2(\epsilon)$ is the two-dimensional density of states and ϕ_{tot} is the total angle which is cut out of the full constant-energy circle by the border of the triangle. ϕ_{tot} can be the sum of a number of subangles. For example, consider a case when the origin lies inside the triangle. For small energies, there is no intersection and $\phi_{\text{tot}}=2\pi$, correctly giving $D_2(\epsilon)=\pi$. As ϵ increases and the circle

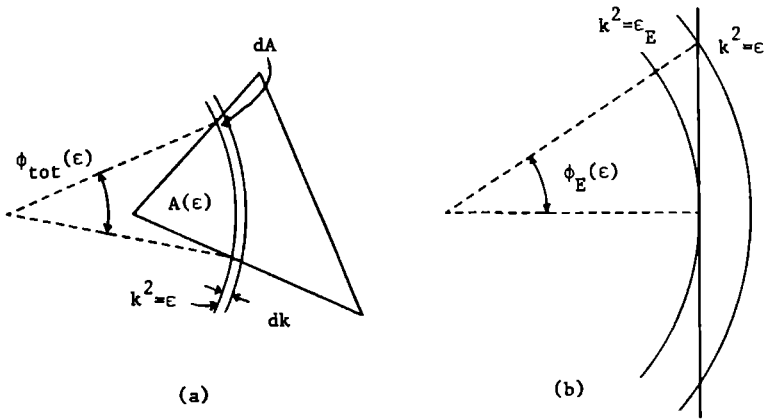


Figure 1. Quantities needed to evaluate the two-dimensional density of states $D_2(\epsilon)$ for the dispersion relation $\epsilon=k^2$ and a triangular region of integration. (a) The connection between $D_2(\epsilon)$ and the cut-out angle. (b) Definition of the angle $\phi_E(\epsilon)$ and the energy ϵ_E for a given edge.

expands, the sides of the triangle cut sectors out of the circle. In this way ϕ_{tot} and $D_2(\epsilon)$ are reduced. Finally, for ϵ larger than all three vertex energies, ϕ_{tot} and $D_2(\epsilon)$ are both zero.

Next, we express ϕ_{tot} using expressions which depend only on characteristic energies of the triangle. These are of two types: first, the three energies at the vertices and second, the three energies at which the line defined by an edge is tangent to the circle. These are denoted by symbols ϵ_V and ϵ_E , respectively. With a given edge is associated the angle $\phi_E(\epsilon)$ as illustrated in Fig. 1b. As a function of energy, ϕ_E is given by

$$\phi_E(\epsilon) = \arcsin \sqrt{1 - \frac{\epsilon E}{\epsilon}} = \arccos \sqrt{\frac{\epsilon_E}{\epsilon}}.$$

The desired total angle ϕ_{tot} is obtained by adding the ϕ_E together with the proper signs. At each energy ϵ , one angle ϕ_E is included in the sum for each intersection of the circle with the triangle edges. Thus each of the three ϕ_E can appear 0, 1 or 2 times in the sum. The sign is in each case +1 if the triangle and the origin lie on the same side of the edge and -1 otherwise. The number and type of terms which contribute to the sum can only change at the energies ϵ_V and ϵ_E , in addition to the energy $\epsilon=0$ if the origin lies inside the triangle. Thus these energies divide the energy range into intervals in a natural way. Within each interval, density of states and ϕ_{tot} are analytic, given by an expression such as

$$\phi_{\text{tot}}(\epsilon) = \sum_{\text{intersections}} (\pm) \phi_{E,i}(\epsilon) + C.$$

C is a different constant in each interval, that is, a step function. It is easy to see that ϕ_{tot} is continuous (except for the jump of 2π at $\epsilon=0$ if the triangle contains the origin) and this is enough information to fix the constant term in each interval.

In practice, the results stated above are used to construct ϕ_{tot} in the following way. First, the energies bounding the intervals are determined. In each interval, the relevant angles $\phi_{Ei}(\epsilon)$ are added with proper weight and sign. The result is a function which is equal to ϕ_{tot} except for a (different) constant in each interval. To complete the calculation, one scans through the intervals from negative to positive energy, adding the proper constants to make the function continuous. Should the origin lie inside the triangle, then ϕ_{tot} is set equal to 2π in the first interval (from $\epsilon=0$ to the smallest ϵ_E).

Next, we generalize the results above to elliptical dispersion relations: $E(\mathbf{k})=k^T B \mathbf{k}$ with $\det B > 0$. This is easy to do since the geometry of the triangle enters only over the special energies ϵ_V , ϵ_E , and $\epsilon=0$. The elliptical case can be solved by reducing it to the circular case. A linear transformation is applied which maps the ellipses of constant energy onto circles. Under this transformation, the special energies are invariant: the equivalent spherical case has the same vertex and edge energies. Thus the only effect of the transformation is to multiply areas by the Jacobean. We conclude that the formalism is valid the way it stands provided that the final result for $D_2(\epsilon)$ is divided by $\sqrt{\det B}$.

Finally, we turn to the case of $\det B < 0$. One proceeds as above but now starts from the standard hyperbolic case $E(\mathbf{k})=k_x^2 - k_y^2$ in place of $E(\mathbf{k})=k_x^2 + k_y^2$. Since the steps are very similar, we only state the results: The edge and vertex energies again play the role of dividing the energy range into intervals (with the minor difference that energies can be negative.) However, ϕ_{tot} and ϕ_ϵ are now hyperbolic angles:

$$\phi_E(\epsilon) = \begin{cases} -\operatorname{arsinh} \sqrt{\frac{-\epsilon_0}{\epsilon}} & \text{if } \frac{\epsilon_0}{\epsilon} < 0 \\ -\operatorname{arsinh} \sqrt{\frac{\epsilon_0}{\epsilon} - 1} & \text{if } \frac{\epsilon_0}{\epsilon} > 0. \end{cases}$$

ϕ_{tot} is assembled out of the three functions $\phi_{E_i}(\epsilon)$ as before. The only change is that ϕ_{tot} is continuous at all energies including $\epsilon=0$. Finally, the transformation of a general dispersion relation with $\det B < 0$ to the standard hyperbolic case is also the same as above except that $\sqrt{(-\det B)}$ takes the place of $\sqrt{(\det B)}$.

III. Application examples

We have applied the analytic quadratic method with linear matrix elements to a number of examples to illustrate both the benefits and some of the problems one may encounter in using this scheme.

(A) Green function integrals

As a first example we consider the Green function integrals for the simple cubic tight-binding band:

$$E(\mathbf{k}) = -(\cos\pi k_x + \cos\pi k_y + \cos\pi k_z)/3$$

$$u(\mathbf{k}) = e^{i\mathbf{k} \cdot \mathbf{R}}$$

The Brillouin zone is given by $-1 \leq k_i \leq 1$ and \mathbf{R} is a real-space lattice vector. By exploiting the cubic symmetry of the band, the integral reduces to 1/48-th of the zone where $u(\mathbf{k})$ is now the corresponding Slater-Koster function [83]. As typical cases we have chosen the functions $u = \cos(m\pi k_x) + \cos(m\pi k_y) + \cos(m\pi k_z)$ for $m=1$ and $m=6$. Fig. 2 shows the results for $F(\epsilon)$ and $dF/d\epsilon$ calculated by both the linear and the analytic-quadratic method. Eight times as many tetrahedra were used in the linear case since the linear interpolation needs only the four corner values. Thus both methods work with exactly the same input data. For the quadratic case, the local linear interpolation for $u(\mathbf{k})$ in each tetrahedron was a least-squares fit to the ten values of u at corners and mid-edges. The linear method takes u constant throughout single tetrahedra, equal to the mean value of the four corner values.

Characteristic for the integrals calculated by the linear method are artificial oscillations as function of energy, especially near the Van Hove singularities at $\epsilon = -1, -1/3, 1/3$ and 1 . This error was already observed in the density of states (MBM) and it has the same origin here. For any Brillouin zone integral, the result of the linear method is always a smooth, piecewise quadratic function of energy and the energy derivative is piecewise linear and continuous. This behaviour is evident in Fig. 2. Thus the oscillations in $F(\epsilon)$ result from trying to use unsuited smooth functions to describe the sharp corners and infinite derivatives of the real function. These singular features can only be approximated by overshooting strongly. An integral evaluated using the quadratic method, however, has the exact analytic behaviour at each Van Hove singularity. (In fact, the derivatives at $\epsilon=1$ for the quadratic result in Fig. 2 really are infinite and seem finite only due to the discrete energy grid.) It is therefore not surprising that the spurious oscillations are completely eliminated when the analytic-quadratic method is used.

It is of interest to compare the two methods as the number of oscillations in the plane wave part of the integrand increases. Of course, the k -point grid used must in any case be fine enough to resolve these oscillations. However, it is seen that the linear method introduces serious errors into the shape of the function early. For example, in the case of case of Fig. 2b, there are still four planes of grid points for each period of the plane wave. From Fig. 2 one can observe that the derivative $dF/d\epsilon$ for the quadratic method approaches a triangle-wave type of behaviour as the period of u becomes comparable to the spacing of the k -point grid. This means that the smooth oscillations which the true function $F(\epsilon)$ has between the Van Hove singularities are being modeled by second order polynomials, which is an adequate approximation in many cases.

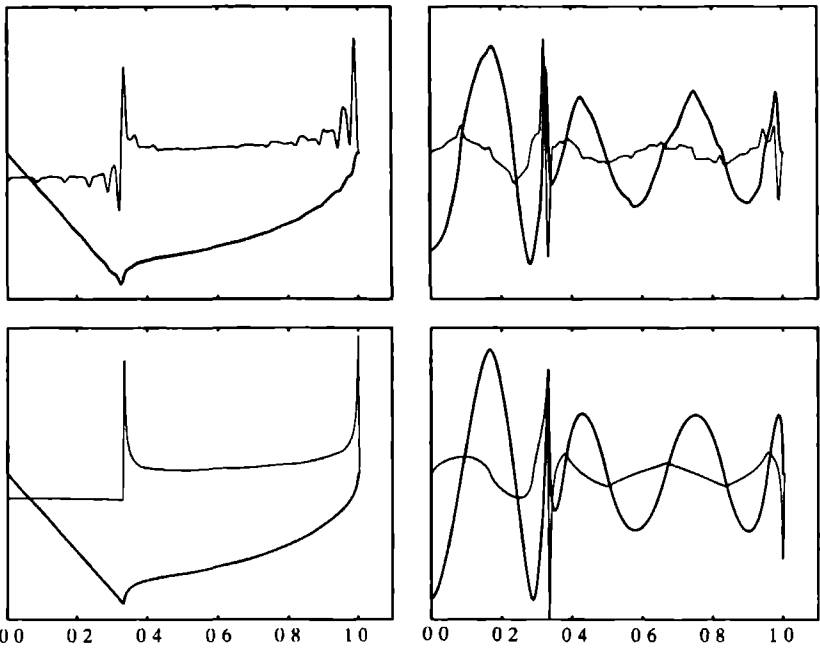


Figure 2. Comparison of the Green function integrals for the simple-cubic tight binding band for $m=1$ (left) and $m=6$ (right) when calculated by the linear (top) and analytic-quadratic method (bottom). The light curve is the energy derivative. Only the positive energy range is shown. The number of tetrahedra used was 1728 and 216 for the linear and quadratic case, respectively.

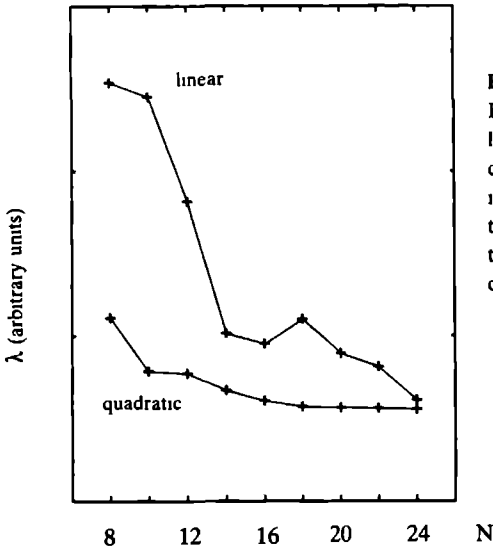


Figure 3. Phonon-correction Fermi surface integral λ as calculated by the two methods for increasing numbers of tetrahedra N . N is the number of divisions from Γ to X and defines the fineness of the k -point mesh for the input data.

(B) Fermi surface integrals

In many applications, one is not interested in F as a function of ϵ but instead requires only the value of F at one fixed energy. Usually this is the Fermi energy and the task is to calculate some integral over the Fermi surface. Our second example compares the convergence rates of the two methods for such a case. We start from the measured Fermi surface of copper as determined by de Haas-van Alphen and cyclotron mass experiments. As described by Halse [35], the Fermi surface is given by three functions $H(\mathbf{k})$, $H^+(\mathbf{k})$ and $H^-(\mathbf{k})$. Points on the Fermi surface satisfy $H(\mathbf{k})=0$ and points on adjacent energy surfaces to $\epsilon_F \pm \delta\epsilon$ are given by $H^\pm(\mathbf{k})=0$. The functions are smooth enough to be given as seven-term Fourier series. It is necessary to use more than one function since otherwise there is no information over $|\nabla E(\mathbf{k})|$ on the Fermi surface. An integral over the Fermi surface can be transformed in the following way

$$\begin{aligned} F(\epsilon_F) &= \int u(\mathbf{k}) \delta[\epsilon_F - E(\mathbf{k})] d^3k \\ &= \int u(\mathbf{k}) W(\mathbf{k}) \delta[F(\mathbf{k})] d^3k \end{aligned}$$

where $W(\mathbf{k})$ is an additional weight function defined as

$$W(\mathbf{k}) = \frac{H^- - H^+}{\delta\epsilon} \frac{|\nabla H|^2}{\nabla H \cdot (\nabla H^+ + \nabla H^-)}$$

For our example, this was evaluated for

$$u(\mathbf{k}) = \frac{1}{(\mathbf{k} - \mathbf{k}_0)^2 + k_{\text{TF}}^2}$$

The integral (denoted by λ) describes the phonon correction to the electron energies (Ashcroft and Mermin [5]). \mathbf{k}_0 lies on the Fermi surface on the line Γ to X . In Fig. 3, we have plotted the resulting values for λ as calculated by the two different methods for increasing numbers of tetrahedra. The faster convergence of the quadratic method is evident. We also note that whereas the quadratic result converges smoothly, the linear method again shows irregular and oscillatory behaviour. The oscillations as function of N arise for the same reason of those in $F(\epsilon)$ in the previous example. As the number of tetrahedra is increased, the oscillations in $F(\epsilon)$ gradually become smaller but also narrower, moving towards the closest Van Hove singularity. At the same time they pass across the Fermi energy and thereby introduce the corresponding spurious peaks in $F(\epsilon_F)$ at certain values of N . The consequence is that, since one in general does not know whether one is at a peak or a valley, the error bars become

correspondingly larger.

IV. Conclusions

In this paper, we have shown how the analytic-quadratic method for the density of states can be generalized to the evaluation of general singular integrals. Application examples have shown that the method is substantially more efficient and precise than analogous linear schemes in two cases: first, when the integral is needed over some energy range and second, when only the value of the integral at one fixed energy (for example the Fermi energy) is needed.

APPENDIX A: Mathematical Formulae

This appendix is a collection of additional mathematical formulae. A large part is concerned with the differential operator $\mathfrak{Y}_L(-i\nabla)$.

FOURIER TRANSFORMS

The 3-dimensional Fourier transform of $f(\mathbf{r})$ is denoted by $\hat{f}(\mathbf{q})$ and will be defined according to the convention [13]

$$\begin{aligned}\hat{f}(\mathbf{q}) &= \int e^{-i\mathbf{q} \cdot \mathbf{r}} f(\mathbf{r}) d\mathbf{r} \\ f(\mathbf{r}) &= \frac{1}{(2\pi)^3} \int e^{+i\mathbf{q} \cdot \mathbf{r}} \hat{f}(\mathbf{q}) d\mathbf{q}.\end{aligned}\tag{A1}$$

For functions given in a Y_L -representation, one has

$$\begin{aligned}f(\mathbf{r}) &= \frac{u(r)}{r} Y_L(\mathbf{r}) \mapsto \hat{f}(\mathbf{q}) = \frac{v(q)}{q} Y_L(\mathbf{q}) \\ v(q) &= 4\pi(-i)^\ell \int_0^\infty u(r) j_\ell(qr) qr dr \\ u(r) &= \frac{4\pi(-i)^\ell}{(2\pi)^3} \int_0^\infty v(q) j_\ell(qr) qr dq\end{aligned}\tag{A2}$$

where j_ℓ is the spherical Bessel function. The radial functions $u(r)$ and $v(q)$ are Hankel transforms of each other. Useful special cases are

$$\begin{aligned}e^{-a^2 r^2} &\mapsto \frac{\pi^{3/2}}{a^3} e^{-q^2/4a^2} \\ \frac{e^{-ar}}{r} &\mapsto \frac{4\pi}{q^2+a^2} \\ \delta(\mathbf{r}) &\mapsto 1.\end{aligned}\tag{A3}$$

DEFINITION OF $y_L(-i\nabla)$

Nozawa [75] generates the solid Hankel functions for the angular momentum quantum numbers (ℓ, m) out of $h_0(\mathbf{r}) := e^{i\mathbf{r}\cdot\mathbf{r}}$ in the following way:

$$\begin{aligned} H_{\ell}^m(\mathbf{r}) &= i^{\ell} h_{\ell}(\mathbf{r}) Y_{\ell}^m(\mathbf{r}) \\ &= (-1)^m C_{\ell}^m [(-i\partial_x) + i(-i\partial_y)]^m P_{\ell}^{(m)}(-i\partial_z) h_0(\mathbf{r}). \end{aligned} \quad (\text{A4})$$

where $P_{\ell}^{(m)}$ is the m -th derivative of the Legendre polynomial and C_{ℓ}^m normalizes the spherical harmonic Y_{ℓ}^m [67]:

$$Y_{\ell}^m(\mathbf{r}) = (-1)^m C_{\ell}^m \left[\frac{x+iy}{r} \right]^m P_{\ell}^{(m)}\left(\frac{z}{r}\right). \quad (\text{A5})$$

In the form (A4) the operator is not useful in the context of chapter 3 because it ignores the point $\mathbf{r}=0$ where it generates unwanted distribution terms. For example, for the case $\ell=2, m=0$ one has $P_2^{(0)}(z) = 3z^2 - 1$. To evaluate (A4) one needs

$$\partial_z^2 h_0(\mathbf{r}) = e^{i\mathbf{r}\cdot\mathbf{r}} \left\{ \frac{i}{r^2} - \frac{1+z^2}{r^3} - \frac{3iz^2}{r^4} + \frac{3z^2}{r^5} \right\} - \frac{4\pi}{3} \delta(\mathbf{r}). \quad (\text{A6})$$

The existence of δ -function term is proven by adding similar expressions for the three components and noting that $\Delta h_0 = -h_0 - 4\pi\delta$. Thus (A4) in fact generates the function

$$\begin{aligned} H_2^0(\mathbf{r}) &= C_2^0 [-3\partial_z^2 - 1] h_0(\mathbf{r}) \\ &= C_2^0 [-3e^{i\mathbf{r}\cdot\mathbf{r}} \{ \dots \} - \frac{e^{i\mathbf{r}\cdot\mathbf{r}}}{r} + 4\pi\delta(\mathbf{r})]. \end{aligned} \quad (\text{A7})$$

The contents of the brackets are the same as in the last equation. The unwanted δ -function part can be avoided by using the following definition instead:

$$\begin{aligned} H_2^0(\mathbf{r}) &= C_2^0 [-3\partial_z^2 + \Delta] h_0(\mathbf{r}) \\ &= C_2^0 [-3e^{i\mathbf{r}\cdot\mathbf{r}} \{ \dots \} - \frac{e^{i\mathbf{r}\cdot\mathbf{r}}}{r}]. \end{aligned} \quad (\text{A8})$$

The difference is that -1 has been replaced by Δ . Because $\Delta h_0 = -h_0$ for $\mathbf{r} \neq 0$, the two different operators give results which differ only at the origin. For the general (ℓ, m) case the corresponding modification is to use the function

$r^{\ell-m} P_{\ell}^{(m)}(z/r)$ in place of $P_{\ell}^{(m)}(z)$. From (A5), the spheric harmonic polynomials are

$$\mathcal{Y}_L^m(\mathbf{r}) = r^{\ell} Y_{\ell}^m(\mathbf{r}) = (-1)^m C_{\ell}^m [x+iy]^m r^{\ell-m} P_{\ell}^{(m)}\left(\frac{z}{r}\right) \quad (\text{A9})$$

so that the modified differential operator is just $\mathcal{Y}_L^m(-i\nabla)$ and

$$H_{\ell}^m(\mathbf{r}) = \mathcal{Y}_L^m(-i\nabla) h_0(\mathbf{r}). \quad (\text{A10})$$

This equation is now valid at all points including $\mathbf{r}=0$ meaning that neither side has a distributional part. Since z is not a special direction it is more useful to work with real linear combinations of $Y_{\ell}^m(\mathbf{r})$ and $Y_{\ell}^{-m}(\mathbf{r})$. These will be denoted by $Y_L(\mathbf{r})$.

FUNCTIONS GENERATED USING $\mathcal{Y}_L(-i\nabla)$

The following presents some general properties for functions which are generated using $\mathcal{Y}_L(-i\nabla)$. For a function $f(\mathbf{r})$, depending only on $r=|\mathbf{r}|$, define

$$F_L(\mathbf{r}) = \mathcal{Y}_L(-i\nabla) f(\mathbf{r}). \quad (\text{A11})$$

Then F_L is the product of a radial function times $Y_L(\mathbf{r})$ and the radial part can be derived from $f(\mathbf{r})$ by differentiation:

$$\begin{aligned} F_L(\mathbf{r}) &= i^{\ell} f_{\ell}(r) Y_L(\mathbf{r}) \\ f_{\ell}(r) &= r^{\ell} \left(-\frac{1}{r} \partial_r\right)^{\ell} f(r) \\ &= \left[-\partial_r + \frac{\ell-1}{r}\right] f_{\ell-1}(r). \end{aligned} \quad (\text{A12})$$

Specifically, $f_0=f$. To derive (A12), note that the Fourier transform of $F_L(\mathbf{r})$ is:

$$\hat{F}_L(\mathbf{q}) = \mathcal{Y}_L(\mathbf{q}) \hat{f}(\mathbf{q}). \quad (\text{A13})$$

By means of (A2) with $v(\mathbf{q})=q^{\ell+1} \hat{f}(\mathbf{q})$, the back transform for $F_L(\mathbf{q})$ is evaluated, giving

$$F_L(\mathbf{r}) = i^{\ell} \left\{ \frac{4\pi}{(2\pi)^3} \int_0^{\infty} q^{\ell+1} \hat{f}(\mathbf{q}) j_{\ell}(qr) q dq \right\} Y_L(\mathbf{r}) \quad (\text{A14})$$

and the quantity between curly brackets is identified as $f_{\ell}(r)$. The only dependence on r here comes through the Bessel function. The recursion relation for

f_ℓ then follows immediately by substituting the known recursion relation for $j_\ell(qr)$ under the integral:

$$j_\ell(r) = [-\partial_r + \frac{\ell-1}{r}]j_{\ell-1}(r)$$

$$\Rightarrow j_\ell(qr) = \frac{1}{q} [-\partial_r + \frac{\ell-1}{r}]j_{\ell-1}(qr). \quad (A15)$$

Equation (A12) shows that the $f_\ell(r)$ always satisfy the first of the two recursion relations which are familiar from the spherical Hankel and Bessel functions. To get something similar to the second relation, more information about $f(r)$ is needed. For example, a common situation is that $\Delta f = g$ for a known function $g(r)$. By applying $\mathcal{Y}_L(-i\nabla)$ to both sides and exchanging the operators, one obtains $\Delta F_L = G_L$. Here $G_L(r)$ equals $i^\ell g_\ell(r) Y_L(r)$ and is derived from $g(r)$ by using $\mathcal{Y}_L(-i\nabla)$. The differential equation which connects f_ℓ and g_ℓ follows by using the Laplace operator in polar coordinates:

$$\partial_r^2 f_\ell + \frac{2}{r} \partial_r f_\ell - \frac{\ell(\ell+1)}{r^2} f_\ell = g_\ell. \quad (A16)$$

By use of (A12) this can be shown to be equivalent to

$$[\partial_r + \frac{\ell+1}{r}]f_\ell(r) = -g_{\ell-1}(r). \quad (A17)$$

Finally, (A12) and (A17) together are used to eliminate the derivative, resulting in

$$\frac{2\ell+1}{r} f_\ell = f_{\ell+1} - g_{\ell-1}. \quad (A18)$$

The relations for the spherical Bessel and Hankel functions are recovered by setting $g = -f$ since these functions satisfy $\Delta f = -f$ for $r > 0$. In many cases $f(r)$ is an analytic function of r at all points including $r = 0$. Then the same is true for the $F_L(r)$ so that the leading term in $f_\ell(r)$ is proportional to r^ℓ . For the functions $\chi_\ell := r^{-\ell} f_\ell$, one has $F_L = i^\ell \chi_\ell(r) \mathcal{Y}_L(r)$ and eqs. (A12), (A18) go over to

$$\chi_{\ell+1} = -\frac{1}{r} \partial_r \chi_\ell \quad (A19a)$$

$$r^2 \chi_{\ell+1} = (2\ell+1) \chi_\ell + r^{-(\ell-1)} g_{\ell-1}. \quad (A19b)$$

The recursion relations make it possible to calculate explicit expressions for the functions $F_L(r)$. For example, $f(r)$ can be taken equal to the normalized

Gaussian $(a^2/\pi)^{3/2} e^{-a^2 r^2}$. Then $\chi_0=f$ and the only effect of applying $(-1/r)\partial_r$ is to bring down a factor of $2a^2$. Therefore

$$\begin{aligned} G_L(\mathbf{r}) &:= \mathcal{Y}_L(-i\nabla)(a^2/\pi)^{3/2} e^{-a^2 r^2} \\ &= (a^2/\pi)^{3/2} (2a^2)^\ell e^{-a^2 r^2} r^\ell \mathcal{Y}_L(\mathbf{r}). \end{aligned} \quad (\text{A20})$$

To demonstrate that the solid Hankel and Bessel functions (eq. 3.2) are indeed generated as in eq. (3.11), first the functions for $\ell=0$ are shown to be the same; then the standard recursion relations for the Hankel and Bessel functions together with the relations above show equality for all values of ℓ .

The smoothed Hankel functions (eq. 3.20) are generated from the function $f(\mathbf{r})$ which satisfies

$$\Delta f = -\epsilon f - 4\pi C e^{-a^2 r^2} \quad \text{with } C = \frac{a^3}{\pi^{3/2}} e^{\epsilon/4a^2}. \quad (\text{A21})$$

The zero-order function $\chi_0(\mathbf{r})$ is known explicitly and the next function can be obtained by differentiation (eq. A19a). The recursion relation (A19b) is used to calculate all higher functions, whereby the right-hand side of the differential equation (A21) plays the role of $g(\mathbf{r})$, so that

$$r^2 \chi_{\ell+1} = (2\ell+1) \chi_\ell - \epsilon \chi_{\ell-1} - 4\pi C (2a^2)^\ell e^{-a^2 r^2}. \quad (\text{A22})$$

Of special interest are the distributions generated from the δ -function: $D_L(\mathbf{r}) = \mathcal{Y}_L(-i\nabla)\delta(\mathbf{r})$. Their properties can be derived by describing D_L as the limit of the Gaussians (A21) for $a \rightarrow \infty$. Since D_L is a distribution, multiplying it by a testfunction $\phi(\mathbf{r})$ and integrating will pick out some linear combination of the derivatives of ϕ at $\mathbf{r}=0$. By integrating in polar coordinates one can calculate

$$\begin{aligned} \int G_L(\mathbf{r}) r^{2m} \mathcal{Y}_K(\mathbf{r}) d\mathbf{r} &= i^\ell \frac{(2m+2\ell+1)!!}{4\pi(2a^2)^m} \delta_{KL} \\ \int D_L(\mathbf{r}) r^{2m} \mathcal{Y}_K(\mathbf{r}) d\mathbf{r} &= i^\ell \frac{(2\ell+1)!!}{4\pi} \delta_{KL} \delta_{m0}. \end{aligned} \quad (\text{A23})$$

The first integral leads to a standard integration and the second is the limit of the first for $a \rightarrow \infty$. (A23) shows that when ϕ is expanded as in (3.6), D_L can be defined as the distribution which picks out the $L,0$ -th term. To get the terms for higher values of n , $\Delta^n D_L$ must be used:

$$\int \Delta^n D_L(\mathbf{r}) r^{2m} \mathcal{Y}_K(\mathbf{r}) d\mathbf{r} = i^\ell \frac{(2\ell+1)!!}{4\pi} \frac{2^m m!}{(m-n)!} \frac{(2m+2k+1)!!}{(2m+2k-2n+1)!} \delta_{KL} \delta_{mn}. \quad (\text{A24})$$

This is derived by shifting the operator Δ^n under the integral to the function $r^{2m} y_K(r)$ and then using (A23). Altogether, this means that the distributions $\Delta^n D_L$ produce the coefficients of the 'spherical Taylor series' (3.6) just as the partial derivatives of the δ -function do for a Taylor expansion in cartesian coordinates.

The smoothing of the interstitial potential in section 4.2 requires integrals over all space of products containing Gaussians and smoothed Hankel functions at different sites. In fact, all 2-center integrals in a family containing both types of functions are easy to evaluate. Define the functions $w_p(r)$ by their Fourier transforms

$$\hat{w}_p(q) = -4\pi e^{\gamma(\epsilon-q^2)} (\epsilon-q^2)^p \quad (A25)$$

and set $W_{pL}(r) = y_L(-i\nabla)w_p(r)$. For $p=0$ and $p=-1$ these are Gaussians and smoothed Hankel functions, respectively, with a decay given by $\gamma=1/4a^2$. The functions W_{pL} for $p>0$ are linear combinations of the $\Delta^k W_{0L}$, $k=0 \dots p$, as follows from

$$(\Delta + \epsilon)W_{pL} = W_{p+1L} \quad (A26)$$

The functions with $p \geq 0$ are restricted to the range of $e^{-a^2 r^2}$ while those with $p < 0$ are extended. The two-center integral between any two functions can be calculated using Parseval's equality. The Fourier transform of W_{pL} is $y_L(q)\hat{w}_p(q)$ so that the Fourier transform of the function centered at \mathbf{R} is

$$W_{pL}(\mathbf{r}-\mathbf{R}) \mapsto -4\pi e^{\gamma(\epsilon-q^2)} (\epsilon-q^2)^p y_L(q) e^{-iq \cdot \mathbf{R}} \quad (A27)$$

Then, permitting two functions to have different centers as well as different decays a, b and setting $c^2 = a^2 b^2 / (a^2 + b^2)$,

$$\begin{aligned} I &= \int W_{pL}^*(\mathbf{r}-\mathbf{R}) W_{sK}(\mathbf{r}-\mathbf{S}) d\mathbf{r} \\ &= \frac{1}{(2\pi)^3} (4\pi)^2 \int e^{(\epsilon-q^2)/4c^2} (\epsilon-q^2)^{p+s} y_L(q) y_K(q) e^{iq \cdot (\mathbf{R}-\mathbf{S})} dq \\ &= -4\pi \sum_{\text{MLM}} C_{KLM} \frac{-4\pi}{(2\pi)^3} \int q^{k+\ell-m} e^{(\epsilon-q^2)/4c^2} (\epsilon-q^2)^{p+s} y_M(q) e^{iq \cdot (\mathbf{R}-\mathbf{S})} dq \end{aligned}$$

The last integral is just the back transform of an expression such as (A27) with an additional even power of q . Therefore

$$I = -4\pi \sum_M C_{KLM} (-\Delta)^{(k+\ell-m)/2} W_{p+s,M}(\mathbf{R}-\mathbf{S}) \quad (\text{A28})$$

where the functions $W_{p+s,M}$ are defined for $\gamma=1/4c^2$. This expresses the 2-center integral in closed form using the same type of functions, evaluated for the vector connecting the centers

LATTICE SUMS AND STRUCTURE CONSTANTS

For a periodic system, the Bloch sums of the solid Hankel functions are of importance. Using the expression for the Fourier transform of H_L (eq. 3.14) these can alternatively be written as a sum over the reciprocal lattice:

$$\mathcal{H}_L(\mathbf{r}) = \sum_{\mathbf{R}} e^{i\mathbf{k}\cdot\mathbf{R}} H_L(\mathbf{r}-\mathbf{R}) \quad (\text{A29a})$$

$$= -\frac{4\pi}{\Omega} \sum_{\mathbf{G}} \frac{y_L(\mathbf{k}+\mathbf{G})}{\epsilon-(\mathbf{k}+\mathbf{G})^2} e^{i(\mathbf{k}+\mathbf{G})\cdot\mathbf{r}} \quad (\text{A29b})$$

Both expressions are not suitable for practical calculation. The real space sum is difficult because the functions H_L are long ranged unless the energy is large and negative. The sum over reciprocal lattice vectors is only conditionally convergent because of the spherical harmonic polynomial. The slowly decaying Fourier terms are necessary to make the singularity of \mathcal{H}_L . The Ewald method [36] treats the singularity separately by splitting the functions into two parts before doing the Bloch summation.

$$H_L(\mathbf{r}) = H_L^{\text{sm}}(\mathbf{r}) + H_L^{\text{d}}(\mathbf{r}) \quad (\text{A30})$$

Here H_L^{sm} is the smoothed Hankel function (eq. 3.20) which is equal to H_L for $e^{-a^2 r^2} \approx 0$. Therefore the difference H_L^{d} is 'damped' in that it is zero where $e^{-a^2 r^2} \approx 0$. By taking a Bloch sum over (A30) and then using a Fourier sum to evaluate the contribution from the smooth functions, one has

$$\begin{aligned} \mathcal{H}_L(\mathbf{r}) &= -\frac{4\pi}{\Omega} \sum_{\mathbf{G}} \frac{y_L(\mathbf{k}+\mathbf{G}) e^{(\epsilon-(\mathbf{k}+\mathbf{G})^2)/4a^2}}{\epsilon-(\mathbf{k}+\mathbf{G})^2} e^{i(\mathbf{k}+\mathbf{G})\cdot\mathbf{r}} \\ &\quad + \sum_{\mathbf{R}} e^{i\mathbf{k}\cdot\mathbf{R}} H_L^{\text{d}}(\mathbf{r}-\mathbf{R}) \\ &=: \mathcal{H}_L^{\text{sm}}(\mathbf{r}) + \mathcal{H}_L^{\text{d}}(\mathbf{r}) \end{aligned} \quad (\text{A31})$$

Both summations need only a small number of terms: the reciprocal sum because of the exponential factor and the real-space sum because H_L^{d} quickly goes

to zero for large arguments. The principle of the method is to treat the long-ranged and the singular parts of H_L differently. The evaluation of the functions $H_L^d(\mathbf{r}-\mathbf{R})$ can be done in closed form (using the explicit expression (3.21) and the recursion relations) but is often done in the form of an integral. For example, for $\epsilon = -\kappa^2 < 0$ the zero-order function is $f(r) = (u_+ - u_-)/2r$ with

$$\begin{aligned} u_{\pm}(r) &= e^{\mp \kappa r} \left[1 - \operatorname{erfc} \left(\frac{\kappa}{2a} \mp ar \right) \right] \\ &= \frac{2}{\sqrt{\pi}} \int_a^{\infty} e^{-r^2 \xi^2} e^{\epsilon/4\xi^2} \left(-\frac{\kappa}{2\xi^2} \mp r \right) d\xi. \end{aligned} \quad (\text{A32})$$

The second expression follows from the first by using the definition of the error function as an integral over e^{-z^2} [1] and the substitution $z = \kappa/2\xi \mp r\xi$. One of the terms cancels when u_+ and u_- are subtracted, giving

$$f(r) = -\frac{2}{\sqrt{\pi}} \int_a^{\infty} e^{\epsilon/4\xi^2} e^{-\xi^2 r^2} d\xi. \quad (\text{A33})$$

A third and more efficient method to calculate $f(r)$ is to use a power series in the energy. This is useful because the explicit expression (3.21) uses the complex error function for positive energies which might not be available. From (A33) it follows that f satisfies the differential equation

$$4\epsilon \frac{\partial^2 f}{\partial \epsilon^2} + \frac{\partial f}{\partial \epsilon} + r^2 f = -\frac{1}{a\sqrt{\pi}} e^{\epsilon/4a^2} e^{-a^2 r^2}. \quad (\text{A34})$$

Writing f as a power series in ϵ leads to a one-step recursion relation for the coefficients:

$$\begin{aligned} f &= \sum_n C_n \epsilon^n \\ -2n(2n-1)C_n &= r^2 C_{n-1} + \frac{e^{-a^2 r^2}}{a\sqrt{\pi}} \frac{1}{(n-1)!} \left(\frac{1}{4a^2} \right)^{n-1}. \end{aligned} \quad (\text{A35})$$

Unless $|\epsilon/4a^2|$ gets unreasonably big, the series converges fast in practice. The choice of the coefficient C_0 determines how much of the homogeneous solution of (A34) is included. The proper choice is $C_0 = \operatorname{erfc}(ar)/r$ to produce the damped Hankel function. This simple program generates $f(r)$:

```

SUBROUTINE IDPP(P,F,A,F)
IMPLICIT REAL*8 (A-H,I-Z)
DATA SPP1/1.77245385100/
FAC=.2500*PI/A/A
CII=DERFC(A*R)/P
F=CN
XXX=-DEXP(-A*A*P*P)/(A*SPP1)
DO 10 N=1,100
  CN=-E*(R*R*CI+XXX)/(2*I*(2*I-1))
  F=F+CN
  IF(DABS(CN).LT.1.D-15) RIM10N
10 XXX=XXX*FAC/N
RETURN
END

```

The *site-diagonal* structure constants in eq. (3.19) describe the function $\mathcal{H}_L(\mathbf{r})$ near the singularity, that is, for $\mathbf{r} \rightarrow 0$. The singularity of \mathcal{H}_L comes from the Hankel function centered at $\mathbf{R}=0$ in (A29a) so that the 'scattered-in part' is

$$\mathcal{H}_L^{\text{sc}}(\mathbf{r}) = \mathcal{H}_L(\mathbf{r}) - H_L(\mathbf{r}).$$

By the Ewald method (A31) this comes out to

$$\mathcal{H}_L^{\text{sc}}(\mathbf{r}) = \mathcal{H}_L^{\text{sm}}(\mathbf{r}) + \sum_{\mathbf{R} \neq 0} e^{i\mathbf{k} \cdot \mathbf{R}} H_L^{\text{d}}(\mathbf{r} - \mathbf{R}) - H_L^{\text{sm}}(\mathbf{r}). \quad (\text{A36})$$

The last term on the right-hand side (usually denoted by $\mathcal{O}^{\ell(3)}$ [36]) is non-zero only if $\ell=0$ and can be calculated from the explicit expression eq. (3.21).

MULTIPOLE MOMENTS FOR SOLID HANKEL AND BESSEL FUNCTIONS

Here eq. (4.39) is derived. All functions are taken to be real so that they have been generated by the operator $\mathcal{Y}_L(-\nabla)$. Since $\Delta H_L = -\epsilon H_L - 4\pi D_L$ and $\Delta \mathcal{Y}_L = 0$, one has

$$\begin{aligned}
I &:= \oint_S [H_L \nabla \mathcal{Y}_L - \mathcal{Y}_L \nabla H_L] \cdot d\mathbf{a} \quad (\text{A37}) \\
&= \int_S [H_L \Delta \mathcal{Y}_L - \mathcal{Y}_L \Delta H_L] d\mathbf{r} = \epsilon \int_S \mathcal{Y}_L H_L d\mathbf{r} + 4\pi \int_S \mathcal{Y}_L D_L d\mathbf{r}.
\end{aligned}$$

Writing H_L in the form $H_L(\mathbf{r}) = f_\ell(r) Y_L(\mathbf{r})$, the surface integral gives

$$\begin{aligned}
I &= \oint_S \{f_\ell Y_L \ell r^{\ell-1} Y_L - r \ell Y_L \frac{\partial f}{\partial r} Y_L\} d\mathbf{a} \\
&= R^{\ell+2} \left\{ -\frac{d}{dr} + \frac{\ell}{r} \right\} f_\ell(R)
\end{aligned}$$

$$= R^{\ell+2} f_{\ell+1}(R)$$

where the recursion relation (A12) was used in the last step.

The integral over $y_L D_L$ in (A37) is $(2\ell+1)!!$ by eq. (A23) and solving for $\int y_L H_L dr$ then gives the desired result. The Bessel function integral is calculated in the same way, using $\Delta J_L = -\epsilon J_L$:

$$\begin{aligned} I &= \oint_{\partial S} [J_L \nabla y_L - y_L \nabla J_L] \cdot da = \epsilon \int y_L J_L \\ &= \epsilon^{-\ell} R^{\ell+1} \left\{ -\frac{d}{dr} + \frac{\ell}{r} \right\} g_\ell(r) \\ &= \epsilon^{-\ell} R^{\ell+2} g_{\ell+1}(R) \end{aligned}$$

where the factor $\epsilon^{-\ell}$ comes from the definition (3.11) of J_L and the function was written as $J_L = g_\ell(r) Y_L(\mathbf{r})$.

APPENDIX B: Singular Part of the Multipole Green Function

This Appendix gives additional calculational details which were not included in section 3.3(B).

BIORTHOGONAL POLYNOMIALS

Consider a series of functions $\psi_p(z), p=0,1,\dots$, all analytic at $z=0$, such that the leading term in ψ_p is proportional to z^p . Written as a power series the functions are:

$$\psi_p(z) = \sum_{n=p}^{\infty} P_p(n)z^n. \quad (B1)$$

The aim is to represent a given analytic function $\xi(z)$ as a linear combination of the ψ_p :

$$\xi(z) = \sum_{p=0}^{\infty} a_p \phi_p(z). \quad (B2)$$

This kind of expansion is called a Neumann series [1]. The coefficients a_p are found using 'biorthogonal polynomials' $\beta_q(z), q=0,1,\dots$ which satisfy

$$2\pi i \delta_{pq} = \oint \beta_q(z) \phi_p(z) dz \quad (B3)$$

where the contour integrals are taken over a closed counterclockwise loop around the origin containing no singularities of ξ . It can be shown that β_q is a polynomial of order $q+1$ in $1/z$:

$$\beta_q(z) = \sum_{s=0}^q B_q(s) \frac{1}{z^{s+1}}. \quad (B4)$$

By multiplying (B2) with $\beta_q(z)$ and integrating over the contour it follows that

$$\begin{aligned} a_q &= \frac{1}{2\pi i} \oint \beta_q(z) \xi(z) dz \\ &= \sum_{s=0}^q B_q(s) \frac{1}{2\pi i} \oint \frac{\xi(z)}{z^{s+1}} dz \end{aligned} \quad (B5)$$

$$= \sum_{s=0}^q B_q(s) [\xi(z)]_s.$$

The symbol $[\dots]_s$ is used to denote the coefficient of order s in the Taylor expansion at $z=0$, that is $[\xi(z)]_s = \partial_z^{(s)} \xi(0)/s!$.

NEUMANN SERIES FOR $\phi^{(0)}$

In the following, the solid Hankel functions will be taken as real and will be defined as (for some energy ϵ_0)

$$H_L(r) = f_\ell(r) Y_L(r)$$

$$f_\ell(r) = \begin{cases} k^{\ell+1} n_\ell(kr) & \epsilon_0 = k^2 > 0 \\ (i\kappa)^{\ell+1} n_\ell(i\kappa r) & \epsilon_0 = -\kappa^2 < 0. \end{cases} \quad (B6)$$

They are generated as in (A11) from the first function which is

$$f(r) = \begin{cases} \frac{\cos kr}{r} & \epsilon_0 > 0 \\ \frac{\cosh \kappa r}{r} & \epsilon_0 < 0. \end{cases} \quad (B7)$$

From (A19) and because the operation $-(1/r)\partial_r$ does not mix even and odd powers of r it follows that $f_\ell(r)$ only has even or odd powers depending on whether ℓ is even or odd. That is, each H_L contains *only* singular terms. Later a suitable analytic part will be added for the case $\epsilon_0 < 0$ to go over to the old definition of H_L (eq. 3.4). The functions

$$H_L^{(p)} = \left(\frac{\partial}{\partial \epsilon_0}\right)^{(p)} H_L = f_\ell^{(p)} Y_L(r) \quad (B8)$$

will be used to represent the singularity of the multipole Green function as in (3.31). The equation to be solved is

$$[\Delta + \epsilon - V_I(r)]\phi(r) = 0 \quad r > 0, \quad (B9)$$

whereby ϕ must have a prescribed singularity at $r=0$. In the Y_L -representation for ϕ (eq. 3.27) one must solve the coupled radial equations

$$\Delta_\ell R_L = \sum_K W_{LK} R_K - \varepsilon R_L$$

$$\text{with } \Delta_\ell := \frac{1}{r^2} \partial_r r^2 \partial_r - \frac{\ell(\ell+1)}{r^2}. \quad (\text{B10})$$

By expanding R_L in the functions f_ℓ and using that $(\Delta_\ell + \varepsilon_0)f_\ell^{(p)} = -p f_\ell^{(p-1)}$, the coupled equations are rewritten:

$$\begin{aligned} R_L &= \sum_p C_{Lp} f_\ell^{(p)} \\ 0 &= \sum_p (p+1) C_{L,p+1} f_\ell^{(p)} + \sum_p (\varepsilon_0 - \varepsilon) C_{Lp} f_\ell^{(p)} + \sum_{Kp} W_{LK} C_{Kp} f_k^{(p)}. \end{aligned} \quad (\text{B11})$$

The coupling potential $W_{LK}(r)$ is given in (3.29). Equation (B11) is multiplied by $r^{\ell+1}$ to eliminate all singular terms, giving

$$0 = \sum_p (p+1) C_{L,p+1} \psi_\ell^{(p)} + \sum_p (\varepsilon_0 - \varepsilon) C_{Lp} \psi_\ell^{(p)} + \sum_{Kp} F_{LK} C_{Kp} \psi_k^{(p)}. \quad (\text{B12})$$

The new functions are defined as

$$\begin{aligned} \psi_\ell^{(p)}(r) &= r^{\ell+1} f_\ell(r) =: \sum_{n=p}^{\infty} P_\ell^{(p)}(n) r^{2n} \\ F_{LK}(r) &= r^{\ell-k} W_{LK}(r). \end{aligned} \quad (\text{B13})$$

The sum shows that only even powers of r appear in $\psi_\ell^{(p)}$ and that the leading term is proportional to r^{2p} . $F_{LK}(r)$ also has only even positive powers of r so that eq. (B12) is in fact a relation connecting functions of the variable $z=r^2$. For every separate ℓ the functions $\psi_\ell^{(p)}(z)$, $p=0,1,2,\dots$ have a corresponding set of biorthogonal polynomials $\beta_\ell^{(q)}$:

$$\beta_\ell^{(q)}(z) = \sum_{s=0}^q B_\ell^{(q)}(s) \frac{1}{z^{s+1}}. \quad (\text{B14})$$

To isolate a coefficient in eq. (B12), the equation is multiplied by $\beta_\ell^{(q)}(z)/2\pi i$ and integrated over the contour, giving

$$\begin{aligned} 0 &= (q+1) C_{L,q+1} + (\varepsilon_0 - \varepsilon) C_{Lq} \\ &+ \sum_{s=0}^q B_\ell^{(q)}(s) \sum_K \left[F_{LK}(z) \sum_{p=0}^{\infty} C_{Kp} \psi_k^{(p)}(z) \right]_s. \end{aligned} \quad (\text{B15})$$

In the last term, eq. (B5) and the explicit form (B14) were used. Equation

(B15) does not seem to be a recursion relation at first sight because the right-hand side contains the functions $R_K(r)$ which are to be calculated: the sum inside the brackets $[[\]]$ is just $r^{\ell+1}R_K(r)$ by equation (B11). However, this sum has all terms of orders z^0, z^2, \dots, z^q correct as soon as the coefficients C_{Kp} are known for $p \leq q$. This follows because the leading term in $\psi_K^{(p)}$ is proportional to z^p . Since $F_{LK}(z)$ only contains positive powers of z , all terms up to the order q are correct for the contents of $[[\dots]]$ so that the sum over s can be evaluated. In practice, this means that at each step in the recursion over q , the current expressions for the functions R_K can be used when solving (B15) for $C_{L,q+1}$. To start the recursion for the function with a singularity of type L_0 , the coefficient $C_{L,0}$ is set to one and all other C_{L0} to zero. The coefficients up to the desired order $q = p_{\max}$ then give the desired expansion (3.31). For the case that the energy ϵ_0 of the Hankel functions has been chosen negative, the coefficients calculated above also give the proper linear combination of the solid Hankel functions generated from $e^{-\kappa r}/r$ as in (3.11) instead of from $\cosh(\kappa r)/r$ as in eq. (B7). The difference between corresponding functions of the different sets is analytic so that the proper description of the singularity is not harmed. One has in effect added a smooth function at the last moment to get a final result which satisfies the boundary conditions (regularity for $r \rightarrow \infty$).

In principle there exists no algorithm for solving the matrix eigenvalue problem $HC = \epsilon S$ if neither matrix is definite, even if it is known that eigenstates exist (Wilkinson [97]). However, the following method was found to be adequate for the problem at hand. Assume there exists an energy ϵ' so that $H - \epsilon'S$ is positive definite. This should be possible if H and S make any sense at all by choosing ϵ' to lie below the expected bands. The following eigenvalue problem is solved by usual means:

$$\begin{aligned} SB_\mu &= \lambda_\mu [H - \epsilon'S]B_\mu \\ B_\mu^+ [H - \epsilon'S]B_\nu &= \delta_{\mu\nu} \end{aligned} \quad (C1)$$

giving a complete set of eigenstates B_μ, λ_μ . Trying to transform back to the original problem, one finds

$$\begin{aligned} HB_\mu &= \epsilon_\mu SB_\mu \quad \text{with} \quad \epsilon_\mu = \epsilon' + \lambda_\mu^{-1} \\ B_\mu^+ SB_\nu &= \delta_{\mu\nu} (\epsilon_\mu - \epsilon')^{-1} \end{aligned} \quad (C2)$$

so that everything is in order except for the normalization of the eigenstates. The difficulty is that the states with $\epsilon_\mu < \epsilon'_0$ cannot be normalized respective to S . However, we do the best we can by defining $C_\mu = \sqrt{|\epsilon_\mu - \epsilon'|} B_\mu$ for all μ , giving

$$\begin{aligned} HC_\mu &= \epsilon_\mu SC_\mu \\ C_\mu^+ SC_\nu &= \delta_{\mu\nu} \text{sign}(\epsilon_\mu - \epsilon'). \end{aligned} \quad (C3)$$

This means that the C_μ are column vectors of a matrix C which transforms H and S to diagonal matrices simultaneously:

$$C^+ SC = \begin{bmatrix} \sigma_1 & & \\ & \cdot & \\ & & \sigma_N \end{bmatrix}, \quad C^+ HC = \begin{bmatrix} \epsilon_1 \sigma_1 & & \\ & \cdot & \\ & & \epsilon_N \sigma_N \end{bmatrix}. \quad (C4)$$

For the case that none of the σ_μ are negative, this is just the result of the usual diagonalization of $HC = \epsilon SC$.

Acceptable eigenstates are those solutions with $\lambda_\mu > 0$ or equivalently $\epsilon_\mu > \epsilon'_0$. The solutions with $\epsilon_\mu < \epsilon'_0$ must be discarded. These solutions arise when an eigenvalue of the overlap matrix shifts from positive to negative. What then happens is that one of the states from the upper artificial set has dropped to a

this By choosing ϵ' to lie below the true bands but above the dropped states and then taking the top part of the λ spectrum, the proper states are selected automatically In practice, a good choice was to take ϵ' about 0.5 Ry below the expected minimum of the band

Since the use of two functions per angular momentum leads to an almost-degenerate basis, the question arises whether it is possible to use matrices of minimal size and still include sufficient degrees of freedom for the interstitial wave function This is motivated by efficiency but also by the desire to think in chemical or tight-binding terms The following approach is made possible by the fact that a single minimal basis to either energy parameter produces bands which are almost correct By orthogonalizing the functions from the second set on those of the first, the overlap and Hamiltonian matrices take the form

$$H = \begin{bmatrix} H_{11} & H_{12} \\ H_{12}^\dagger & H_{22} \end{bmatrix}, \quad S = \begin{bmatrix} S_{11} & 0 \\ 0 & S_{22} \end{bmatrix} \quad (C5)$$

The upper-left blocks alone give almost correct eigenvalues so that orthogonalization forces the remaining basis functions into directions which give very bad eigenvalues when taken alone Because of the minimal property of the Hamiltonian these energies lie high above the true bands The effect of the coupling H_{12} between the diagonal blocks is to push the two sets of bands apart The bands calculated by the H_{11} and S_{11} alone are slightly too high since the single basis does not have all the required degrees of freedom The repulsion from the upper set corrects for this, yielding the proper eigenvalues For this kind of situation, a simple version of Lowdin perturbation theory is adequate [64] Written out, the eigenvalue equation for the blocked matrices is

$$\begin{aligned} H_{11}C_1 + H_{12}C_2 &= \epsilon S_{11}C_1 \\ H_{12}^\dagger C_1 + H_{22}C_2 &= \epsilon S_{22}C_2 \end{aligned} \quad (C6)$$

The second equation is solved for C_2 which is then substituted in the first, giving

$$\{ H_{11} - H_{12}(H_{22} - \epsilon S_{22})^{-1} H_{12}^\dagger \} C_1 = \epsilon S_{11} C_1$$

The second term in the curly brackets can be approximated by replacing ϵ by some guess ϵ_0 of the energy, for example, ϵ_0 can be chosen somewhere in the middle of the band. To see that this is adequate, go to a representation in which H_{22} and S_{22} are diagonal, then a typical (say the i,i -th) element of $H_{22} - \epsilon S_{22}$ is

$$h_{11} - \epsilon s_{11} = (\epsilon_1 - \epsilon) s_{11}$$

where ϵ_1 is an eigenvalue to H_{22}, S_{22} . The difference $\epsilon_1 - \epsilon$ is large because ϵ_1 lies in the upper complex of bands and ϵ in the lower. Thus the difference between the guessed energy ϵ_0 and ϵ is much smaller than $\epsilon_1 - \epsilon$, meaning that the replacement of ϵ by ϵ_0 does not introduce a large error. Furthermore, since the extra term in the curly brackets is a small correction, it is adequate to treat it in an approximate way. The solutions of the following eigenvalue problem therefore are good approximations to the eigenstates of the full double-basis problem:

$$\bar{H}_{11} C_1 = \epsilon S_{11} C_1$$

$$\bar{H}_{11} := H_{11} - H_{12}(H_{22} - \epsilon_0 S_{22})^{-1} H_{12}^\dagger. \quad (C7)$$

It is clear that a large gap between the upper and lower bands is necessary for the scheme to work. This is only the case if the double basis is nearly degenerate.

SUMMARY

The first part of this thesis (chapters 1 to 5) is concerned with multiple scattering theory, which is a useful and frequently followed approach when solving the Schrodinger equation in concrete applications. The aim is to go beyond the muffin-tin potential approximation which is at present a precondition for applying this theory in practice. Chapter 1 is intended as an introduction to the subject.

Chapter 2 presents the basic facts of multiple scattering theory insofar as they are relevant here. It is assumed from the beginning that a spherical region around each nucleus is treated separately from the 'interstitial region' between the atoms. There are strong arguments for doing this if all electrons (including the core states) are to be treated properly, a completely different approach is to eliminate the problems connected with the core by use of a pseudopotential.

Given this 'muffin-tin geometry', one can now proceed in two ways. First, by using a straightforward plane wave expansion for all quantities in the interstitial region, the potential can be treated without approximation. This results in the linear augmented plane wave method (LAPW). This method has proven to be very useful, but it has a number of disadvantages: (1) it makes a large basis set necessary, (2) it is restricted to periodic systems, and (3) it uses basis functions which are unrelated to any kind of intuitive atomic-orbital picture. The second way to proceed is to approximate the interstitial potential by a constant value so that the wave function there can be derived from the (analytically known) free electron propagator. In a natural way this leads to the multiple-scattering description in which each atom is seen as a scatterer embedded in a homogeneous medium. A number of methods (such as KKR) have been developed from this principle, which eliminate the three disadvantages stated above. Specifically, multiple scattering theory can be applied to systems such as surfaces, molecules, and impurities as well as to periodic structures. The major disadvantage is the necessity of a flat interstitial potential, which is an inadequate approximation except for close-packed systems of high symmetry.

Chapter 3 presents a new practical way to generalize multiple scattering theory to potentials of arbitrary shape. The basic idea of the approach is to consider the atomic spheres as scatterers embedded in an *inhomogeneous* (but well-behaved) medium. The problem to be solved is to find a description for the propagation of waves between the scatterers, once this is known, one can proceed as in the existing methods. The solution consists in probing the response of the medium to multipole disturbances at the various atomic sites. This is equivalent

to determining the Green function for the medium. The functions used hereby are the 'multipole Green functions', which reduce to the Hankel functions of conventional multiple scattering theory for a flat interstitial potential. It is demonstrated that these functions contain in a compact way exactly the minimum of information which is needed about the interstitial potential when solving the Schrodinger equation for the full system. It is also shown how the functions can be calculated in practice. This is done by splitting off the singular part for separate treatment in a manner analogous to the Ewald method for evaluating lattice sums, for example when Madelung potentials are calculated.

In chapter 4, a computer implementation of the ideas of chapter 3 for periodic systems is described. Apart from some technical details, most emphasis is placed on making the method self-consistent in the framework of local density theory. In this way, the electron-electron interaction is included adequately for most ground-state properties. The central variable of local density theory is the charge density, so that a convenient representation for it must be found. For the implementation, a new simple scheme was chosen which fits periodic Hankel functions to the value and slope of the true charge density on the sphere surfaces (that is, on the boundary of the interstitial region). This has the advantages that only a small effort is required to accumulate the charge density, that the electrostatic potential (needed to attain self-consistency) is easy to calculate, and that the total-energy integrals can be evaluated analytically.

Chapter 5 demonstrates, that the band-structure method in the final self-consistent form is able to describe well the electronic structure of realistic systems. The covalent semiconductor silicon was taken as test case, since it is the prototype of a structure for which a flat interstitial potential fails. The comparisons with experiment and previous calculations show that the method is as precise as the other state of the art first-principles methods. The present basis is much smaller than all others which are in use, so that a compact representation of the effect of the interstitial potential has indeed been found. However, this must be paid for to some extent when the multipole Green functions are constructed. When overall efficiency is considered, it is probable that the computational effort of the present method is comparable to that of the other approaches. This shows once again that a certain minimal amount of effort is unavoidable when the interstitial potential is treated properly. Thus, it is not claimed that the present method solves all problems connected with electronic structure calculations for general potentials more efficiently. It is, however, a new approach to the problem which is inequivalent and complementary to the existing methods. The techniques developed here should make it possible to find new attacks on related problems such as electronic structure calculations for surfaces, impurities, or atomic clusters. In addition, the calculations in

chapter 5 demonstrate that the simple charge density representation is adequate even for such small effects as the energy change caused by a frozen phonon perturbation. This is of importance for other full-potential methods as for example the LAPW method.

Chapter 6 is devoted to a different problem which is frequently encountered in solid-state physics, namely, the evaluation of singular Brillouin zone integrals. Characteristic for these is that there is an energy-conserving Dirac δ -function under the integral; the simplest example is the density of states. For some given energy, the δ -function restricts the integration to the corresponding constant-energy surface of the electron (or phonon) band in question, with an additional weight function depending on the magnitude of the gradient of the energy band. The weight function becomes infinite at points for which the gradient disappears. This leads to singularities in the integral as a function of energy, called Van Hove singularities. The numerical evaluation is usually done by the linear integration method. The Brillouin zone is cut into a large number of small tetrahedra and the band is interpolated linearly in each of these. Simple analytical expressions are available for the contribution of each tetrahedron. This procedure gives large errors for tetrahedra in the vicinity of critical points (where the gradient is zero), since there the linear term vanishes and the second-order term is leading in a Taylor expansion. Thus, it is desirable to base a numeric integration method on a local *quadratic* approximation. The three papers in chapter 6 show that simple analytic expressions also exist in this case. The resulting scheme is denoted as the analytic-quadratic integration method.

The first two papers present the method for the special case of the density of states. Geometrically, the quantity to be calculated is the area which is cut out of the quadratic constant-energy surface by the tetrahedron, measured in a metric defined by means of the corresponding quadratic form. The central formula connects this to the sum of the angles in the corners of this piece of the surface. The density-of-states contribution can in this way be evaluated easily. A number of tests prove that the new method has an improved convergence rate when compared to the linear method (as the number of tetrahedra is increased) and that it can resolve the Van Hove singularities perfectly.

The third paper included in this chapter extends the method to the general case when an arbitrary well-behaved function stands under the integral as well as the δ -function. Corresponding to the quadratic expression used to interpolate the band, this new function must be approximated linearly. It is shown that the extra terms which must then be evaluated can be transformed to integrals over the tetrahedron surface. In this formulation, the additional terms are recognized to be functions of the two-dimensional density of states associated with the triangular faces of the tetrahedron. Thus, the difficult general case is reduced to

the calculation of densities of states in two and three dimensions, so that it can be evaluated analytically as before. Test calculations for typical applications show that the same big advantages with respect to the linear methods are found for the case of general singular integrals. Thus, it is now possible to determine such quantities as Fermi surface integrals more efficiently and to a higher precision than in the past.

SAMENVATTING

Het eerste deel van dit proefschrift gaat over de theorie van meervoudige verstrooiing, in de praktijk een nuttige en veelgebruikte aanpak om de Schrodingervergelijking op te lossen. Hoofdstuk 1 is een inleiding.

Hoofdstuk 2 geeft een overzicht van het deel van de theorie van meervoudige verstrooiing dat we hier nodig hebben. Terwijl tot nu toe de muffin-tin (poffertjespan) benadering voor de potentiaal gemaakt moest worden om de theorie toe te passen, is het hier de bedoeling om deze benadering te laten varen. Wel zal van het begin af aan de muffin-tin opdeling van de ruimte gebruikt worden, dat wil zeggen dat rond elke atoomkern een bol apart van de tusseliggende ruimte wordt behandeld. Hiervoor zijn goede redenen als men alle elektronen (met inbegrip van de binnenste schillen) nauwkeurig wil behandelen, een volstrekt andere benadering is om de problemen die te maken hebben met de binnenste schillen, op te lossen door gebruik te maken van een pseudopotential.

Uitgaande van de muffin-tin opdeling van de ruimte kan men nu op twee manieren verder gaan. Ten eerste kan men alle grootheden in het gebied tussen de bollen uitdrukken in een som over vlakke golven. Dit leidt tot de LAPW (Linear Augmented Plane Wave) methode. Deze methode heeft haar nut ruimschoots bewezen, maar kent een aantal nadelen: a) zij heeft een erg grote basis nodig, b) zij kan alleen toegepast worden op periodieke systemen en c) zij gebruikt een basis die los staat van elk gevoelsmatig beeld van atomaire toestanden. De andere manier om verder te komen is om de potentiaal in het tusseliggende gebied te benaderen met een constante waarde zodat de golf functie hier verkregen kan worden uit de analytisch bekende voortplantingseigenschappen van vrije elektrongolven. Op natuurlijke wijze leidt dit tot het beeld van de meervoudige verstrooiing, waarin ieder atoom werkt als een verstrooier van elektronen in een homogeen medium. Een aantal methoden, zoals KKR (Korringa, Kohn en Rostoker), is ontwikkeld langs deze lijn, die de eerder genoemde drie nadelen niet kent. In het bijzonder kan meervoudige verstrooiingstheorie toegepast worden op bijvoorbeeld oppervlakken, moleculen en

onzuiverheden, maar ook op periodieke systemen. Het grootste bezwaar is het gebruik van een vlakke potentiaal, dat eigenlijk alleen echt gerechtvaardigd is bij dicht gestapelde systemen met een hoge symmetrie.

In hoofdstuk 3 wordt een nieuwe praktische manier gepresenteerd om de theorie van de meervoudige verstrooiing uit te breiden zodat zij toegepast kan worden op potentialen met een willekeurige vorm. Het uitgangspunt hierbij is de atomen te beschouwen als verstrooiers in een *inhomogeen* medium. De opgave is om ook nu de voortplanting van de golven tussen de verstrooiers te beschrijven, verder is alles als in de bestaande methoden. Voor de oplossing moet men nagaan hoe het medium reageert op een multipoolstoring op de diverse atomaire posities. Dit is hetzelfde als het bepalen van Green's functie voor het medium. De functies die hiervoor gebruikt worden zullen hier 'multipool Greenfuncties' heten, die in het geval van een vlakke potentiaal neerkomen op de Hankelfuncties van de gewone theorie van meervoudige verstrooiing. Van deze functies wordt aangetoond, dat ze precies alle informatie over de potentiaal in het tussenliggende gebied bevatten die nodig is om de Schrodinger-vergelijking voor het hele systeem op te lossen. Ook wordt aangegeven hoe deze functies in de praktijk berekend kunnen worden, namelijk door de functie te splitsen in een singulier korte dracht gedeelte en een lange dracht gedeelte dat glad is, zoals bij de methode van Ewald voor het berekenen van de Madelungpotentiaal van kristalroosters.

In hoofdstuk 4 wordt een computerimplementatie van de ideeën uit hoofdstuk 3 voor periodieke systemen beschreven. Naast aandacht voor enige technische details wordt de nadruk gelegd op het zelf-consistent maken van de methode binnen de benadering van de plaatselijke dichtheid (het Zweedse elektronengas). Deze benadering is in staat de elektron-elektronwisselwerking in de grondtoestand redelijk goed te beschrijven. De centrale variabele in de theorie van de plaatselijke dichtheid is de ladingsdichtheid. Hiervoor moet een handige weergave gevonden worden. Voor de implementatie werd een nieuw en eenvoudig schema ontworpen, dat periodieke Hankelfuncties aanpast aan de waarde en afgeleide van de werkelijke ladingsdichtheid op de boloppervlakken (dat wil zeggen op de rand van het tussengelegen gebied). Dit heeft als voordeel, dat het weinig moeite kost om de totale ladingsdichtheid samen te stellen, dat de elektrostatische potentiaal (die nodig is om zelf-consistentie te bereiken) makkelijk te berekenen is, en dat de totale-energieintegralen analytisch uitgewerkt kunnen worden.

Hoofdstuk 5 laat zien dat de bandenstructuurmethode in haar uiteindelijke zelf-consistente vorm in staat is om de elektronenstructuur van realistische systemen goed te beschrijven. Als proef is de covalente halfgeleider silicium gekozen, omdat het een typisch voorbeeld is van een structuur waarvoor een vlakke

interstitiele potentiaal het laat afweten. De vergelijking met experimenten en eerdere berekeningen laten zien dat de methode net zo nauwkeurig is als de best bestaande methoden. De basis die hier wordt gebruikt is echter veel kleiner dan die van alle andere, zodat er inderdaad een zeer compacte manier om het effect van de interstitiele potentiaal te beschrijven is gevonden. De prijs die hier echter tot op zekere hoogte voor betaald moet worden zit in de constructie van de multipool Greenfuncties. Over het geheel genomen is de hoeveelheid rekenwerk in deze methode waarschijnlijk vergelijkbaar met die van de andere. Dit toont weer eens aan dat men onder een zekere hoeveelheid werk niet uit komt als de potentiaal in het tussengelegen gebied op de juiste wijze behandeld wordt. Er wordt dus niet gesteld dat deze methode alle problemen met betrekking tot elektronenstructuurberekeningen voor willekeurige potentialen op de meest doelmatige wijze oplost. Maar het is wel een nieuwe aanpak die los staat van een aanvulling is op de bestaande methoden. De technieken die hier zijn ontwikkeld bieden een gereedschap waarmee aanverwante zaken als elektronenstructuurberekeningen van oppervlakken, onzuiverheden of atomaire clusters aangepakt zouden kunnen worden. Bovendien tonen de berekeningen van hoofdstuk 5 aan dat de eenvoudige weergave van de ladingsdichtheid zelfs goed genoeg is voor zulke kleine effecten als de energieverandering ten gevolge van een verstoring door een fonon. Dit is van belang voor andere methoden die de volledige potentiaal gebruiken zoals LAPW.

Hoofdstuk 6 is gewijd aan een ander probleem dat vaak opduikt in de natuurkunde van de vaste stof, namelijk het uitwerken van singuliere integralen over de Brillouin zone. Karakteristiek voor deze integralen is dat de integrand een energiebehoudende Dirac deltafunctie bevat. Het eenvoudigste voorbeeld is de toestandsdichtheid. De deltafunctie beperkt de integratie tot een oppervlak van een zekere constante energie van de elektron (of fonon) band met een gewichtsfunctie gelijk aan één gedeeld door de gradient van de integrand. De gewichtsfunctie wordt oneindig als de gradient nul wordt. Dit leidt tot singulariteiten in de integraal als een functie van energie, die Van Hove singulariteiten heten. De berekening wordt in de praktijk meestal gedaan met de zogenaamde lineaire integratiemethode. De band wordt in een groot aantal tetraeders telkens door een lineaire functie benaderd. Dit geeft voor de bijdrage van elke tetraeder een eenvoudige analytische uitdrukking. Dit leidt tot grote fouten in de buurt van kritische punten, (waar de gradient nul is), aangezien de kwadratische term daar leidt. Er is daarom behoefte aan een integratiemethode die gebaseerd is op een gebiedsgewijs *kwadratische* benadering. De drie artikelen in hoofdstuk 6 laten zien dat eenvoudige analytische uitdrukkingen ook in dit geval bestaan. De zo ontwikkelde methode wordt de Analytisch Kwadratische Methode genoemd.

De eerste twee artikelen behandelen de methode voor het bijzondere geval van de toestandsdichtheid. Meetkundig beschouwd moeten we de grootte bepalen van dat deel van het energie-oppervlak dat door een tetraëder wordt begrensd, waarbij we een maat gebruiken die door de kwadratische term gegeven wordt. De formule die centraal staat legt het verband tussen deze grootte en de som van de hoeken van dit oppervlak. De toestandsdichtheid volgt dan eenvoudig. Bij een aantal toepassingen is aangetoond dat de nieuwe methode sneller convergeert dan de lineaire (bij toenemend aantal tetraëders) en dat de Van Hove singulariteiten uitstekend worden weergegeven.

In het derde artikel wordt de methode uitgebreid tot het algemene geval waarbij de integrand bestaat uit het produkt van een willekeurige nette functie met de deltafunctie. Bij een kwadratische benadering van de band hoort een lineaire benadering van de functie. Aangetoond wordt dat de extra termen die zodoende ontstaan teruggebracht worden tot integralen over het oppervlak van de tetraëder. In deze formulering van het probleem kan men de extra termen herkennen als twee-dimensionale toestandsdichtheden die horen bij de driehoekige zijvlakken van de tetraëder. Zo is het moeilijke algemene geval teruggebracht tot de berekening van toestandsdichtheden in twee en drie dimensies, zodat zij weer analytisch uitgedrukt kan worden. Typische toepassingen laten weer dezelfde voordelen ten opzichte van de lineaire methode zien. Het is nu dus mogelijk geworden om grootheden als Fermi-oppervlakken efficiënter en nauwkeuriger te berekenen dan vroeger.

REFERENCES

- [1] Abramowitz, M., and I. Stegun, *Handbook of Mathematical Functions* (Dover, New York, 1972)
- [2] Aldred, P.J.E., and M. Hart, Proc. R. Soc. London Ser. A **332**, 223 (1973)
- [3] Andersen, O.K., and R.G. Woolley, Mol. Phys. **26**, 905 (1973)
- [4] Andersen, O.K., Phys. Rev. B **12**, 3060 (1975)
- [5] Ashcroft, N.W., and N.D. Mermin, *Solid State Physics* (Holt-Saunders, New York, 1976)
- [6] Bachelet, G.B., D.R. Hamann, M. Schlüter, Phys. Rev. B **26**, 4199 (1982)
- [7] Beleznyay, F., and M.J. Lawrence, J. Phys. C **1**, 1288 (1968)
- [8] Bendt, P., and A. Zunger, Phys. Rev. B **26**, 3114 (1982)
- [9] Boon, M.H., M.S. Methfessel, and F.M. Mueller, to be published in J. Phys. C
- [10] Born, M., and J.R. Oppenheimer, Am. J. Phys. **84**, 451 (1927)
- [11] Bross, H., and K.H. Anthony, Phys. Status Solidi **22**, 667 (1967)
- [12] Chadi, D.J., and M.L. Cohen, Phys. Rev. B **8**, 5747 (1973)
- [13] Champeney D.C., *Fourier Transforms and their Physical Applications* (Academic, London, 1973)
- [14] Chelikowsky, J.R., and S.G. Louie, Phys. Rev. B **29**, 3470 (1984)
- [15] Christensen, N.E., Phys. Rev. B **29**, 5547 (1984)
- [16] Conolly, J.W.D., and J.R. Sabin, J. Chem. Phys. **56**, 5529 (1972)
- [17] Cooke, J.F., and R.F. Wood, Phys. Rev. B **5**, 1276 (1972)
- [18] Danese, J.B., J. Chem. Phys. **61**, 3071 (1974)
- [19] Danos, M., and L.C. Maximon, J. Math. Phys. **6**, 766 (1965)
- [20] Dederichs, P.H., and R. Zeller, Phys. Rev. B **28**, 5462 (1983)
- [21] Denteneer, P.J.H., and W. van Haeringen, J. Phys. C **18**, 4127 (1985)
- [22] Dimmock, J.O., Solid State Phys. **26**, 103 (1971)
- [23] Ehrenreich, H., and L.M. Schwartz, Solid State Physics **31**, 149 (1976)
- [24] Eisenhart, L.P., *Introduction to Differential Geometry* (van Nostrand, Princeton, 1947)
- [25] Ellis, D.E., and G.S. Painter, Phys. Rev. B **2**, 2887 (1970)
- [26] Elyashar, N., and D.D. Koelling, Phys. Rev. B **13**, 5362 (1976)

- [27] Ewald, P.P., *Ann. Phys. (Germany)* **64**, 253 (1921)
- [28] Gelatt Jr., C.D., H. Ehrenreich, and R.E. Watson, *Phys. Rev. B* **15**, 1613 (1977)
- [29] Glötzel, D., B. Segall, and O.K. Andersen, *Solid State Commun.* **36**, 403 (1980)
- [30] Gonis, A., and G.M. Stocks, *Phys. Rev. B* **25**, 659 (1982)
- [31] Groot, R.A. de, F.M. Mueller, P.G. van Engen, and K.H.J. Buschow, *Phys. Rev. Lett.* **50**, 2024 (1983)
- [32] Gschneidner, K.A., *Solid State Phys.* **16**, 275 (1964)
- [33] Gunnarsson, O., and B.I. Lundqvist, *Phys. Rev. B* **13**, 4274 (1976)
- [34] Gunnarsson, O., J. Harris, and R.O. Jones, *Phys. Rev. B* **15**, 3027 (1977)
- [35] Halse, M.R., *Proc. Roy. Soc. London* **265**, 507 (1969)
- [36] Ham, F.S., and B. Segall, *Phys. Rev.* **124**, 1786 (1961)
- [37] Hamann, D.R., M. Schlüter, and C. Chiang, *Phys. Rev. Lett.* **43**, 1494 (1979)
- [38] Hamann, D.R., *Phys. Rev. Lett.* **42**, 662 (1979)
- [39] Harmon, B.N., W. Weber, and D.R. Hamann, *Phys. Rev. B* **25**, 1109 (1982)
- [40] Harris, J., and G.S. Painter, *Phys. Rev. B* **22**, 2614 (1980)
- [41] Hedin, L., and B.I. Lundqvist, *J. Phys. C* **4**, 2064 (1971)
- [42] Herring, C., *Phys. Rev.* **57**, 1169 (1940)
- [43] Hohenberg, P., and W. Kohn, *Phys. Rev.* **136**, B864 (1964)
- [44] Holzwarth, N.A.W., S.G. Louie, and S. Rabii, *Phys. Rev. B* **26**, 5382 (1982)
- [45] Jackson, J.D., *Classical Electrodynamics* (Wiley, New York, 1975)
- [46] Janak, J.F., *Phys. Rev. B* **18**, 7165 (1978)
- [47] Jarlborg, T., and A.J. Freeman, *Phys. Lett.* **74A**, 349 (1979)
- [48] Jepsen, O., and O.K. Andersen, *Solid State Commun.* **9**, 1763 (1971)
- [49] Johnson, K.H., *Adv. Quantum Chemistry* **7**, 143 (1973)
- [50] Johnson, K.H., *J. Chem. Phys.* **45**, 3085 (1966)
- [51] Kane, E.O., *Phys. Rev. B* **4**, 1917 (1971)
- [52] Kasterin, N., *Proc. Acad. Sci. Amsterdam* **6**, 460 (1897)
- [53] Koelling, D.D., and G.O. Arbman, *J. Phys. F* **5**, 2041 (1975)
- [54] Koelling, D.D., *Phys. Rev.* **188**, 1049 (1969)
- [55] Kohn, W., and L.J. Sham, *Phys. Rev.* **140**, A1133 (1965)
- [56] Kohn, W., and N. Rostoker, *Phys. Rev.* **94**, 1111 (1954)
- [57] Korringa, J., *Physica* **13**, 392 (1947)

- [58] Kübler, J., A.R. Williams, and C.B. Sommers, Phys. Rev. B **28**, 1745 (1983)
- [59] Kübler, J., Physica **127B**, 257 (1984)
- [60] Kunc, K., and R.M. Martin, Phys. Rev. Lett. **48**, 406 (1982)
- [61] Lehmann, G., and M. Taut, Phys. Status Solidi B **54**, 469 (1972)
- [62] Lloyd, P., and P.V. Smith, Adv. Phys. **21**, 69 (1972)
- [63] Loucks, T.L., *Augmented Plane Wave Method* (Benjamin, New York, 1967)
- [64] Löwdin, P., J. Chem. Phys. **19**, 1396 (1951)
- [65] Maradudin, A.A., E.W. Montroll, and G.H. Weiss, *Theory of Lattice Dynamics in the Harmonic Approximation* p.65, (Academic, New York, 1963)
- [66] Merzbacher, E., *Quantum Mechanics* (Wiley, New York, 1970)
- [67] Messiah, A., *Quantum Mechanics* (North-Holland, Amsterdam, 1978)
- [68] Methfessel, M., and J. Kübler, J. Phys. F **12**, 141 (1982)
- [69] Methfessel, M.S., M.H. Boon, and F.M. Mueller, J. Phys. C **16**, L949 (1983)
- [70] Miedema, A.R., F.R. de Boer, and P.F. de Chatel, J. Phys. F **3**, 1558 (1973)
- [71] Morita, T., and T. Horiguchi, J. Math. Phys. **12**, 981 (1971)
- [72] Morse, M., *Functional Topology and Abstract Variational Theory* (Gauthiers, Villars, Paris, 1939)
- [73] Moruzzi, V.L., J.F. Janak, and A.R. Williams, *Calculated Electronic Properties of Metals* (Pergamon, New York, 1978)
- [74] Mueller, F.M., J.W. Garland, M.H. Cohen, and K.H. Bennemann, Ann. Phys. (Germany) **67**, 19 (1971)
- [75] Nozawa, R., J. Math. Phys. **7**, 1841 (1966)
- [76] Painter, G.S., and D.E. Ellis, Phys. Rev. B **1**, 4747 (1970)
- [77] Painter, G.S., J.S. Faulkner, and G.M. Stocks, Phys. Rev. B **9**, 2448 (1974)
- [78] Perdew, J.P., Chem. Phys. Lett. **64**, 127 (1979)
- [79] Phillips, J.C., Phys. Rev. **104**, 1263 (1956)
- [80] Roberto, J.B., B.W. Batterman, and D.T. Keating, Phys. Rev. B **15**, 2590 (1974)
- [81] Rompa, H.W.A.M., M.F.H. Schuurmans, and F. Williams, Phys. Rev. Lett. **52**, 675 (1984)
- [82] Segall, B., Phys. Rev. **105**, 108 (1957)

- [83] Slater, J C , and G F Koster, Phys Rev **94**, 1498 (1954)
- [84] Slater, J C , Phys Rev **51**, 846 (1937)
- [85] Slater, J C , Phys Rev **81**, 385 (1951)
- [86] Springelkamp, F , R A de Groot, W Geertsma, W van der Lugt, and F M Mueller, Phys Rev B **32**, 2319 (1985)
- [87] Stohr, H , and H Bross, Phys Status Solidi B **90**, 497 (1978)
- [88] Stukel, D J , and R N Euwema, Phys Rev B **1**, 1635 (1970)
- [89] Talman, J D , *Special Functions* (Benjamin, New York, 1968)
- [90] Treusch, J , and R Sandrock, Phys Status Solidi **16**, 487 (1966)
- [91] Van Hove, L , Phys Rev **89**, 1189 (1953)
- [92] Wang, C S , and B M Klein, Phys Rev B **24**, 3393 (1981)
- [93] Weinert, M , J Math Phys **22**, 2433 (1981)
- [94] Wendel, H , and R M Martin, Phys Rev B **19**, 5251 (1979)
- [95] Wigner, E , Phys Rev **46**, 1002 (1934)
- [96] Wigner, E , and F Seitz, Phys Rev **43**, 804 (1933)
- [97] Wilkinson, J H , *The Algebraic Eigenvalue Problem* (Clarendon, Oxford, 1965)
- [98] Williams, A R , J Kubler, and C D Gelatt Jr , Phys Rev B **19**, 6094 (1979)
- [99] Williams, A R , Phys Rev B **1**, 3417 (1970)
- [100] Wimmer, E , H Krakauer, M Weinert, and A J Freeman, Phys Rev B **24**, 864 (1981)
- [101] Yang, Y W , and P Coppins, Solid State Commun **15**, 1555 (1974)
- [102] Yin, M T , and M L Cohen, Phys Rev B **26**, 5668 (1982)
- [103] Yin, M T , and M L Cohen, Phys Rev B **26**, 3259 (1982)
- [104] Zeller, R , and P J Braspenning, Solid State Commun **42**, 701 (1982)
- [105] Ziman, J M , Proc Phys Soc **86**, 337 (1965)
- [106] Zunger, A , and A J Freeman, Phys Rev B **15**, 5049 (1977)
- [107] Zunger, A , and M L Cohen, Phys Rev B **18**, 5449 (1978)
- [108] Zunger, A , and M L Cohen, Phys Rev B **20**, 4082 (1979)
- [109] Zunger, A , Phys Rev B **21**, 4785 (1980)

CURRICULUM VITAE

- Geboren 12 september 1954 te Clausthal-Zellerfeld (Bondsrepubliek Duitsland).
- Middelbare school: van 1966 tot 1969 Hendrik Hudson High School in Montrose, New York, U.S.A.; daarna Graf Engelbert-Gymnasium in Bochum (Duitsland) tot aan het eindexamen in 1973.
- Vanaf september 1973 studie theoretische Natuurkunde en Wiskunde aan de Ruhr-Universität Bochum tot aan het doctoraalexamen (Diplom).
- Van april 1981 tot maart 1986 in dienst van de Stichting Fundamenteel Onderzoek der Materie, en werkzaam als wetenschappelijk medewerker bij de afdeling Banden Structuur Berekeningen van de Katholieke Universiteit Nijmegen.

Stellingen

- 1 The disadvantage of the Ewald method for calculating the KKR structure constants is usually seen in the numerical radial integrations needed to evaluate the real-space lattice sums. These integrals can be expressed in closed analytic form.
(M. Abramowitz and I. Stegun, Handbook of Mathematical Functions, 7.4.33 and 34)
- 2 The distinction between a spherical-wave and a plane-wave representation for the interstitial wavefunction in a muffin-tin potential is not superficial, because only the spherical-wave basis is tailored to include exactly the required degrees of freedom. This explains the efficiency of the KKR, ASW and LMTO methods.
- 3 The simplicity of Weinert's method for solving the Poisson equation in crystals is obscured because plane waves are used to expand the charge densities. If atom-centered periodic Hankel-functions are used instead, the formalism becomes much simpler.
(M. Weinert, J. Math. Phys. **22**, 2433 (1981))
- 4 Self-consistent electronic structure calculations using non-local norm-conserving pseudopotentials are so complicated that the advantages are marginal when compared to all-electron full-potential methods.
- 5 'There is a rebellious soul in things which must be overcome by powerful charms and incantations'. This sentence by Joseph Conrad describes the activities of a medicine man in Borneo. It also characterizes the impression which is produced on an outsider who listens to scientific specialists discussing an intricate problem.
- 6 Quantum mechanics has taught to scientists something which has long been accepted by many philosophies, namely, that there are questions which do not have an answer on a rational level.
- 7 Die führenden Autoren der Trivialliteratur sind Hedwig Courths-Mahler, Johannes Mario Simmel, und Fritjof Capra
(Fritjof Capra, 'The Tao of Physics')

- 8 Het gebruik van woorden uit een vreemde taal dient niet uit de weg te worden gegaan, aangezien zelfs voor de meest eenvoudige woorden geen nauwkeurige vertaling bestaat
9. A tough exercise in self-discipline is to sit still next to someone who is programming a computer
- 10 A fairer democratic system would result if each person were permitted to divide his vote among a number of candidates
- 11 Our ratio-dominated society abounds with paradoxes such as the production of surplus food by unhealthy methods and, of course, peace by means of nuclear threat. An understandable reaction of many people is to refuse to participate in logical discussions about such subjects.
- 12 Die alten chinesischen Kaiser mussten die 'vier Künste' beherrschen: Malerei, Kalligraphie, Schach und Musik. Im Interesse der Allgemeinheit sollte man heutzutage dasselbe von allen leitenden Politikern fordern.

M Methfessel

29 mei 1986

